AD NUMBER

AD818673

LIMITATION CHANGES

TO:

Approved for public release; distribution is unlimited.

FROM:

Distribution authorized to U.S. Gov't. agencies and their contractors; Critical Technology; 31 JUL 1967. Other requests shall be referred to Air Force Technical Applications Center, Washington, DC 20333. This document contains export-controlled technical data.

AUTHORITY

USAF ltr dtd 28 Feb 1972

FINAL REPORT
CONTRACT AF33(657)-15919
SDL OPERATIONS
18 FEBRUARY 1966 - 1 MARCH 1967

31 JULY 1967

Prepared for

AIR FORCE TECHNICAL APPLICATIONS CENTER

Washington, D. C.

By

EARTH SCIENCES DIVISION
TELEDYNE INDUSTRIES, INC.

Under

Project VELA UNIFORM

Sponsored By

ADVANCED RESEARCH PROJECTS AGENCY
Nuclear Test Detection Office
ARPA Order No. 624

FINAL REPORT - CONTRACT AF33(657)-15919

SDL Operations 18 February 1966 - 1 March 1967

AFTAC Project No.:	VELA T/6702
Project Title:	Seismic Data Laboratory
ARPA Order No.:	624
ARPA Program Code No.:	5810
Name of Contractor:	EARTH SCIENCES DIVISION TELEDYNE INDUSTRIES, INC.
Contract No.:	AF 33(657)-15919
Date of Contract:	18 February 1966
Amount of Contract:	$ 1,842,884
Contract Expiration Date:	17 February 1967
Project Manager:	William C. Dean (703) 836-7644

P. O. Box 334, Alexandria, Virginia

This work reported herein was supported by the Advanced Research Projects Agency, Nuclear Test Detection Office, and was monitored by the Air Force Technical Applications Center under Contract AF 33(657)-15919.

Neither the Advanced Research Project Agency nor the Air Force Technical Applications Center will be responsible for information contained herein which may have been supplied by other organizations or contractors, and this document is subject to later revision as may be necessary.

TABLE OF CONTENTS

		Page No.
I.	INTRODUCTION	1
II.	FACILITIES	4
	A. Office Lay-Out	4
	B. Personnel and Management	5
	C. Electronic Data Processing Equipment	6
III.	DATA STORAGE AND RETRIEVAL	9
	A. Magnetic Tape and Film	9
	B. Data Tape Compression Program	9
	C. Composite Tapes	10
	D. Digitized Data	11
	E. Digital Programs	12
	F. U. A. Coast and Geodetic Survey Epicenters	12
	G. Earthquake Bulletin Data	13
	H. Shot Report Data	13
IV.	SERVICE FUNCTIONS	13
	A. Computational Services for Other Vela Participants	13
	B. Automated Bulletin Process	14
V.	DESCRIPTIVE ANALYSES OF EARTHQUAKES & EXPLOSIONS	15

TABLE OF CONTENTS
(continued)

		Page No.
VI.	RESEARCH	19
	A. General	19
	B. LASA Studies	19
	C. Teleseismic Signal Measurements at Vertical Arrays	31
	D. Rayleigh Wave Rejection by Optimum Filtering of Vertical Arrays	34
	E. Detection of Surface Waves at Teleseismic Distances	37
	F. Rectilinear Motion Detection	43
	G. Energy Fluctuations in Seismic Noise	51
	H. The Coherency Analysis of Seismic Noise	53
	I. Analysis of Seismic Noise at the Yellowknife Array, Canada	58
	J. Finite Fourier Transform Theory & Its Application to the Computation of Convolutions, Correlations and Spectra	61

APPENDIX A - Bibliography of Reports Issued Under Contract AF 33(657)-15919

LIST OF ILLUSTRATIONS

FIGURE		Follows Page No.
1.	Seismic Data Laboratory Floor Plan	4
2.	Seismic Data Laboratory Organization Chart	5
3.	Schematic Diagram of Digital Computer Equipment	6
4.	Schematic Diagram of Analog Processing Equipment	6
5.	Amplitude Measurement Procedures for Statistical Summary Reports	17
6.	Typical LASA Seismograms for 4 November 1965 - Argentina Event	20
7.	Subarray Amplitude Variations for 4 November 1965 Event	20
8.	Subarray S/N Variations for 4 November 1965 Event	20
9.	10 November 1965 Processed Traces (Prefiltered Data)	22
10.	10 November 1965 Processed Traces (Prefiltered Data)	22
11.	Computed Anomalies Before & After Shifts, Subarray F3	28
12.	Type of LASA Travel-Time Data Computed by the SDL	28
13.	Vertical Component Vertical Array Measurements-- Aleutians, USCGS Focus 67 km, Magnitude 5.2 Date 6/17/65 Time 19:05:9.1	33
14.	Deghosted Vertical Array Measurements, Method I	33
15.	Deghosted Vertical Array Measuremtns, Method II (Reflection Coefficient 0.7)	33
16.	Optimum Filters Estimating Four Modes (The Signal & Three Rayleigh Modes) from Synthetic Data with all Four Modes Present	36
17.	Real Signal Test Case	41
18.	Real Signal Test Case	41
19.	Real Signal Test Case	41
20.	Peru Event	45
21.	Polarization Measurements Using REMODE Filters	47
22.	Input S/N Ratio R	49

LIST OF ILLUSTRATIONS
(continued)

		Follows Page No.
FIGURE		
23.	Input S/N Ratio R	49
24.	Input S/N Ratio R	49
25.	Input S/N Ratio R	49
26.	Relative Frequency of Occurrence (Ordinate) Versus Energy Level (Abscissa)	52
27.	Relative Frequency of Occurrence (Ordinate) Versus Energy Level (Abscissa)	52
28.	Seismic Array at CPSO	55
29.	Sample A -- Proportion of Noise Power Accounted For With Outer Seismometers Added First	56
30.	Sample A -- Proportion of Noise Power Accounted For With Inner Seismometers Added First	57
31.	Yellowknife Array	58
32.	System Response at Yellowknife Array	58
33.	Yellowknife Array Noise Sample; Original and Transcription	60
34.	Auto-Spectra, R1, Low Resolution (.2 cps) for Yellowknife Array Noise	60
TABLES		
1.	List of Users of SDL Data	13
2.	Unified Magnitudes from P_n or P Waves for Statistical Summary Reports	17
3.	Data From Explosions Analyzed by the Seismic Data Laboratory	18
4.	Summary of Signal/Noise Ratio Improvement (decibels above bandpass-filtered single seismometer)	22
5.	REMODE Comparisons for Detection Thresholds and S/N Improvements	49
6.	Ordinary Coherence of 10 with other Seismometers	56
7.	Linear Filter Relation Between Sub-Array Elements and Center Element (10)	57

I. INTRODUCTION

This final report covers the period 18 February 1966 through 1 March 1967, the period of performance under contract AF 33(657)-15919. The purpose is to accumulate, in one report, a concise discussion of the research, the operations, and the capabilities of the Seismic Data Laboratory (SDL) as they relate to the VELA UNIFORM Program.

The Seismic Data Laboratory was originally established under Contract AF 33(657)-7427 and was operated as the Data Analysis and Technique Development Center from October 1961 through 16 August 1963. Basically, this contract period was devoted to the design and establishment of a permanent facility which would serve not only as a repository for all the data accumulated for use under the VELA UNIFORM Program, but also as an organization to analyze the data, conduct basic research in seismic phenomena, and to perform data services for the entire VELA UNIFORM community.

These goals were essentially completed in February 1963 when the SDL moved into its present facility at 300 N. Washington Street, Alexandria, Virginia. By this time, the organization structure was established, personnel with the qualifications needed to perform the work were on the job, routine operating procedures had been established, the electronic data processing equipment configuration was complete, and a research plan had been established to attack the problem of the detection and identification of earthquakes and nuclear explosions.

Thus the objectives of this earlier period had been attained, and the Seismic Data Laboratory began its operations as an integral part of the VELA UNIFORM Program under contract AF 33(657)-12447.

The work performed and the accomplishments attained under this contract were reported in the final report issued on 15 April 1966.

Essentially, the work performed under the present contract was a continuation of the tasks outlined under prior SDL contract periods. The actual work statement is as follows:

1. Tasks

a. Perform data analyses and seismological research as directed by the AFTAC project officer. The following task assignments are included:

(1) Design, develop, and apply new analytical techniques and procedures for processing seismological data.

(2) Analyze and evaluate data from explosions and selected earthquakes.

(3) Compile and report basic data from explosions and earthquakes, which may include the variation of amplitude with distance as a function of frequency, travel times of body and surface waves, travel-time anomalies, variation of amplitude with yield or explosion environment, wave-form characteristics, and other information as specified.

(4) Evaluate existing identification criteria and develop and apply new identification criteria for distinguishing between seismic waves from natural and artificial sources.

(5) Develop data processing techniques that will improve the detection and identification capability of station networks and associated analysis centers.

(6) Process seismological data from the Large Aperture Seismic Array as directed by the AFTAC project officer.

b. Maintain data services and plant facilities as follows:

(1) Maintain a central data file, to include a system for cataloging and classifying incoming seismic data, that include means for rapid access to significant data.

(2) Maintain a file of all digitized seismograms.

(3) Continually evaluate the equipment, facilities, and staff of the Seismic Data Laboratory (SDL); make recommendations for modifications as required, and effect such modifications as approved by the Government.

(4) Obtain and prepare digital and analog computer programs for cataloging, processing, and analyzing the data.

(5) Furnish copies of seismological recordings or processed seismological data to other VELA UNIFORM participants, provide facilities for visiting scientists to review data within the SDL, provide computational services to other VELA participants, conduct mathematical analyses, and other activities as approved by the AFTAC project officer.

(6) Compress the data on analog magnetic tapes so that the original tapes can be degaussed and returned to the field for further use as directed by the AFTAC project officer.

These tasks essentially cover the work which has been performed during this period and the summary discussion which follows is based on all the detailed reports and memoranda which have been issued under the contract.

Section II discusses the general SDL facilities, including analog and digital machine data processing. Section III is concerned with the storage and retrieval of film and tape, tape compression, and the data which have been processed in-house. Section IV covers the types of service functions which SDL offers to other VELA UNIFORM participants. Section V is a descriptive discussion of the statistical summary analyses completed on earthquake and explosion events, and Section VI gives a concise summary of the research studies which have been undertaken.

II. FACILITIES

A. Office Lay-Out

The Seismic Data Laboratory is housed in the second and third floors of a seven-story building at 300 North Washington Street, Alexandria, Virginia. A floor plan of these two floors is shown in Figure 1. In general, the offices are on the third floor while the second floor is restricted to computer activities and the Central Data Files. Owing to security requirements, normal access to the laboratory is entirely through the third floor lobby door that is constantly attended by a receptionist during the daytime shift. Other exits are provided into the stairwells but can be used only in case of emergency by breaking a security seal. Also, as needed, freight can be entered either through an outside freight door in the maintenance room or the second floor elevator door that is normally kept locked.

In addition to the regular SDL staff, office space is provided for the AFTAC Project Officer, for other AFTAC personnel, and for SDL visitors. This provision fulfills one of the functions of SDL. Visitors, either VELA UNIFORM participants or approved foreign scientists, are encouraged to use the facilities provided to study the data stored in SDL.

The present building includes many features required specifically for the computing facilities. These features include extra electric power, separate high-capacity air conditioners, and a raised floor to accommodate wiring and to serve as an air conditioning plenum under the computer room and adjacent maintenance area. The regular concrete flooring under this area has, in addition, extra reinforcing steel for special loading.

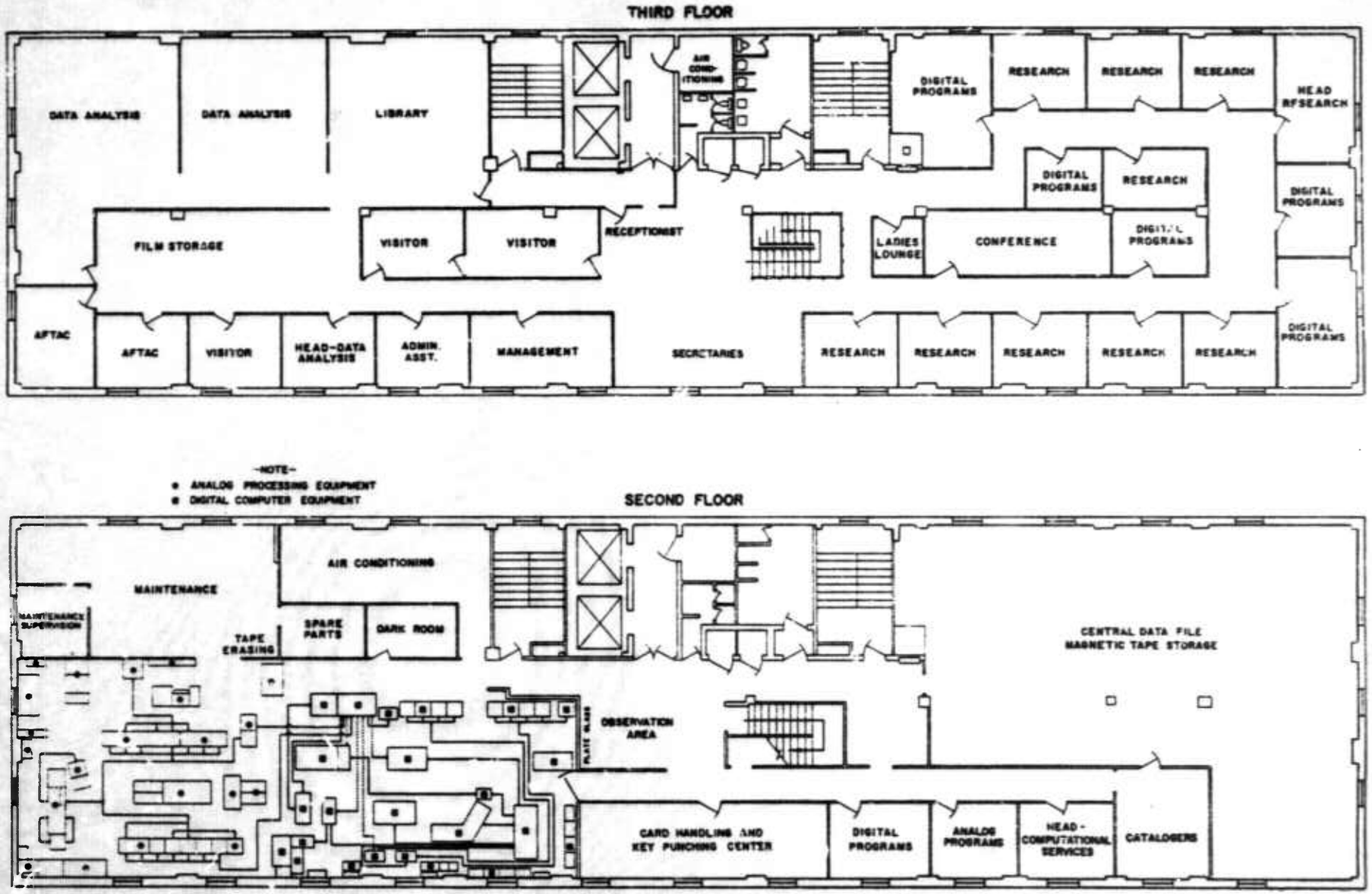

Figure 1. Seismic Data Laboratory Floor Plan

The Central Data Files provides space for 250 three-foot shelf sections, each of which holds 102 magnetic tapes. The total storage capacity is approximately 25,550 tapes. A large portion of data over one year old is being compressed, thus increasing greatly the actual amount of data that can eventually be stored here. The compressed data tapes are stored at another near-by facility in order that the most current data will be readily available for processing.

Approximately 300 square feet is also devoted to storing analog film at SDL. New techniques for storing digital tapes have enabled us to store all our digital tapes in the computing area.

B. Personnel and Management

The SDL is organized into three sections in accordance with Figure 2. The Data Analysis Section consists of trained geophysicists who make routine examination of seismic records; the Research Section consists of scientists on the Ph.D. level and is responsible for the original research conducted; and the Computational Services Section provides the electronic data processing function. As a secondary function, the Data Analysis and Computational Services sections perform service for other VELA UNIFORM participants.

The execution of a research program is ideally performed on a project basis rather than an organization basis. The project leader is one of the senior research scientists supported by one or more computational assistants, analysts or programmers. Since a research worker cannot keep the same number of support people busy all the time, pooling the various specialties makes

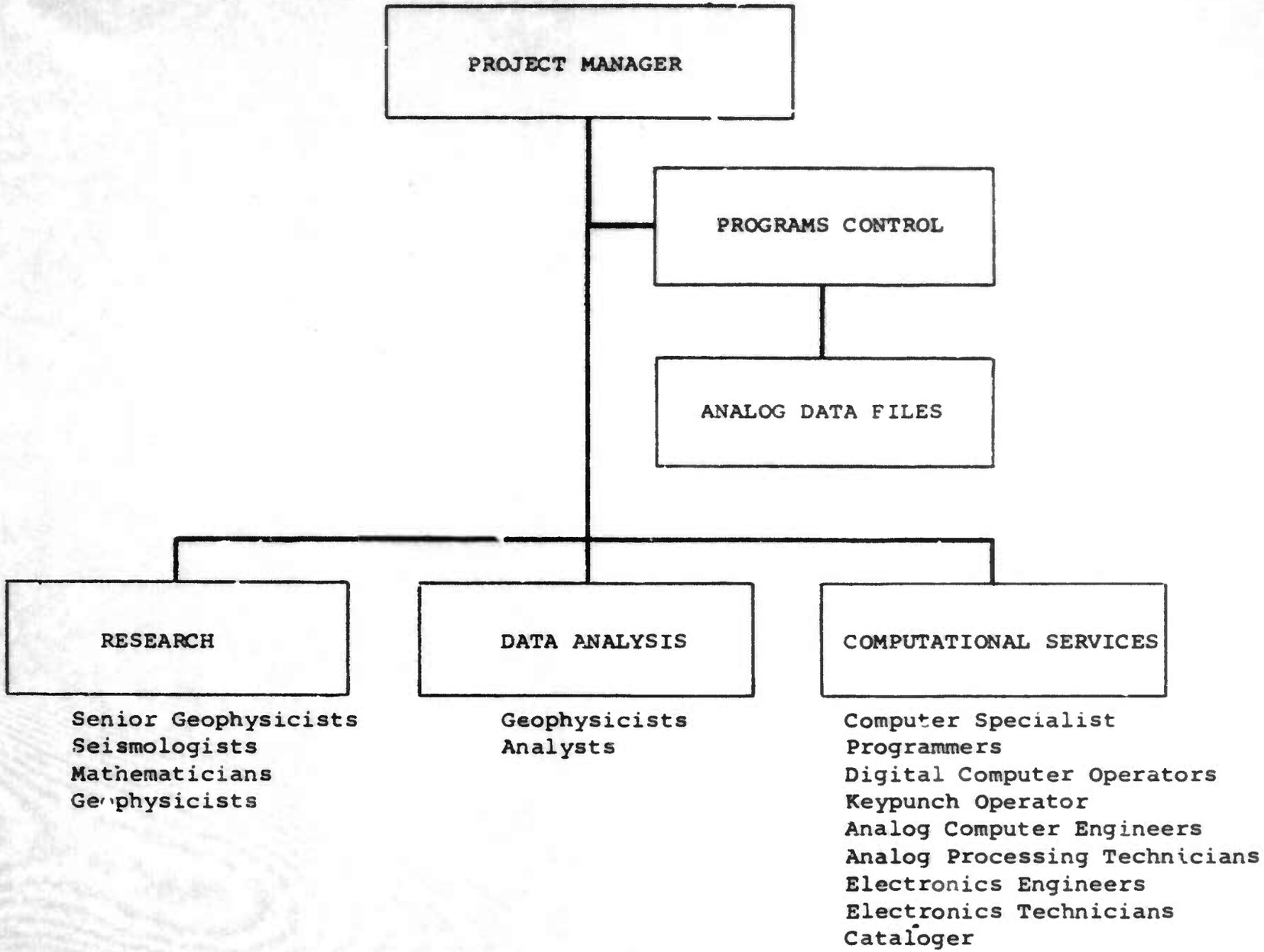

Figure 2. Seismic Data Laboratory Organization Chart

for more efficient use of personnel. The use of service pools is also an efficient way of providing necessary support for non-SDL requests without untenable interruption of research programs. This applies to both analysts and programmers.

The SDL has made use of consultants to design experiments, to follow their progress, and to help interpret the results; the actual work being done by geophysicists or senior analysts assigned full time to the projects and supervision being furnished by appropriate SDL personnel.

C. Electronic Data Processing Equipment

The equipment configuration is indicated schematically in Figures 3 and 4. This equipment may be roughly classified into functional groups as follows: (1) magnetic tape playback, including filters, spectrum analyzers, etc., (2) analog computer, (3) time code generator and the analog-to-digital converter, (4) electronics for compressing data on magnetic tape, and (5) digital computer and its supporting equipment.

The various modes of data flow through the digital computer are shown schematically in Figure 3. The most convenient aspects of this system are: (1) The small CDC 160-A that performs offline operations freeing the 1604 computer for the bigger jobs, and (2) the plotter that has been used almost universally to present the output in a form readily understood by visual inspection. Plotting will now be shared by the recently completed D/A conversion system, including the analog plotter.

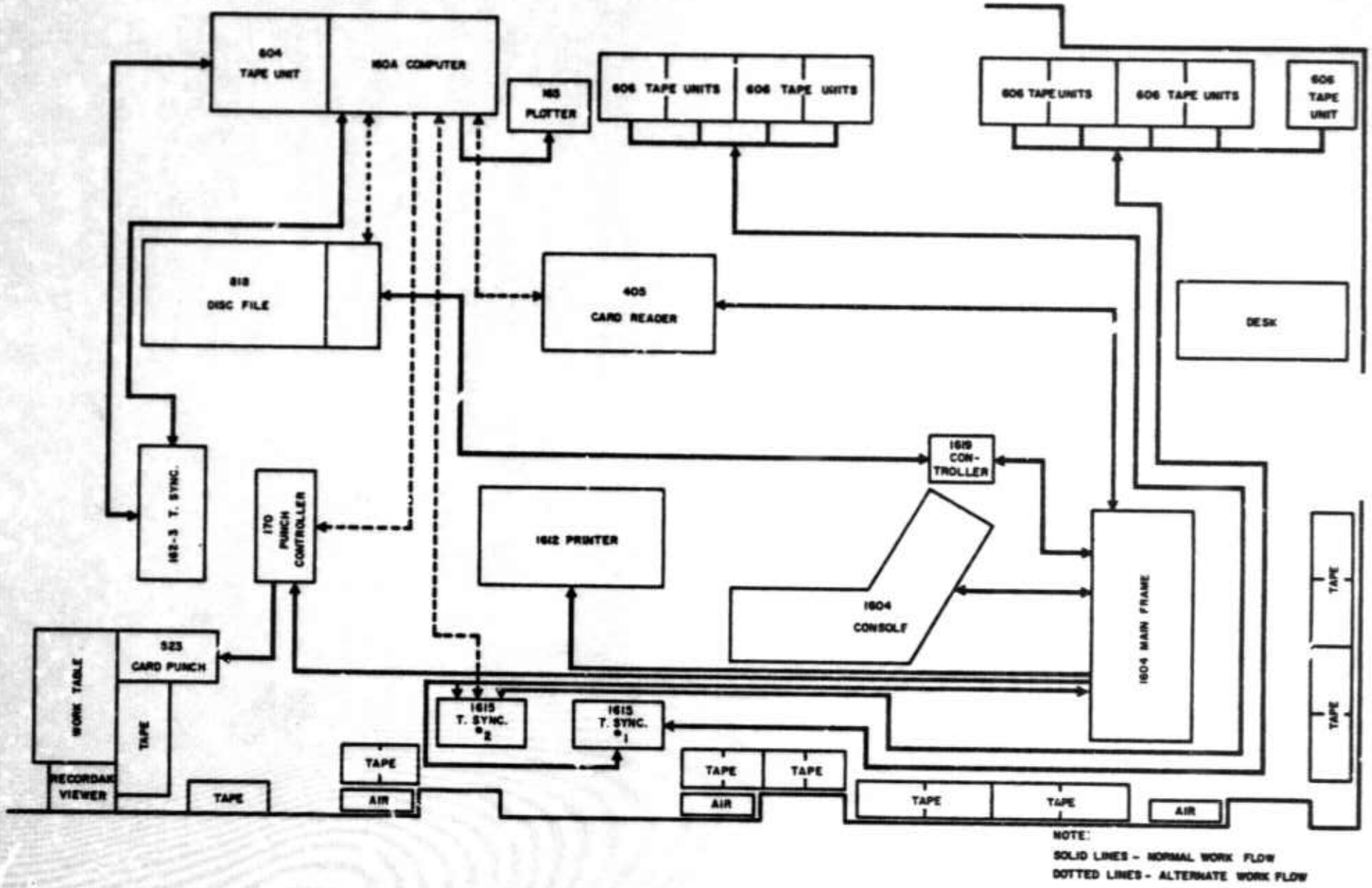

Figure 3. Schematic Diagram of Digital Computer Equipment

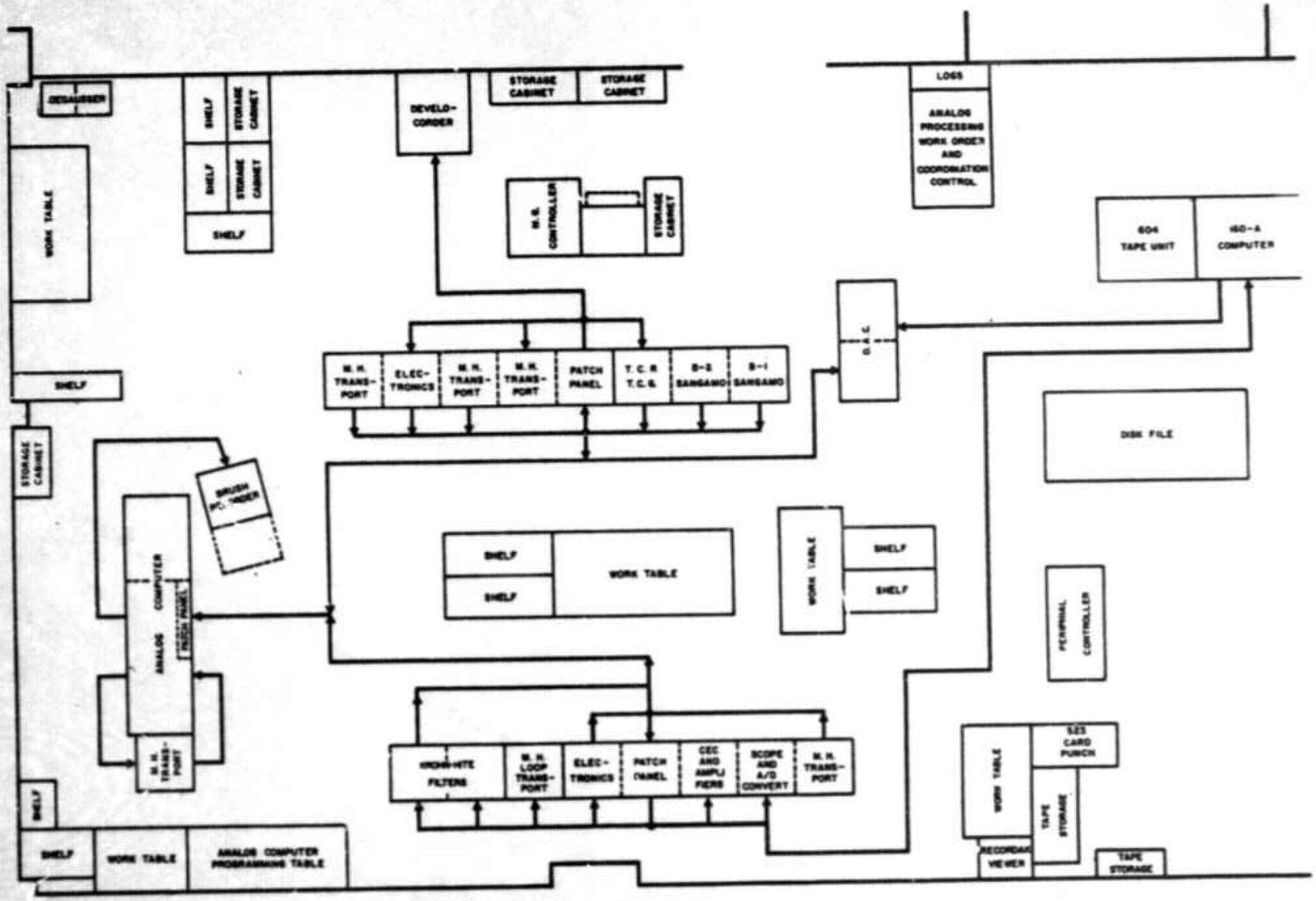

Figure 4. Schematic Diagram of Analog Processing Equipment

In order to machine process LASA data as set forth in the work statement, the equipment configuration was modified to include the following additions:

- One CDC 604 magnetic tape drive
- One CDC 818 disk file
- One CDC 162-3 controller
- A digital-to-analog sub-system

The disk file, tape drive, and the controller were supplied and installed by the Control Data Corporation. Because of our specialized requirements, the individual parts of the D/A sub-system were purchased, assembled and made operational by SDL engineering personnel.

The analog sections of the equipment are characterized by high flexibility. Any element can be connected through patch-panels to any other element. The various elements in the system are shown in their relative floor arrangement in Figure 4; the connecting points for the trunk cables between the patch panels are as shown.

The following operations can now be performed, many simultaneously, with the analog processing system:

1. Transcribe the magnetic recordings from one tape to another, either to make a duplicate tape or to produce a composite tape consisting of selected portions of many original tapes. Whereas the original tape is recorded at 0.3 ips, the transcription can be performed at speeds up to 60 ips, that is, 200 times faster;

2. Make paper records, or film playouts, from magnetic recordings;

3. Make power spectra analysis and plot the results automatically;

4. Digitize analog tapes for further analysis on the digital computer. The digital tapes are in an IBM compatible format;

5. Generate and read VELA Time Code;

6. Filter data using Krohn-Hite filters or special analog computer circuits;

7. Make develocorder films from analog tape;

8. Read and write analog tapes compatible with the British 24-channel system;

9. Compress data from field tapes on new tapes in the ratio of 10:1, thus freeing nine tapes out of ten for re-use in the Field Measurement program;

10. Transcribe data from standard IRIG ½-inch magnetic tapes to the one-inch tapes normally used at SDL; and

11. Perform any general analog computer operations.

III. DATA STORAGE AND RETRIEVAL

A. Magnetic Tape and Film

Seismic data comes to the SDL from the Long Range Seismic Measurements (LRSM) field teams, U.S. and foreign observatories, and from the Large Aperture Seismic Array (LASA) located at Billings, Montana. The FM analog magnetic tapes and operational logs are stored in the Central Data Files and the digital tapes from LASA are stored in the digital computer area. For working convenience, both 16 mm and 35 mm film, together with operational logs, are stored adjacent to the Data Analysis Section.

When this data comes in, it is checked against a packing list and a receiving record is prepared. This receiving record contains the recording station's name and the date of recording. The data itself is stored by station and month. When data is needed for processing, the receiving record is checked to see if the data has been received and, if so, the cataloger goes to the appropriate shelving unit where the data is sotıed and checks it out of the files for processing.

B. Data Tape Compression Program

Early in 1963 it became clearly evident that the storage of the analog magnetic tape would soon be a storage problem if all data recorded in the field was to be stored in the SDL facility. Because of this, and to partially solve the high cost of magnetic tapes used in the field program, it was decided to compress this original data by re-recording it on magnetic tape at 10 times its present density; that is to say, the data on 10 original tapes would be recorded on one new tape.

Certain seismic data, particularly that of known nuclear explosions, is maintained in its original form. Originally, data six months old was compressed, but once the initial backlog of data was eliminated, only data at least one year old is compressed.

The basic system requires the use of three tape transports that may be manipulated by a single operator. While the data is being transferred from the tape on one transport to the tape on another transport, a third transport is being loaded and prepared for transcription.

As the original data is being compressed, a log is prepared which contains the recording station and data day, the data compressed, quality control check-off, and the date the tape is erased. The date that the data is compressed is noted in the proper receiving record, discussed above. The box containing the compressed data is marked with the station name and data recording day. The compressed tapes are then stored at another near-by facility where they are readily available.

Compression operations started in September 1963, and the sub-system became fully operational during February 1964. Present production is being maintained at the level needed to meet the requirements of the field measurement program (LRSM teams and U.S. Observatories) and SDL.

C. Composite Tapes

The data library contains analog composite tapes which were either prepared by the SDL or obtained from other contractors for use in the VELA UNIFORM program. A separate area is maintained

within the Central Data Files for storage of these composite tapes and log-books are kept by both the Central Data Files and Analog Processing supervisor. These log-books contain the event name, and the recording stations which are a part of the composite tape. A composite tape for a given event contains each station calibration, 10 minutes of data recorded at each station before the P arrival, and 10-20 minutes of data recorded after the P arrival.

D. Digitized Data

The digital library contains many thousands of digital seismograms, most of which were recorded on analog tape and digitized at SDL. Several hundred events were recorded directly on digital tape using data acquisition systems at Tonto Forest Seismological Observatory and LASA. In each case data have been demultiplexed into a library format which can be input to digital programs already in use.

Digitized data can be punched on cards or written on tape in an IBM compatible format. The data is written in the binary mode at 200 or 556 bits per inch (as specified by the requestor). The tapes contain a variable number of files of 36-bit word binary integers. Each file contains either a vertical or horizontal component from a single station for a specified period of time (up to 13 minutes).

The binary integers range between plus and minus 2048. The data is not necessarily calibrated, but instructions are available for relating digital counts to earth motion at lcps.

The sampling rate can be varied, but is normally 20 samples per second. The data is prefiltered to minimize aliasing. The time of the first digital point can be determined to $\pm$ .1 second.

A separate list is furnished with each tape giving the order of the seismograms written on each tape, sampling rate, number of files per seismogram, number of data points per file, time of first point, component identification, event name, recording station, and filter setting used at time of digitization.

After each seismogram is written in library format, it is plotted on an incremental x-y plotter and sent through a QC procedure. If the QC is satisfactory, magnitude, time of first point, time of first motion, signal-to-noise ratio, channel quality, event information and instrument or configuration data is punched on cards together with the location on magnetic tape of each seismogram. The digitized data can then be searched on any of the above parameters to determine its availability or suitability for a given analysis assignment.

E. Digital Programs

Many of the scientific and systems programs which have either been developed by the SDL or obtained from other sources have been written-up and are on punched cards or tape, or both.

F. U.S. Coast & Geodetic Survey Epicenters

BCD tapes containing epicenters listed on the Preliminary Determination of Epicenters (PDE) cards (January 1960 to date) are on file. Geographic and seismic regions have been computed for each epicenter.

The cards contain:

Origin Time	Magnitude
Latitude	Source of Magnitude
Longitude	Geographic Region Number
Depth (KM)	Seismic Region Number
	Comments

G. Earthquake Bulletin Data

Earthquake bulletin data from the LRSM teams (February 1962 to date) and the VELA observatories (February 1963 to date) have been written on magnetic tape. Data includes the PDE cards, plus all phase information for those stations which recorded the earthquake. Recorded phase arrivals not associated with an epicenter are also on the tape.

H. Shot Report Data

Data from more than 75 shot events have been punched on cards. The data on the punched cards include:

Shot name	First motion (if picked)
Location	Period
Magnitude	Amplitude
Medium	Instrument
Recording station	Component
Phase ID	Azimuth
Arrival Time	Distance

IV. SERVICE FUNCTIONS

A. Computational Services for Other VELA Participants

Manpower and computer time spent in providing services to other VELA participants has increased steadily since the inception of the SDL project. During this contract period, 286 requests were received from 50 organizations and the VELA Seismological Center. Table 1 lists the organizations which received SDL services during the period of this report.

The normal services to VELA participants include copies of 16 and 35 mm film, copies of digital programs, digitized data, copies of analog tape composites, and the use of the 1604 digital computer for checking out new programs or running production programs.

ORGANIZATIONS RECEIVING SDL DATA SERVICES

Advanced Research Projects Agency
AFCRL

Bolt, Beranek, & Newman, Inc.
Boston College
Brown Engineering, Inc.

California Institute of Technology
Canadian Department of Mines
Canadian Pacific Oil & Gas Company
Carnegie Institute of Washington
Continental Oil Company
Control Data Corporation

Dominion Observatory
Department of Commerce

Earth Sciences, Teledyne
Engineering Physics

General Atronics Corporation
Geotech, Teledyne
Graduate Research Center of
the Southwest

IBM Corporation
Institute for Defense Analysis
International Seismological Research
Centre

Lamont Geophysical Observatory
Lawrence Radiation Laboratory
Lincoln Laboratory

Massachusetts Institute of Technology
Mitre Corporation

Oregon State University

Pan American Petroleum
Pennsylvania State University
Philco Corporation
Princeton University

Roland F. Beers, Inc.
Rowe Air Force Base

San Calixto, Bolivia Observatory
Stanford Research Institute
Stanford University
St. Louis University

Texas Instruments, Incorporated
Triangle Institute

Underwater Systems, Inc.
United Kingdom Atomic Energy
Authority
University of Bergen
University of Frankfort, Germany
University of Michigan
University of Minnesota
University of Tasmania
U. S. Coast and Geodetic Survey,
ESSA

Vitro Corporation

Washington Science Center (USCGS)

Xavier University

Table 1

As the seismic community has become familiar with the activities of the SDL and aware of the data which is available, more frequent requests have been received for the following services:

- Digitizing data from specified earthquakes or explosions.
- Running SDL production programs, such as power spectral density and the linear array programs, on specified data.
- Writing digitized data in specified formats for use on other computers.
- Computing lists of earthquakes which meet specified criteria of depth, magnitude, and location.
- Making composite analog tapes of special events.
- Providing space and assistance for visiting scientists to study data and exchange information with the SDL personnel.

Data requests from VELA participants are screened carefully so as not to interfere with normal SDL analysis assignments, and the services performed are approved by the VSC.

B. Automated Bulletin Process

Under VSC's direction, an Automated Bulletin Process (ABP) computer program was developed jointly by SDL and the Geotech Division, Teledyne Industries, Inc. The program associates seismic phase arrivals at a number of stations, with epicenters reported by the U.S. Coast and Geodetic Survey, and identifies up to 23 phases. The ABP is now being used to accelerate the preparation of the monthly earthquake bulletins of the five VELA UNIFORM seismological observatories published by the Geotech Division, Teledyne Industries, Inc.

In terms of time and manpower requirements, most of the work of preparing the earthquake bulletins involves:

1. Measurement of arrival times, amplitude, and period, preliminary phase identification based on signal character, and card-punching these data for each station. Analysts may record from 300 to 2,000 events per month at each station, depending upon the station, time of year, and seismic activity for a given month.

2. Association of phase arrivals with hypocenters reported in the U.S. Coast and Geodetic Survey (USC&GS) Preliminary Determination of Epicenters (PDE) cards, identification of phases, merging of associated and unassociated events, computation of azimuth, distance, magnitude, and ground displacement, and finally, combination of all data from the five observatories into a form suitable for publication.

The ABP was designed to automate the latter task.

The ABP has been written in three parts which can be combined into one program but are usually run independently.

V. DESCRIPTIVE ANALYSES OF EARTHQUAKES AND EXPLOSIONS

A long range seismic measurements (LRSM) program was established under VELA UNIFORM to record and analyze short-period and long-period data from a planned series of U.S. underground nuclear tests. A standard format was established for compiling statistical data from these nuclear explosions and certain earthquakes having special characteristics. After an event was analyzed, reports were issued summarizing these statistics to be used by VELA UNIFORM participants in studying and developing methods for distinguishing between explosive and earthquake sources.

The data from these various events were recorded by operating mobile field teams and the observatories operated at Wichita Mountain, Oklahoma (WMSO), Uinta Basin, Utah (UBSO), Blue Mountain,

Oregon (BMSO), Cumberland Plateau, Tennessee (CPSO), and Tonto Forest, Arizona (TFSO), and from several experimental or temporary stations operated in connection with other research programs.

Instrumentation at each of the mobile stations consists of three-component short-period Benioff and three-component Sprengnether long-period seismographs. Data are recorded on 35 millimeter film and one-inch 14 channel magnetic tape. All of these stations are equipped to record WWV continuously in order to provide accurate time control. Calibration is accomplished once each day and just prior to each shot at operating settings. Specific details of the instrumentation and operating procedures for these stations are given in Field Manual, Long Range Seismic Measurement Program, Technical Report No. 63-17, which can be obtained from the Geotech Division of Teledyne Industries, Inc., Dallas, Texas. All the observatories have both long-period and short-period, three-component instrumentation in addition to their other specialized facilities.

Station site information, presented in these reports, includes the station name and code; the geographic coordinates, distances and azimuths involved; the station elevations; and the type of instruments in use at each location.

For each event analyzed, a status report is included, giving the names of stations and indicating which instruments were operational and which recorded signals, together with an operations map showing the location of each station recording the event and the type of signals recorded.

An explanation of the procedure for amplitude measurements used in these reports is illustrated in Figure 5 . The unified magnitude (m) computations for distances less than 16° are based on AFTAC/VSC extensions of Gutenberg's Tables*. For these purposes, points from 10° to 16° were read from a curve in the Gutenberg-Richter paper and an inverse cube relationship was used to extrapolate from two to ten degrees. A table of the distance factors (B) is shown in Table 2.

A standard hypocenter location program for a digital computer is used to determine the event locations, using data from all stations analyzed. Best-fit values of latitude, longitude, depth of focus, and time of origin were determined statistically by a least squares technique. This utilized a Jeffreys-Bullen travel-time curve as modified by Herrin in 1961 on the basis of Pacific surface-focus recordings. Precision of the computation is limited primarily by the accuracy of arrival times, the validity of the standard travel-time curve, and by local velocity deviations. Since the method is based on P wave arrivals, this particular program does not make use of later phases such as pP and S in the determination of depth or location.

The measurements made of the principal phases from these events are summarized. These include the Pn and P arrival times, the maximum amplitudes (A/T) of Pn, P and Pg motion as seen on the short-period vertical instruments, and the maximum amplitudes (A/T) of the Lg phase as measured on the short-period horizontal tangential component. Long-period Rayleigh wave motions are also tabulated in (A/T) form.

---

*Gutenberg, B. and Richter, C.F., Magnitude and Energy of Earthquakes, Ann. Geofis., 9 (1956), pp. 1-15.

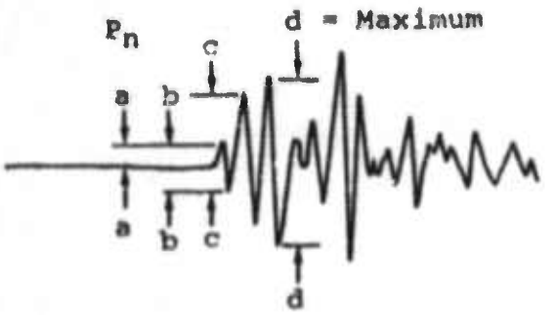

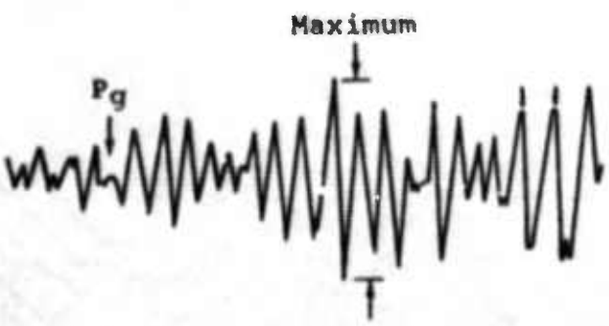

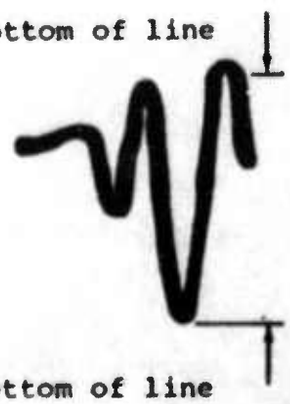

Detail Showing Allowance For Line Width

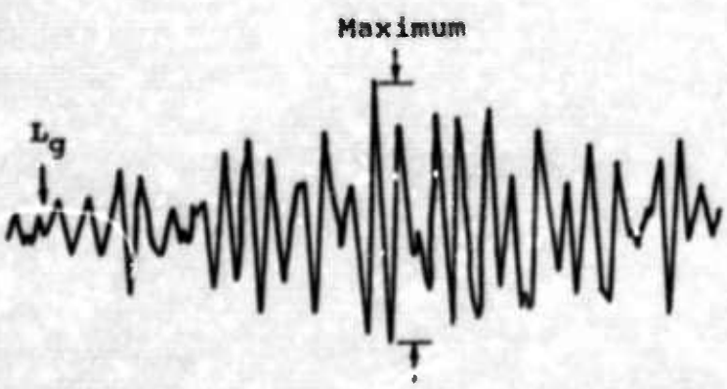

Pick time of Pn at beginning of "a" half cycle.

Pick amplitude of Pn as maximum "$d/_2$" within 2 or 3 cycles of "c".

Pick amplitudes of Pg and Lg at maximum of corresponding motion.

Figure 5. Amplitude Measurements Procedures for Statistical Summary Reports

Unified Magnitude: $m = \log_{10} (A/T), + B$

where

A = zero to peak ground motion in millimicrons

$$= \frac{(mm)\ (1000)}{K}$$

T = signal period in seconds

B = distance factor (see Table below)

mm = record amplitude in millimeters zero to peak

K = magnification in thousands at signal frequency

Table of Distance Factors (B) for Zero Depth

Dist (deg)	B	Dist (deg)	B	Dist (deg)	B	Dist (deg)	B
0°	-	27°	3.5	54°	3.8	80°	3.7
1	-	28	3.6	55	3.8	81	3.8
2	2.2	29	3.6	56	3.8	82	3.9
3	2.7	30	3.6	57	3.8	83	4.0
4	3.1	31	3.7	58	3.8	84	4.0
5	3.4	32	3.7	59	3.8	85	4.0
6	3.6	33	3.7	60	3.8	86	3.9
7	3.8	34	3.7	61	3.9	87	4.0
8	4.0	35	3.7	62	4.0	88	4.1
9	4.2	36	3.6	63	3.9	89	4.0
10	4.3	37	3.5	64	4.0	90	4.0
11	4.2	38	3.5	65	4.0	91	4.1
12	4.1	39	3.4	66	4.0	92	4.1
13	4.0	40	3.4	67	4.0	93	4.2
14	3.6	41	3.5	68	4.0	94	4.1
15	3.3	42	3.5	69	4.0	95	4.2
16	2.9	43	3.5	70	3.9	96	4.3
17	2.9	44	3.5	71	3.9	97	4.4
18	2.9	45	3.7	72	3.9	98	4.5
19	3.0	46	3.8	73	3.9	99	4.5
20	3.0	47	3.9	74	3.8	100	4.4
21	3.1	48	3.9	75	3.8	101	4.3
22	3.2	49	3.8	76	3.9	102	4.4
23	3.3	50	3.7	77	3.9	103	4.5
24	3.3	51	3.7	78	3.9	104	4.6
25	3.5	52	3.7	79	3.8	105	4.7
26	3.4	53	3.7				

Table 2. Unified Magnitudes From P_n or P Waves for Statistical Summary Reports

Other data given in these reports include the travel-time residuals from the Pn and P phases and the amplitudes of Pn and P, Pg and Lg, (which also showed lines proportional to the inverse cube of the distance visually fitted to the observed points), Rayleigh wave amplitudes, and illustrative seismograms showing the signals recorded at a number of locations.

Table 3 gives the events analyzed by SDL together with basic data for each event.

EVENT NAME	EVENT DATE	MEDIUM	MAGNITUDE
Buff	16 December 1965	Tuff	5.14 ± 0.51
Charcoal	10 September 1965	Tuff	5.16 ± 0.29
Chartreuse	6 May 1966	Rhyolite	5.22 ± 0.62
Dumont	19 May 1966	Tuff	5.48 ± 0.56
Duryea	14 April 1966	Rhyolite	5.17 ± 0.50
Half Beak	30 June 1966	Rhyolite	6.02 ± 0.60
Palanquin	14 April 1965	Rhyolite	4.33 ± 0.36
Pin Stripe	25 April 1966	Tuff	4.51 ± 0.56
Redhct	5 March 1966	Tuff	4.11 ± 0.30
Rex	24 February 1966	Tuff	4.80 ± 0.56
Rockville Dam*	3 April 1966	Mine Shaft	4.51 ± 0.93
Tan	3 June 1966	Tuff	5.56 ± 0.49
Yuba	5 June 1963	Tuff	4.36 ± 0.49

*Chemical Explosion

Table 3. Data From Explosions Analyzed by the Seismic Data Laboratory.

VI. RESEARCH

A. General

The basic aim of the VELA UNIFORM Program has been, and is, "to obtain at the earliest practical date a system for the detection of nuclear explosions underground..." Implicit in this objective is the identification of a given seismic event at a nuclear explosion once it has been detected. Thus, the basic problem restated is twofold - detection and identification. To the basic problem we must also add the necessity of developing a system to implement our solution.

Research progress in the Seismic Data Laboratory has paralleled that in the seismological community and has led in most of the specific areas subject to SDL attention. Early research was restricted to recordings of regional and near regional events. As progress was made in the solution of the detection and identification problem at these distances, attention shifted to recordings of explosion and earthquake seismograms at teleseismic distances.

During this reporting period, emphasis has been placed on detection and identification, utilizing data recorded at more sophisticated facilities, such as the LASA in Montana, and utilizing more sophisticated techniques for analyzing such data.

Following is a discussion of the research undertaken at the SDL for which results were reported.

B. LASA Studies

1. LASA Signal and Noise Amplitudes

The objectives of this study were to determine the variability of signal and noise amplitudes within individual subarrays, and across the total LASA, in addition to signal-to-noise

ratio gains produced both by phased and unphased subarray sums. Computations were made of signal amplitudes, rms noise levels, signal-to-noise ratios and phased and unphased subarray summations from Montana LASA recordings of three teleseismic events.

The 1,325 digital seismograms used in this study were recorded on six multiplexed tapes (556 Bpi); three of these tapes contained one cps sine wave calibration data, and the remaining three tapes contained event recordings. Portions of the event seismograms, amounting to 120 seconds of data (70 seconds before P arrival plus 50 seconds of signature), were placed in SDL library format; these library tapes, two for each event, were then used as input to the LASA amplitude program.

Following the data formatting stage, the seismograms were bandpass filtered and demagnified (corrected for system magnification at one cps).

Figure 6 presents the pre-filtered outputs of the subarray center seismometer which are typical (in waveform) of those recorded throughout LASA.

Figures 7 and 8 show subarray amplitude and S/N variations, respectively, computed from the 04 November 1965 data. The mean signal amplitude of 19 subarrays is eight millimicrons, whereas subarray E3 has a mean amplitude of about 20 mμ (about 3 times the LASA mean). Corresponding S/N (Figure 8) also show that subarray E3 is greater than the mean by a factor of three.

The subarray standard errors for signal amplitudes for the three events used averaged about 0.2, signifying that events producing large mean signal amplitudes have correspondingly large standard deviations.

Figure 6. Typical LASA Seismograms for 4 November 1965 - Argentina Event

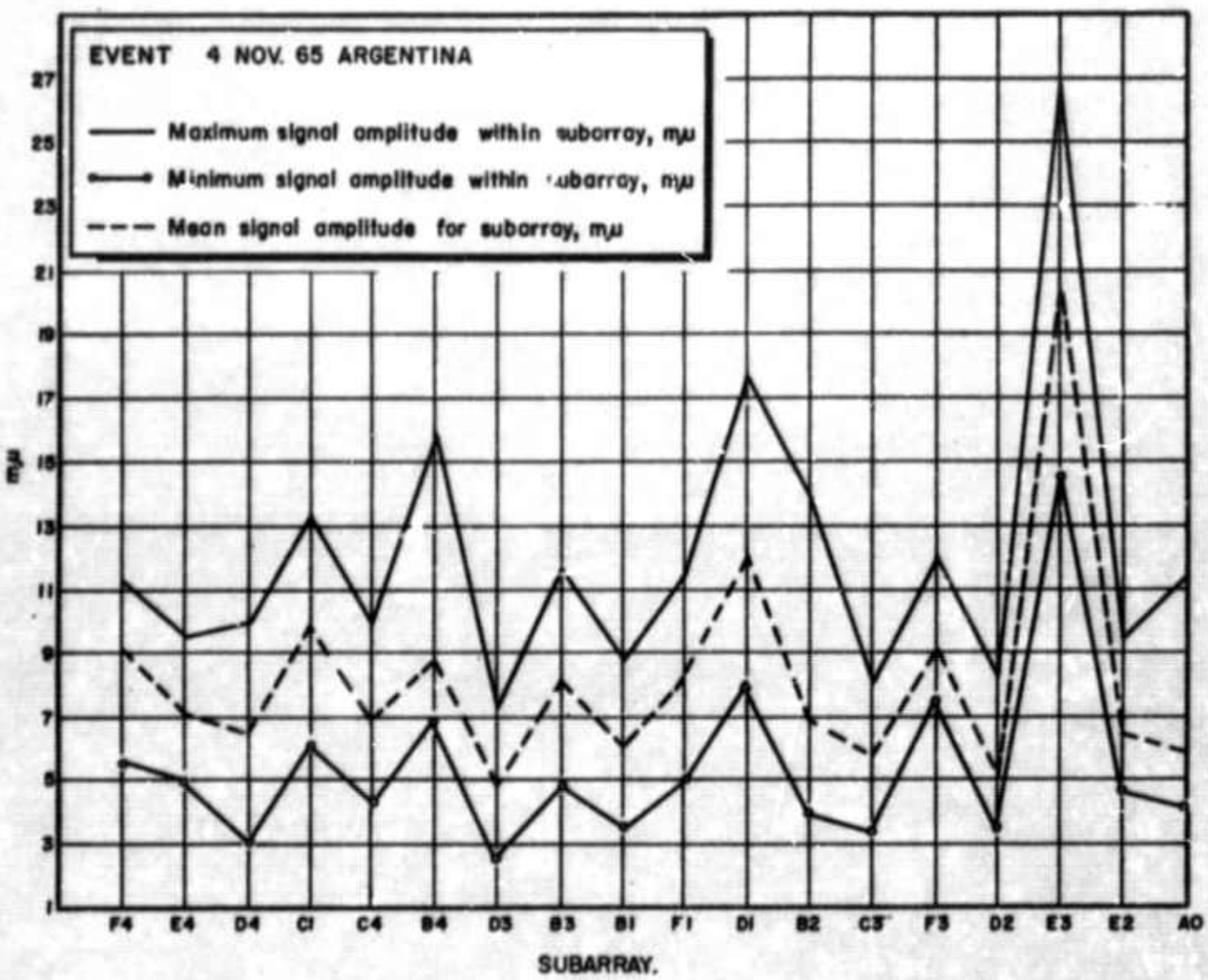

Figure 7. Subarray Amplitude Variations for 4 November 1965 Event

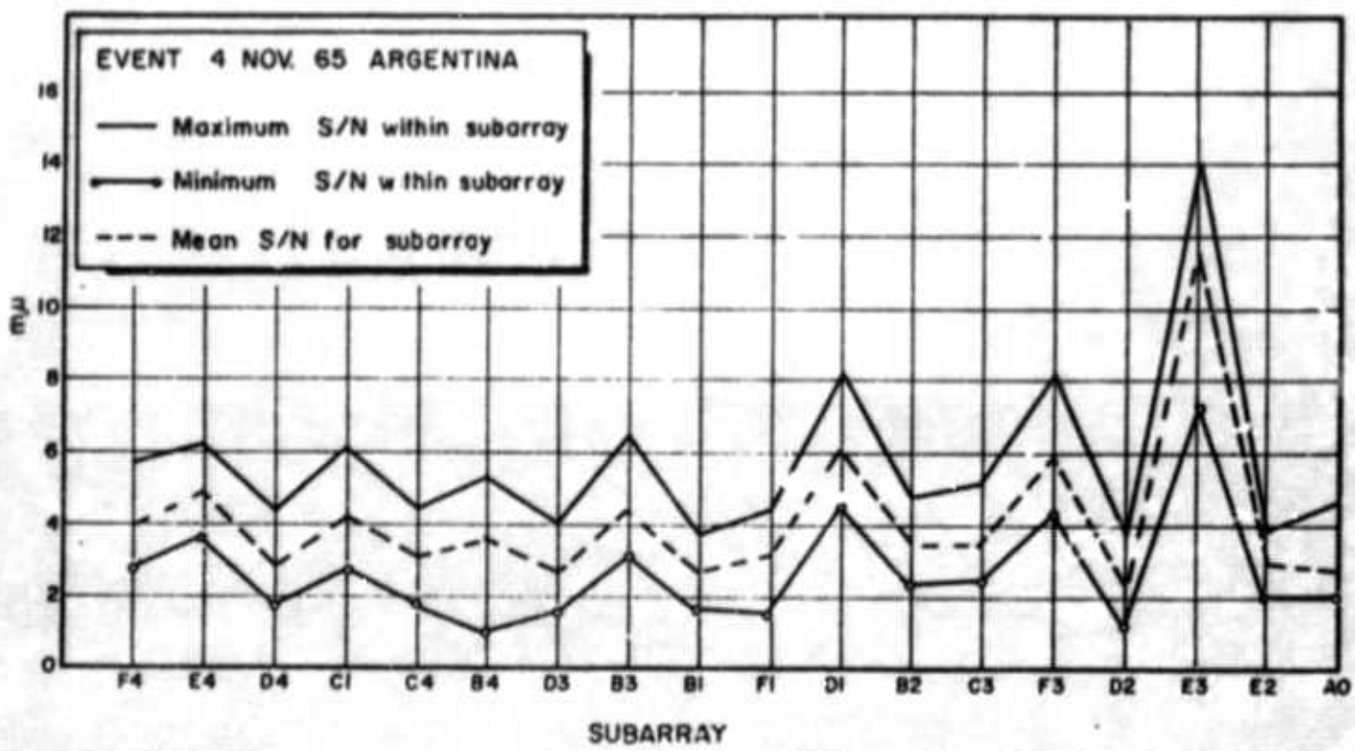

Figure 8. Subarray S/N Variations for 4 November 1965 Event

From the foregoing discussion of LASA signal and noise amplitudes for three earthquakes, the following is concluded:

a. Signal amplitudes vary within a subarray by a factor of three or four;

b. Subarray mean signal amplitudes vary across LASA by a factor of three or four;

c. Noise levels (rms) across the entire LASA appear to be fairly uniform for a given event;

d. Although the mean signal and noise amplitudes computed from seismograms recorded at the subarray centers are lower than their corresponding values computed from all LASA seismograms, the S/N values are about equal;

e. There are no apparent similarities among the observed amplitude variations, e.g., the maximum amplitudes computed from the three events are recorded by different subarrays, although two of the events are from the same direction and within 1000 kilometers of one another;

f. Phased summations of the subarray signal amplitudes are about 2 db better than corresponding unphased sums, but they are slightly smaller than the subarray mean amplitudes;

g. Phased summations of the subarray noise levels (rms) are about the same (actually slightly smaller) as the corresponding unphased sums, but they are about 6 db lower than the subarray mean noise levels; and

h. Subarrays S/N from the phased summations are about 3 db better than the unphased sums, and they are about 6 db better than the subarray mean S/N.

2. Maximum Likelihood Filtering of LASA Seismograms

The objective of this study was to compare the effectiveness and practicality of the maximum-likelihood filtering technique with straightforward time-shifted array summation, i.e., beamforming. We were interested specifically in signal-to-noise ratio improvement, distortion of signal waveform, and cost in digital computing time.

The data were short-period LASA seismograms containing P arrivals from two teleseismic events, 10 November 1965, Aleutian Islands, and 25 November 1965, Kamchatka. Realizable and symmetrical maximum-likelihood filters, two seconds long and based on fitting intervals consisting of 150 seconds of bandpass filtered (0.4 - 3.0 cps) data, were used in processing the data.

The results of the analysis, summarized in Table 4 and illustrated by Figures 9 and 10, indicate that within a subarray the maximum-likelihood filter gives about 1 db more S/N improvement than the phased sum, when the noise reference is outside the fitting interval. The symmetric maximum-likelihood filter performs about 2 db better than its realizable counterpart.

Moreover, when individual subarrays were processed by the realizable filters, and the 21 resulting channels were summed, the S/N improvement was 2-3 db over simply phasing and summing the individual subarray sums; this improvement referred to noise outside the fitting interval.

The symmetric maximum-likelihood filter degrades output signal waveform when signals on the input channels are not identical. The degradation, which is usually not serious within a subarray, takes the form either of precursors to the signal or diminution of the first motion.

			10 Nov 65		25 Nov 65	
			MLR	MLS	MLR	MLS
Average of bandpass filtered center seismometer outputs $(10)_p$			0	0	0	0
Average of subarray phased sums	$P\sum_{JK}(AI)_p$	IN	4.5	4.5	5.5	5.5
		OUT	5.0	5.0	5.5	5.5
Average of subarray maximum-likelihood filter outputs	$ML\sum_{JK}(AI)_p$	IN	9.5	10.8	9.0	11.0
		OUT	6.5	7.5	5.5	7.0
Phased sum of subarray center seismometer outputs	$P\sum_{AI}(10)_p$	IN	10.0	10.0	11.5	11.5
		OUT	11.0	11.0	11.5	11.5
Maximum-Likelihood filtered subarray center seismometer outputs	$ML\sum_{AI}(10)_p$	IN	9.5	12.5	14.5	14.8
		OUT	6.0	7.5	9.5	9.4
Phased sum of subarray phased sums	$P\sum_{AI}\left[P\sum_{JK}(AI)_p\right]$	IN	12.5	12.5	18.0	18.0
		OUT	15.0	15.0	16.5	16.5
Maximum-Likelihood filtered subarray phased sums	$ML\sum_{AI}\left[P\sum_{JK}(AI)_p\right]$	IN	16.0	14.8	20.0	20.8
		OUT	13.5	11.5	14.0	15.0
Phased sum of maximum-likelihood filtered subarray outputs	$P\sum_{AI}\left[ML\sum_{JK}(AI)_p\right]$	IN	17.0	20.6	22.0	21.8
		OUT	18.5	18.9	18.[illegible]	18.4
Maximum-Likelihood filtered subarray maximum-likelihood filter outputs	$ML\sum_{AI}\left[ML\sum_{JK}(AI)_p\right]$	IN	18.0	20.5	23.0	22.5
		OUT	15.0	14.8	16.5	16.2

Table 4. Summary of Signal/Noise Ratio Improvement
(decibels above bandpass-filtered single seismometer)

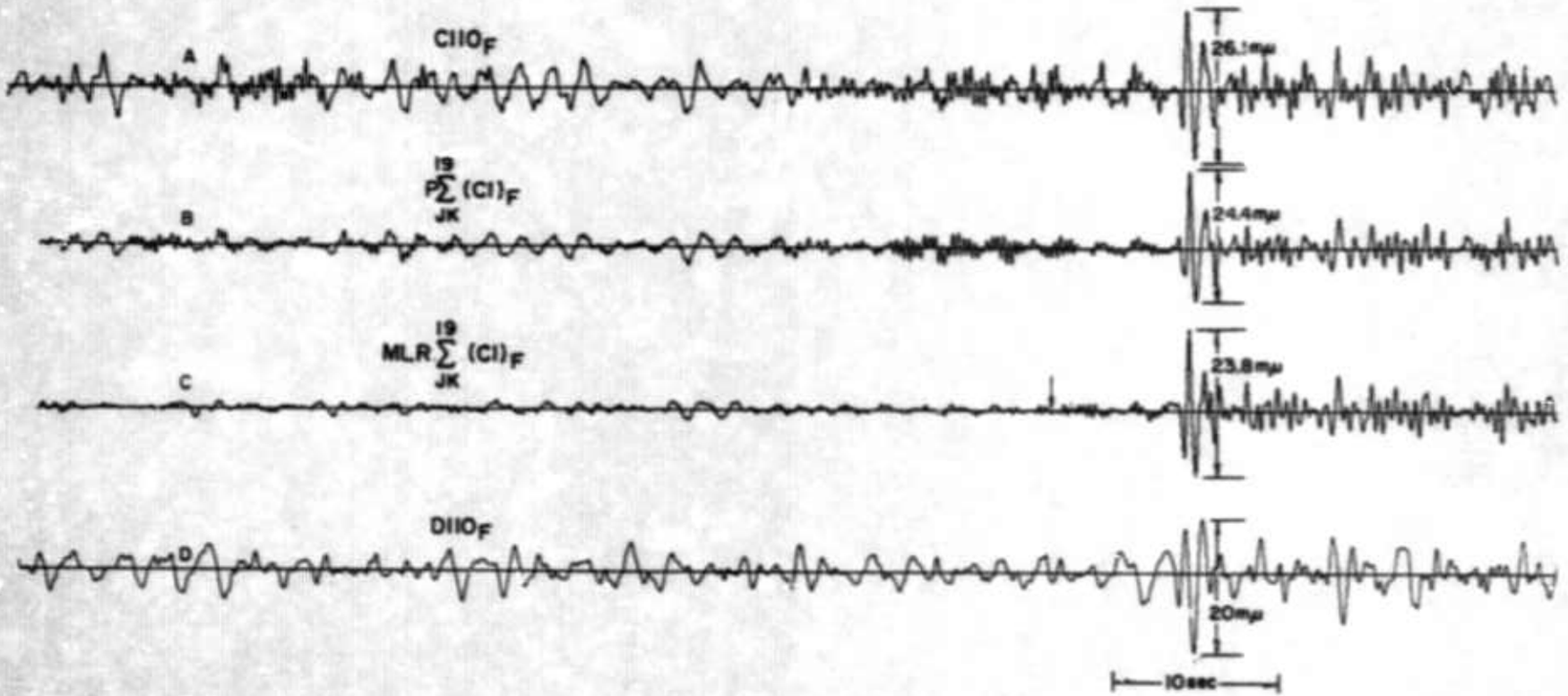

Figure 9. 10 November 1965 Processed Traces (Prefiltered Data)

(A) Output of Center Seismometer, Subarray C1;
(B) Phased Sum of Subarray C1;
(C) Realizable Maximum-Likelihood Filter Output, Subarray C1;
(D) Output of Center Seismometer, Subarray D1.

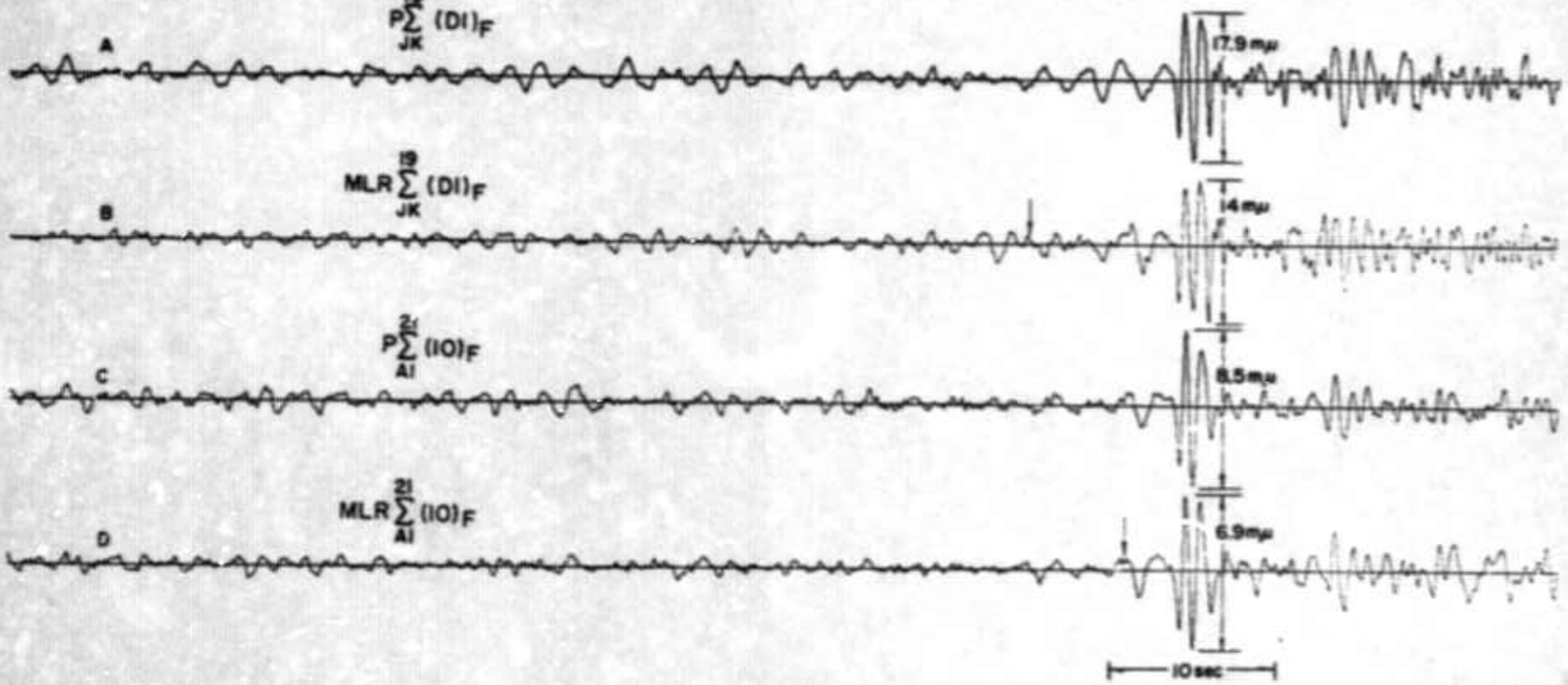

Figure 10. 10 November 1965 Processed Traces (Prefiltered Data)

(A) Phased Sum of Subarray DI;
(B) Realizable Maximum-Likelihood Filter Output, Subarray DI;
(C) Phased Sum of 21 Subarray Center Seismometer Outputs;
(D) Realizable Maximum-Likelihood Filter Output Based on 21 Subarray Center Seismometer Outputs.

3. Maximum-Likelihood Filtering of LASA Noise Seismograms

The purpose of this study was to determine the effectiveness of realizable (MLR) and symmetrical (MLS) maximum-likelihood filters, compared with direct summation, in reducing the rms noise level inside of, immediately adjacent to, and several minutes away from the fitting interval; moreover, we were interested in the comparative behavior of maximum-likelihood filters computed from variable lengths of both raw and bandpass filtered inputs.

Realizable and symmetrical maximum-likelihood filters, two seconds long and based on fitting intervals consisting of 75, 150, 180, and 300 seconds of both raw and bandpass filtered inputs, were computed using seismic noise recorded during the night of 25 March 1966, by nineteen sensors in the A0 subarray at the Montana LASA.

Results showed that, excluding the realizable filter based on raw data, the effect of maximum-likelihood filtering noise samples lying outside the fitting interval is to produce noise levels 1 to 3 db lower than the corresponding direct sum of bandpass filtered data. Moreover, the filters lower the rms noise level slightly more than the square root of N in the data sample lying outside of, but immediately adjacent to, the fitting interval, but fail to yield the square root of N noise reduction if applied to noise fields which are several minutes removed from the interval.

Depending upon the nature of the input data (raw or pre-filtered), the symmetrical filter is 1 to 5 db better than the corresponding realizable filter, but its output appears to be approximately 180 degrees out-of-phase with its realizable counterpart.

It was also found that the fitting interval is not a critical parameter in the design of maximum-likelihood filters for lengths equal to or greater than 150 seconds.

4. The Crosswise Sum Method for Maximum-Likelihood Filtering of LASA Seismograms

In previous maximum-likelihood studies of data from the Montana LASA, individual subarrays were processed and then these subarray outputs were combined to process all of LASA. It may be advantageous to phase and sum, across LASA, one output from each subarray (say, all those sensors having the same identification number -- e.g., the phased sum of all the 10's, the phased sum of all the 21's, etc.) and then to use the resulting 25 traces as input to a maximum-likelihood filtering process.

Adding together samples of noise from all subarrays by combining outputs from corresponding elements from each subarray, would produce 25 traces with more noise correlation than the 21 subarray outputs themselves. Moreover, adding together samples from each subarray would produce 25 signals of similar waveform. Finally, because only one maximum likelihood filter would have to be designed, the crosswise sum method would save a considerable amount of machine time.

Accordingly, it was decided to process the two events reported earlier (10 November 1965 and 25 November 1965) by this crosswise sum method, and to make the necessary comparisons between results.

Results showed that the crosswise sum method produces results within approximately 2 db of the maximum gain indicated by the previous analysis. However, whereas in previous results the subarray maximum-likelihood filters produced gains of 0 to 1.5 db over the corresponding phased sums for noise measured outside the fitting interval, the crosswise sum maximum-likelihood filter seems to lose from 1 to 3 db relative to this corresponding phased sum. This is in accord with previous results for maximum-likelihood filters used to combine subarray outputs, which lost from 1.5 to 4 db relative to their corresponding phased sums of noise measured outside the fitting interval.

The signals on the traces input to the crosswise sum method are remarkably similar in waveform, and they are equal in amplitude. This is reflected in the preservation of signal amplitude through the maximum-likelihood filter. The symmetrical filter does not introduce a precursor. In both realizable and symmetrical cases, the signal appears as it does on the corresponding phased sum.

For each of the inputs to the crosswise sum maximum-likelihood filters, a theoretical gain of 13.2 db is predicted if the noise is completely uncorrelated, because here N = 21 and the square root of N improvement is 13.2 db. For the 25 November event, this is achieved for the average of the input traces. For the 10 November event, it is lower by 3 db.

5. Relative Travel-Time Anomalies at LASA and the Location of Epicenters Using "SHIFT"

The entire set of 180 events selected for the measurement of anomalies were recorded with good signal-to-noise ratios on the films. If any of the subarrays recorded signals were difficult

to read, they were eliminated from all computations. However, if the signals were strong, and if confidence was placed in the readings, the calculated anomalies were kept regardless of their agreement with other results.

Whenever possible, the readings were the arrival times of first motion of P. However, the number of events recorded with sufficiently distinct onsets was small and the data accumulated too slowly. Because all of the instruments at LASA are the same, first peaks or troughs of a number of events were also read to increase the rate of accumulation. When the anomalies obtained by using first motions were closely compared with those obtained using first extrema, no consistent differences were apparent. This result implies that any differences in the phase response characteristics between the subarray center instruments are within the precision of the measurements.

The event locations, necessary for computing expected travel-times, were those listed on the "Preliminary Determination of Epicenters" (PDE) cards supplied by the U.S. Department of Commerce, Environmental Science Services Administration (U.S. Coast and Geodetic Survey). These locations are routinely reported to 0.1° latitude and longitude. Merely for convenience the center subarray of LASA, A0, was selected as the reference station for all calculations.

In general, travel-time anomalies are dependent upon both event direction and distance. It is necessary to measure anomalies from a large number of events occurring in all regions of possible interest. More consistency is obtained if the results are then separated into event direction of approach

and plotted as a function of distance. It was seen that if the anomalies were plotted as a function of direction with no regard for distance, the results would be quite scattered. Similarly, if they were plotted only as a function of distance, the same large scatter would result. Both distance and direction are important and must be separated.

Although the anomalies are plotted by direction and distance, they are more precisely plotted by region. The term "region" as used here is defined as that limited area from which all events will yield the same anomalies.

The travel-time anomalies at LASA were seen to be large, even for stations quite near the reference, A0. For example, subarray D4 recorded signals 0.7 seconds late with respect to A0 for events southeast of LASA at a distance of about 8000 km. The physical causes of the anomalies are presently unknown, but it is probable that differing geological conditions in the crust and the upper mantle beneath each of the subarrays is responsible.

The results showed scatter within some regions much larger than would be expected from reading errors alone. The only reasonable cause of the observed anomaly variation within a region is an error in the assumed location of the event. In this study, all of the epicenters and depths used were those listed on the PDE cards. These locations are meant to be preliminary, and they are accepted to be as such. The reported latitudes and longitudes "have an estimated accuracy of a few tenths of a degree and 25 km in depth" (U.S.C.&.G.S first PDE card). An error of a "few tenths of a degree" can easily explain most of the anomaly variations.

The next logical question is: Can the original epicenters within a region be shifted by some acceptable distance such that the observed scatter about a mean is reduced? To aid in answering this, a computer program, SHIFT, was written which reduces the anomaly errors by shifting the locations. An example of the anomaly improvement at just one of the 20 subarrays using Kurile Islands events is shown in Figure 11, where the results in the upper part indicate the computed anomalies from the original epicenters and the results in the lower part those after the shifts.

6. LASA Travel-Time Data at the SDL

In connection with its many LASA analyses, the SDL is accumulating relative travel-times at the Montana Large Aperture Seismic Array (LASA) with a view towards computing travel-time anomalies at the 21 subarrays. In the belief that these raw data are in demand and may be of use to the seismic community in general, a report was issued which contains LASA travel-time data for approximately 400 events, as read from LASA films.

Figure 12 shows the type of data which has been computed and the following numbered explanation, corresponding to the circled number on the figure, describes the method of presentation:

1. Arbitrary region name
2. Direction of approach
3. Distance range for events included in region
4. Azimuth range for events included in region
5. Event date and name
6. PDE latitude
7. PDE longitude
8. PDE depth
9. PDE origin time
10. Arrival time in seconds (an arrival time of "0" indicated no reading made at that subarray)
11. Arrival time, hour, and minute at LASA

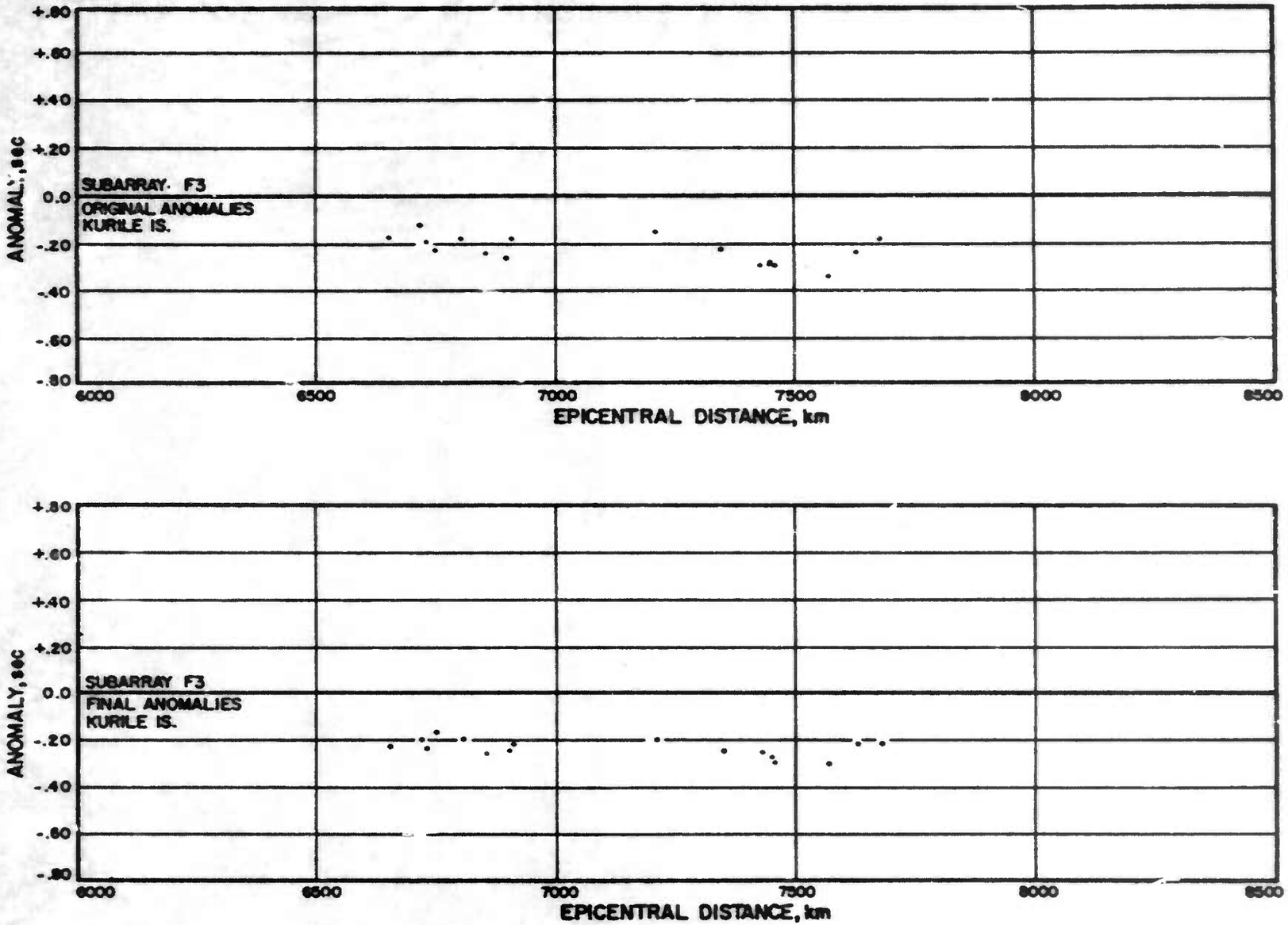

Figure 11. Computed Anomalies Before and After Shifts, Subarray F3

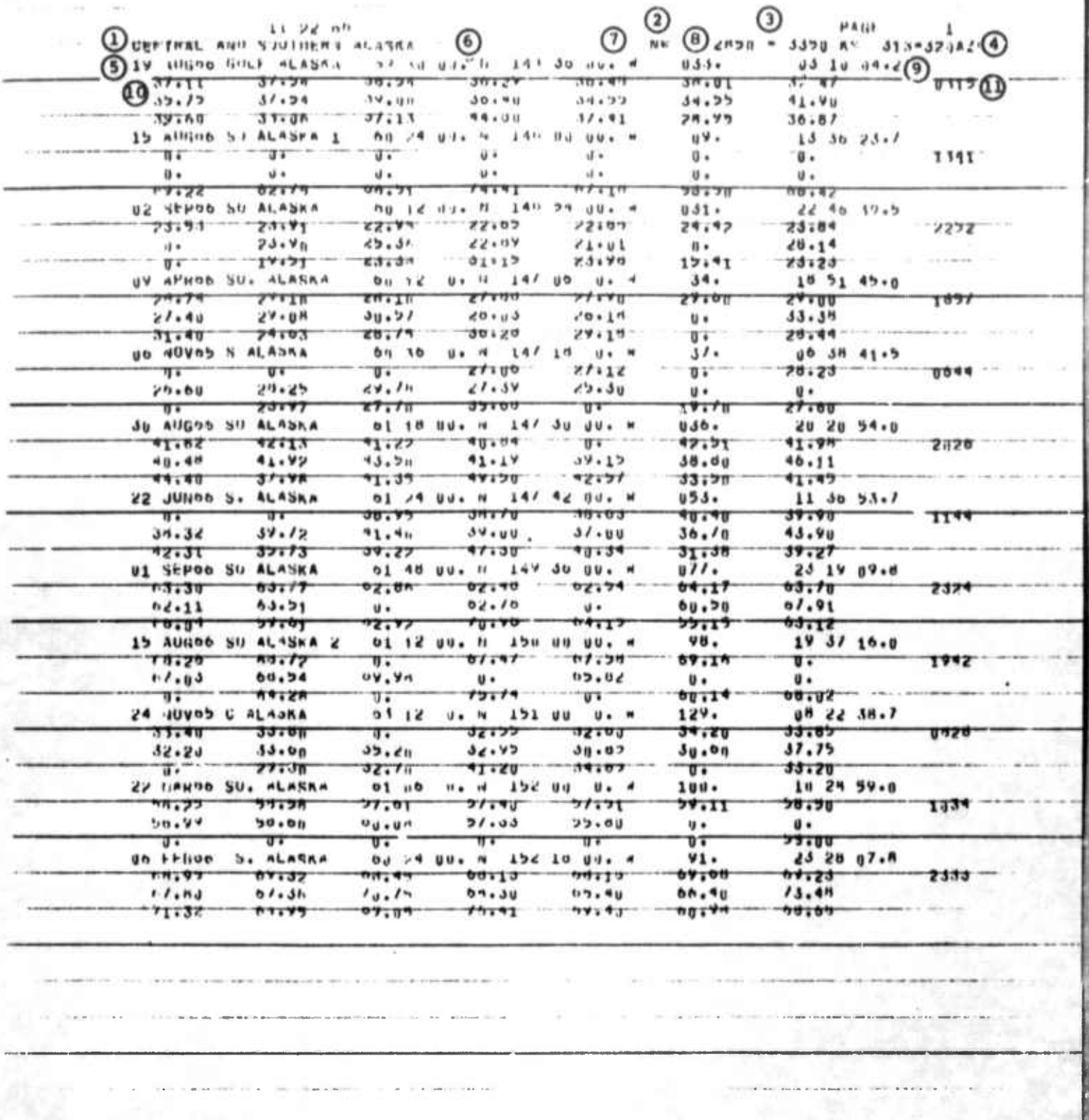

Figure 12. Type of LASA Travel-Time Data Computed by the SDL

7. LASA Travel-Time Anomalies for Various Epicentral Regions

Approximately 350 teleseisms were used to compute P-wave travel-time anomalies, relative to subarray A0, at all subarray center instruments at the Large Aperture Seismic Array (LASA) in Montana. As the anomalies were dependent upon event distance and azimuth (hence, epicentral region), the results were separated into groups such that the subarrays had anomalies which were consistent within each defined region. The total number of regions was 39.

The results were arranged first by general direction (beginning with the northwest and going clockwise) and second by increasing epicentral distance within each directional group, as follows:

Direction	No. of Regions	Distance Range, km	Azimuth Range (Degrees)	No. of Events
Northwest	14	2000-10800	292-320	155
North	2	9300-10900	349-003	14
North-northeast	1	9300- 9900	018-025	3
Northeast	2	4800- 9800	032-054	12
East	1	6000- 6100	070-071	2
East-southeast	2	4800- 5800	112-120	6
Southeast	9	3400- 9800	133-165	90
South	3	2800- 9100	181-188	12
West-southwest	2	9500-10800	239-246	34
Undefined	3			
Atlantic Ridge		5000- 9900	083-101	6
Continental U.S.		800- 1700	124-280	5
Miscellaneous		5300-10000	328-178	6

The following observations are made concerning travel-time anomalies at LASA:

1. The anomaly variations between regions measured at a single subarray are as high as 1.43 seconds. For example, subarray F4 has an average anomaly of +0.65 sec ($N = 8, \sigma_{F4} = 0.06$) for the Eastern Mexico region and an average of -0.78 sec ($N = 17, \sigma_{F4} = 0.05$) for the Fiji Islands region.

2. Subarrays which are quite near the reference subarray A0 can have unusually large anomalies. For example, subarray D4 is located 30.75 km from A0 (center instrument to center instrument) and has an anomaly relative to A0 of +0.71 sec ($N = 12, \sigma_{D4} = 0.06$) for the Peru-Bolivia region.

3. The center instrument at subarray B2 is only 7.50 km from the center at A0, but it has an anomaly of -0.26 sec ($N = 11, \sigma_{B2} = 0.07$) for the Fiji Islands region. This result suggests that the time anomalies <u>within one subarray</u> (7 km diameter) may vary from element to element perhaps as much as 0.30 sec. Signals within a subarray could be significantly misaligned if such large anomalies existed.

4. The anomalies are not slowly varying functions of either distance or azimuth. For example, subarray E1 has an anomaly of +0.78 sec ($N = 12, \sigma_{E1} = 0.06$) computed from events approaching from a southeasterly direction at 7700 km distance (Peru-Bolivia region), but at 9300 km (Central Chile-Argentina Border region), whereas for events bearing about 182° at the same distance (South and West of Easter Island) the anomaly is -0.57 sec ($N = 6, \sigma_{F3} = 0.09$). Hence the anomaly at E1 changes by 0.53 sec in a distance of 1600 km, and at F3 it changes by 0.68 sec in 38° of azimuth.

5. The maximum anomaly range observed at LASA is 1.72 sec; average anomaly at subarray E1 is +0.87 sec for events occurring in the North Colombia region; average anomaly at subarray F3 is -0.85 sec for events from the North Atlantic region.

6. The maximum anomaly range for one particular region (North Atlantic) is 1.18 sec, where the F3 anomaly is -0.85 sec and the F1 anomaly is +0.33 sec.

7. In general, the subarray anomalies computed for a region are consistent within the precision of the measurements. There are, however, discrepancies. For example, events occurring in the North Colombia region yield anomalies which differ more than expected from one event to another, and the subarray and event standard deviations (σ_i and σ_k respectively) are much larger than those computed for other regions. The probable reason for these discrepancies is epicenter mislocation; i.e., these regions may not have adequate seismic control such that spurious locations result.

8. It is estimated that the 36 regions (plus 3 undefined) given in this report yield adequate anomaly information for about 20% of all possible regions and for about 90% of all earthquake regions within 105° of LASA.

C. Teleseismic Signal Measurements at Vertical Arrays

A vertical array records simultaneously on several transducers stacked in a deepwell 3 km or more in depth. The purpose of this study was to investigate the possibility of reducing near surface reverberations by stacking procedures similar to those used in reflection seismology. By reciprocity, the same algorithms developed for stacked sources can be applied to stacked receivers by reversing the sign of the reflection coefficients.

The two deghosting techniques applied are described as follows:

1. When a surface or near surface trace is available, the deghosted trace can be constructed by simply shifting the surface trace by K, multiplying a $\frac{1}{2}\alpha$, and subtracting this resultant from either the deepwell trace (phased vertical array) or the deepwell trace shifted by K/2 (non-phased vertical array).

2. It would seem more plausible to develop a deghosting process that removes the echo without the use of a surface seismogram, a practical technique that would figuratively push the ghost off the end of the deepwell trace.

Given the reflection coefficient α, and the deepwell trace $y_{i,1}$ the phased deghosted trace is formed as follows: First a new trace $Z_{i,1}$ is defined to be

$$Z_{i,1} = Y_{i,1} - X_{(i - NT_1)} \cdot \alpha_1,$$

where NT_1 is equal to the product of the sampling rate and the echo time delay (K). This above equation simply shifts and inverts the ghost to a point NT_1 farther down the seismic record than it originally was. This iterative process is continued until the ghost reflection is pushed off the seismic record.

The individual deghosted traces from the vertical array are then stacked by summing. The signals should now reinforce since after deghosting they tend to agree in waveform and arrival time. The noise background and oscillations created on individual channels by the deghosting process will decrease relative to the signal upon summation.

In addition to the linear summation, a correlation trace is formed which emphasizes the in-phase component on all n channels in the vertical array traces. The correlation trace is formed by first computing a running zero lag correlation, $y_2(t)$, between the first two traces, $x_1(t)$ and $x_2(t)$ in the vertical array.

$$y_2(t) = \frac{1}{2T} \int_{t-T}^{t+T} x_1(u)\ x_2(u)\ du$$

Then the subsequent traces in the vertical array are correlated in a similar way with the correlation trace.

$$y_3(t) = \frac{1}{2T} \int_{t-T}^{t+T} y_2(u)\ x_3(u)\ du$$

$$\vdots$$

$$y_k(t) = \frac{1}{2T} \int_{t-T}^{t+T} y_{k-1}(u)\ x_k(u)\ du$$

For k traces in the vertical array, $y_k(t)$ represents the final correlation trace which is displayed.

Figure 13 shows the original recordings for an Aleutian earthquake recorded at the AP-OK vertical array. The sum trace and the correlation trace are computed with no deghosting applied to the individual traces.

Figure 14 shows this same event with the individual traces deghosted by method I. Figure 15 shows this same event with the individual traces deghosted by method II.

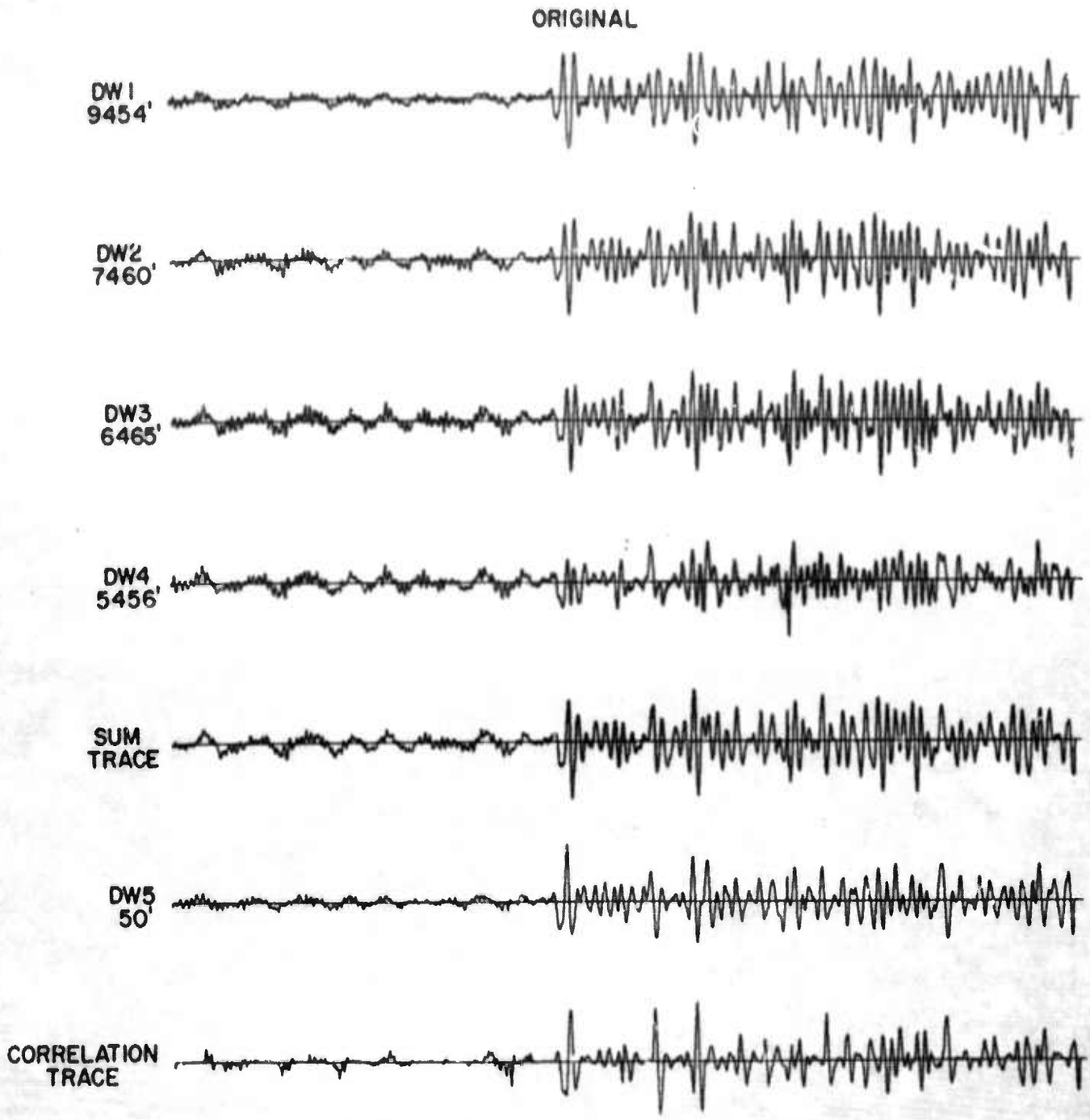

Figure 13. Vertical Component Vertical Array Measurements -- Aleutians, USCGS Focus 67 km, Magnitude 5.2, Date 6/17/65, Time 19:05:9.1

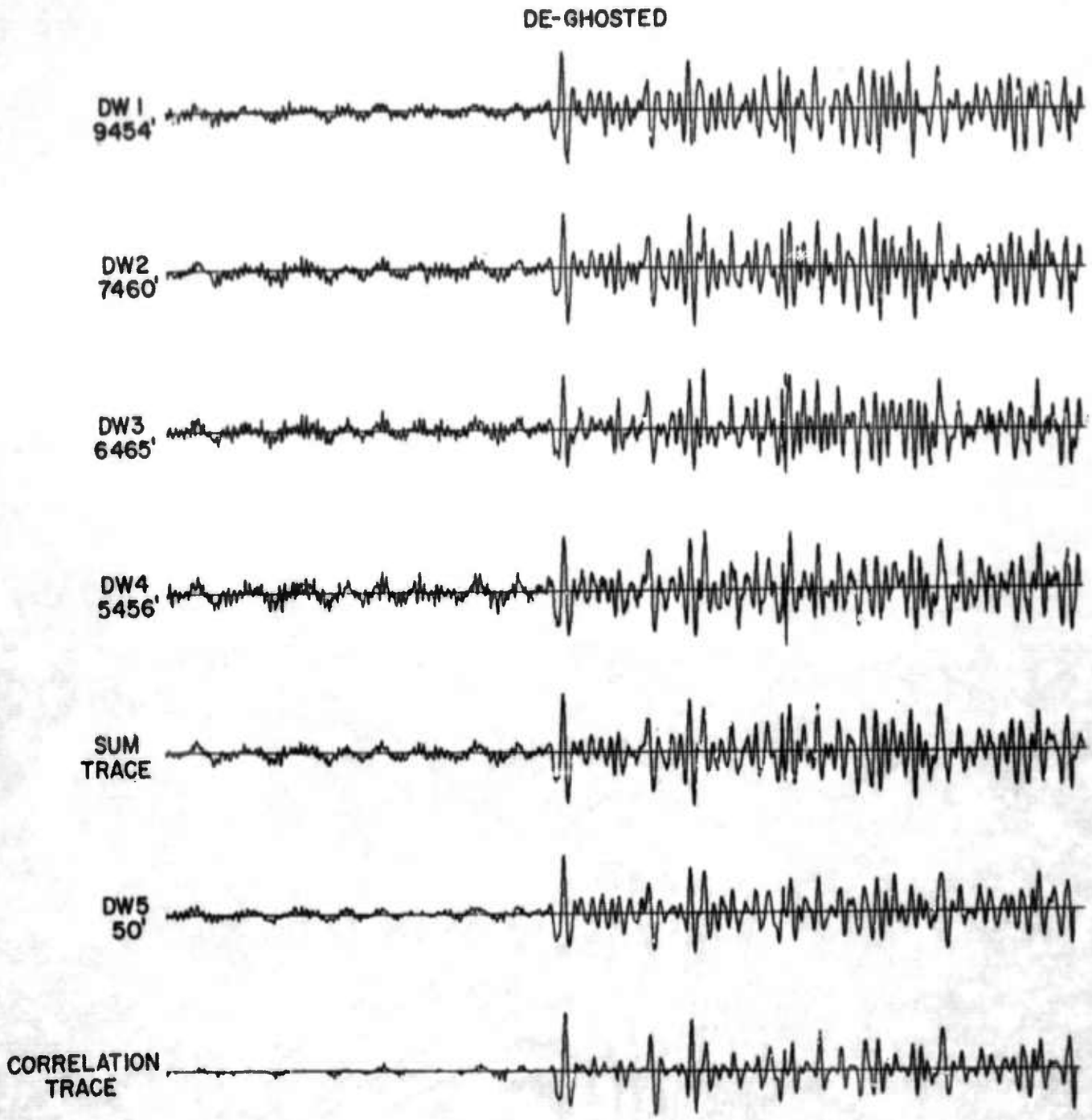

Figure 14. Deghosted Vertical Array Measurements, Method I

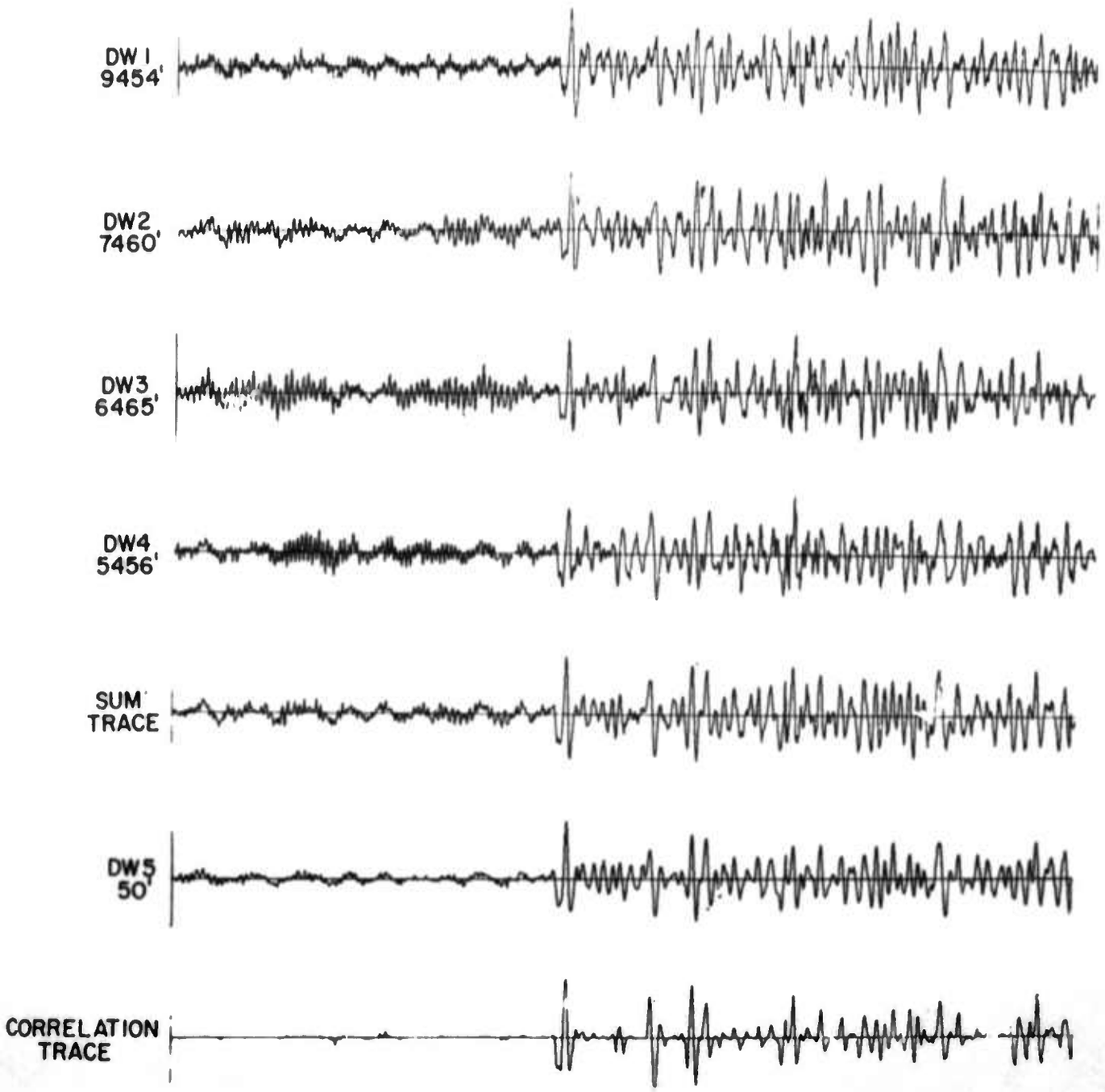

Figure 15. Deghosted Vertical Array Measurements, Method II
(Reflection Coefficient 0.7)

Results show that vertical array processing, based on previous experience with stacked sources, reduces the reverberations and complexity of the coda caused by near surface reverberations at the receiver. Both deghosting methods performed adequately. The correlation trace for the inverse operation had a slightly cleaner coda and this method has the advantage of not requiring a quiet surface trace and exact control of instrument gain. The correlation traces used for detecting the upgoing P-pulses impose the strongest possible requirement that the signal be fixed jointly on all channels.

D. Rayleigh Wave Rejection by Optimum Filtering of Vertical Arrays

Vertical arrays offer some intriguing advantages over other arrangement of seismometers. Assuming the noise to be composed of Rayleigh waves and perhaps some mantle-propagating P-waves, and assuming the signals to be teleseismic P-waves, the noise and signals will be recorded by a vertical array with some rather special characteristics.

We can imagine that each mode of Rayleigh wave noise possesses a random character common to noise functions in general. However, for each Rayleigh wave mode the response versus depth and frequency relative to its response on the surface is predictable. Because the relative depth variation is predictable, the vertical array can be summed to cancel the Rayleigh modes. In contrast, the noise over a surface array is more unpredictable and more variable and, therefore, more difficult to cancel by array summation.

The purpose of this analysis was to test the theory of applying maximum likelihood filters in vertical arrays in order to provide undistorted estimates of the signal or the various Rayleigh modes with the other modes cancelled out.

A vertical array of five vertical component seismometers which existed in a well at the Uinta Basin Seismological Observatory (UBSO) was used for testing this theory. The Rayleigh dispersion curves for this well indicated that the fundamental, first, and second higher Rayleigh modes would all be supported over the signal frequency range of 0.5 to 2.0 cps. Since we wanted more recording levels than modes, these three Rayleigh modes plus a signal mode were the only ones considered to exist in our synthetic modeling of this well.

The optimum filter, G, solutions are the least squares inverse to the Rayleigh signal filter matrix, H. Thus, the matrix products of G and H gives the identity matrix. In our test model we assumed the signal existed with the same size and amplitude on all traces. We derived optimum filter solutions only over the signal range of 0.5 to 2.0 cps. For the frequencies below 0.5, we smoothed the frequency responses to zero according to a sinusoidal gain function for both the H and G frequency responses. We smoothed these responses to zero in a similar way over the range from 2 to 5 cps. Also, the orthogonality of our optimum filter solutions were maintained over the entire frequency range.

In order to demonstrate that our optimum filter solutions were correct, we created some synthetic data which conformed to the well log analysis we assumed for the UBO well. These Rayleigh mode traces were combined with an artificial signal to produce a mixture of signal and Rayleigh modes expected from this well.

Figure 16 shows the data from the five levels of the vertical array if the signal plus the fundamental and the first and second higher Rayleigh modes have been added into the vertical array data. The outputs for the signal and the three Rayleigh modes are reproduced in size and waveform within a few percent of the expected results. The signal trace shows better than a 20 db improvement over the best signal/noise ratio available in the vertical array. Thus, the optimum filters perform as expected when the data properties match the dispersion analysis of the well log.

These solutions were then applied to actual noise data recorded at the vertical array. All of the optimum filters used required inputs from all five levels of noise data. However, we could ask for estimates of only a single mode or for estimates of several modes in the filter outputs. The more modes a set of filters estimate, the larger the filter gains will be. It follows that any errors resulting from incorrect dispersion analysis, instrument calibrations, or non-parallel layering will be amplified much more in these filters with fewer degrees of freedom. Results showed that the signal estimate outputs gave progressively increasing low frequency errors on the estimates of all modes as the degrees of freedom decreased (i.e., as the number of outputs increased).

It was concluded that our optimum filter solutions have the following features:

1. These filters are indeed orthogonal and separate the noise and signal modes as planned.

2. These optimum filters extend for 400 points in time since the frequency interval chosen was 0.5 cps.

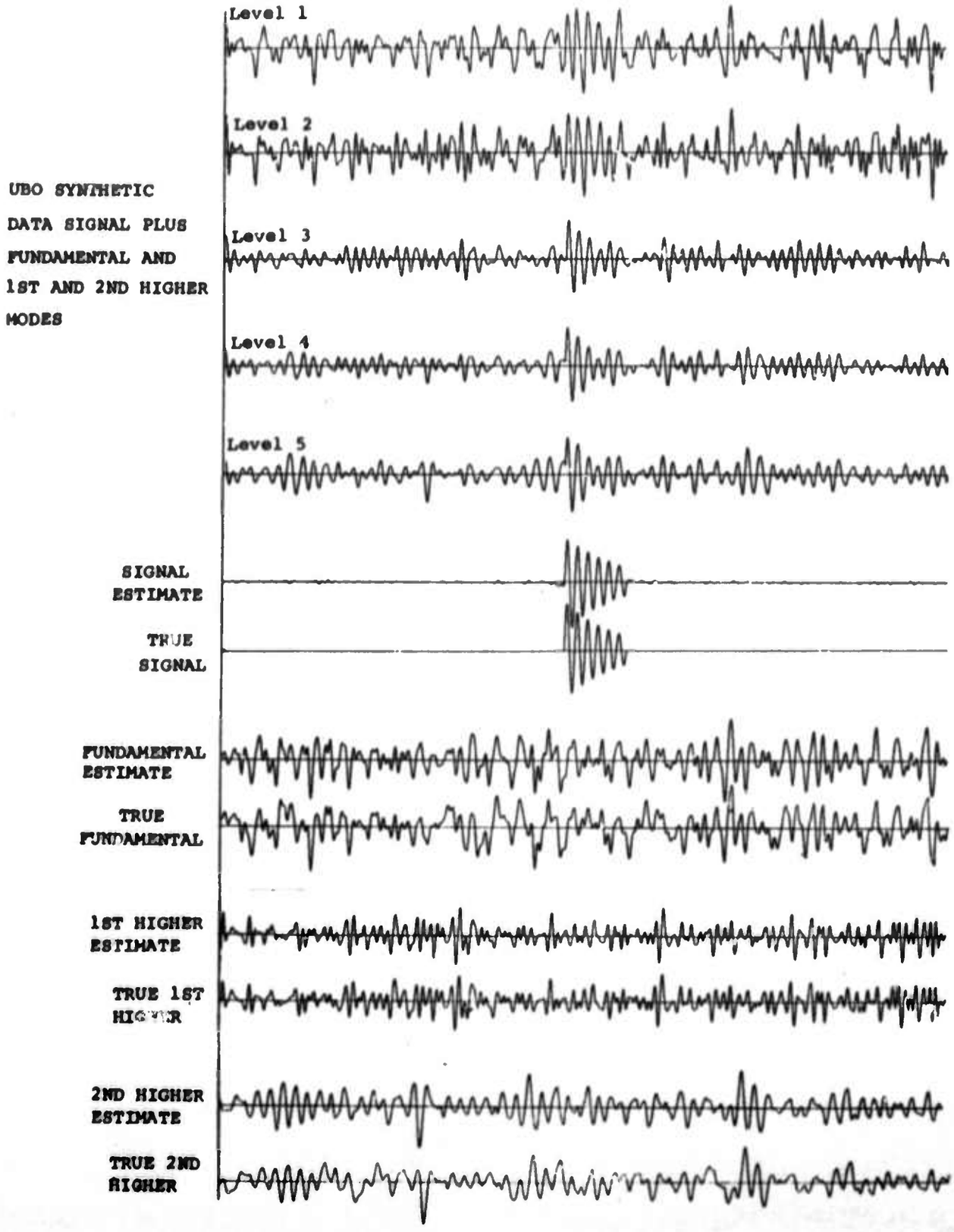

Figure 16. Optimum Filters Estimating Four Modes (The Signal and Three Rayleigh Modes) from Synthetic Data with all Four Modes Present.

3. The gain on the synthetic examples was greater than 20 db with solutions restricted to the 0.5 - 2.0 frequency range. More resolution in frequency could increase this figure.

4. The optimum filters are zero phase shift filters. Therefore, they are algebraically additive.

5. The optimum filters become larger in gains (both positive and negative) as degrees of freedom decrease.

6. The optimum filters become larger in gains (both positive and negative) as the aperture of array goes down. Thus for low frequencies the solutions tend to become unstable.

7. Extra modes not considered and errors in assumptions cause errors in the output. Errors in assumptions can include an incorrect well log, non-parallel layering in surrounding medium, and incorrect calibrations of seismometers.

8. Extra degrees of freedom are needed to cut gains of optimum filters and make optimum solutions more tolerant of errors.

9. Extra degrees of freedom are best obtained by increasing the number of seismometers in the vertical array.

10. More stable solutions (i.e., optimum filters with lower gain) will be obtained from the deeper vertical arrays which have the seismometers distributed rather uniformly throughout the array.

E. Detection of Surface Waves at Teleseismic Distances

We present here a matched filter approach for distinguishing weak teleseismic surface wave signals from background noise. The method discriminates against events not located in a particular source region of interest and provides estimates of magnitude and radiation pattern, when a number of recording stations are available.

Basically the matched filter approach amounts simply to searching a record x(t) for a known waveform y(t). In particular, it is assumed that $x(t) = ay(t) + n(t)$ where $\underline{a}$ is a constant and n(t) is a random noise process. If no further assumptions are made with regard to the nature of the noise process, one can determine the least-squares estimate of $\underline{a}$ which minimizes $J(a,\tau) = \sum_t \left[x(t+\tau) - a\, y(t) \right]^2$ where the summation is over the length of y(t). In the test series x, which is of longer duration than y, the lag τ indicates at what point in x the comparison is begun. The value of $\underline{a}$ obtained by setting $\frac{\partial J}{\partial a} = 0$ is

$$\hat{a} = \sum_t x(t+\tau)\, y(t) / \sum_t y^2(t) \qquad (1)$$

Thus, the matched filter in this case is simply the waveform y(t) and the matched filter output at lag τ is

$$\sum x(t+\tau)\, y(t) = Cxy\,(\tau) \qquad (2)$$

The coherency at lag τ is given by

$$C(\tau) = \sum_t x(t+\tau)\, y(t) / \left[\sum_t x^2(t+\tau) \cdot \sum_t y^2(t) \right]^{\frac{1}{2}} \qquad (3)$$

It always is bounded by $-1 \leq C(\tau) \leq 1$. The maximum in the envelope of $C(\tau)$ occurs at the value of τ where x and y match best in the least-squares sense. The $C_{max}(\tau)$ is the correlation coefficient.

In the present application we have used this simple least squares approach. Estimates of $\underline{a}$, $C_{xy}(\tau)$, and $C(\tau)$ calculated in this way allow us to study test cases and unknown events with a minimum of assumptions.

The matched filter approach requies that one knows the desired or expected waveform in order to search effectively for that waveform in a noisy record. In order to obtain a suitable "expected" waveform and at the same time assure that propagation effects would be properly accounted for, we chose the surface wave from a larger event in the source region of interest as the filter y(t). Thus, no matter how complicated the paths of propagation are, the paths for other events in the same source region will be nearly coincident with those of the larger event which produced y(t), so the only major differences in recorded waveform will be source differences. This coincidence of travel path simply assures that the earth's transfer function is the same for all events occurring in that source region; it does not mean that dispersion during propagation to teleseismic distances is unimportant. To the contrary, it is this physical effect (dispersion) which is vital to the success of the technique, since it transforms the source pulse into an oscillatory signal which is of long duration. As the duration of the signal increases, random correlations of the signal with the noise become poorer, with the result that the "false alarm" level is reduced. From this standpoint the larger the epicentral distance the better the method should work, since the signal increases in duration, the larger the distance. However, the energy density of the signal is reduced due to dispersion and attenuation during propagation, so that the signal to noise ratio is reduced with increasing distance. Therefore, for a given transfer function and noise level, one would expect there to be an optimum observing distance for detecting events using the matched filter. But, because of the different noise levels among available stations and the

variety of propagation paths to these stations, it does not appear to be practical to determine these optimum observing distances experimentally. What we can estimate, however, is the minimum S/N at which the technique will detect observed or expected signal waveforms.

Because of dispersion and frequency-dependent attenuation with distance, the signal waveform will in general be different at each station and thus a different filter for each station and source region must be used. However, this presents no problem since a single large event in a given source region provides for each station a filter suitable for detecting other events located in that region, as well as the temporal pattern of arrival times at the stations. This pattern and the fact that the filters are different for each station can be used to advantage in discriminating against events outside the source region of interest, since one or more of the decision criteria listed earlier will not be satisfied; in particular, the correlation peak values will be degraded, and the arrival times of these peaks will not produce the appropriate pattern of arrival times at the observing stations.

When a small event has been detected by this method, then the question arises as to what details we can extract about the source. The estimates of $\hat{a}$ provide a convenient means of comparing the magnitude of the small event to that of the larger one, since $\hat{a}^2$ is an estimate of the ratio of the energy in the small event to that in y(t). Some care must be taken, however, if the reference event exhibits a strong radiation pattern which is different from that of the smaller event. In fact, the radiation pattern of the small event relative to the reference event can be obtained by plotting $\hat{a}/\sum_t y^2(t)$ vs. source-station azimuth.

Comparisons of $\hat{a}$ vs. distance along a given azimuth allow us to estimate roughly the excitation spectrum of the small event compared to the larger one, since the attenuation with distance is frequency-dependent, which implies that $\hat{a}$ should vary with distance in a way which reflects the shape of the spectrum of the small event compared with that of the reference event. Only if their spectra are identical in shape will $\hat{a}$ be invariant with distance. Since this attenuation factor is of the form $\exp\left[-g(\omega)\ \Delta\right]$, where $g(\omega)$ is an increasing function of frequency and Δ is epicentral distance, $\hat{a}$ will decrease with distance if the spectrum of the small event is peaked at a higher frequency than the reference event.

Thus potentially the matched filter method permits us to:

1. detect the surface waves from a source region of interest, while rejecting events outside the source region;

2. make magnitude estimates for small events relative to the reference event;

3. outline radiation patterns for small events;

4. estimate spectral shape relative to the reference event.

Figures 17, 18, and 19 show the results of adding the signal shown at the top (an actual oceanic Rayleigh wave train recorded at 4686 km distance) to the noise trace at a number of arrival times, with the indicated signal/noise, S/N, and using the signal as the matched filter. We define S/N as $\max_t y(t) / \mathrm{RMS}\left[n(t)\right]$. The number in parentheses is an alternate value of signal/noise (S/N) given by $\mathrm{RMS}\left[y(t)\right] / \mathrm{RMS}\left[n(t)\right]$. The values of $\alpha = \hat{a}$ are printed next to C_{xy} trace, and the correlation coefficients CC next to the C trace. The arrows indicate the

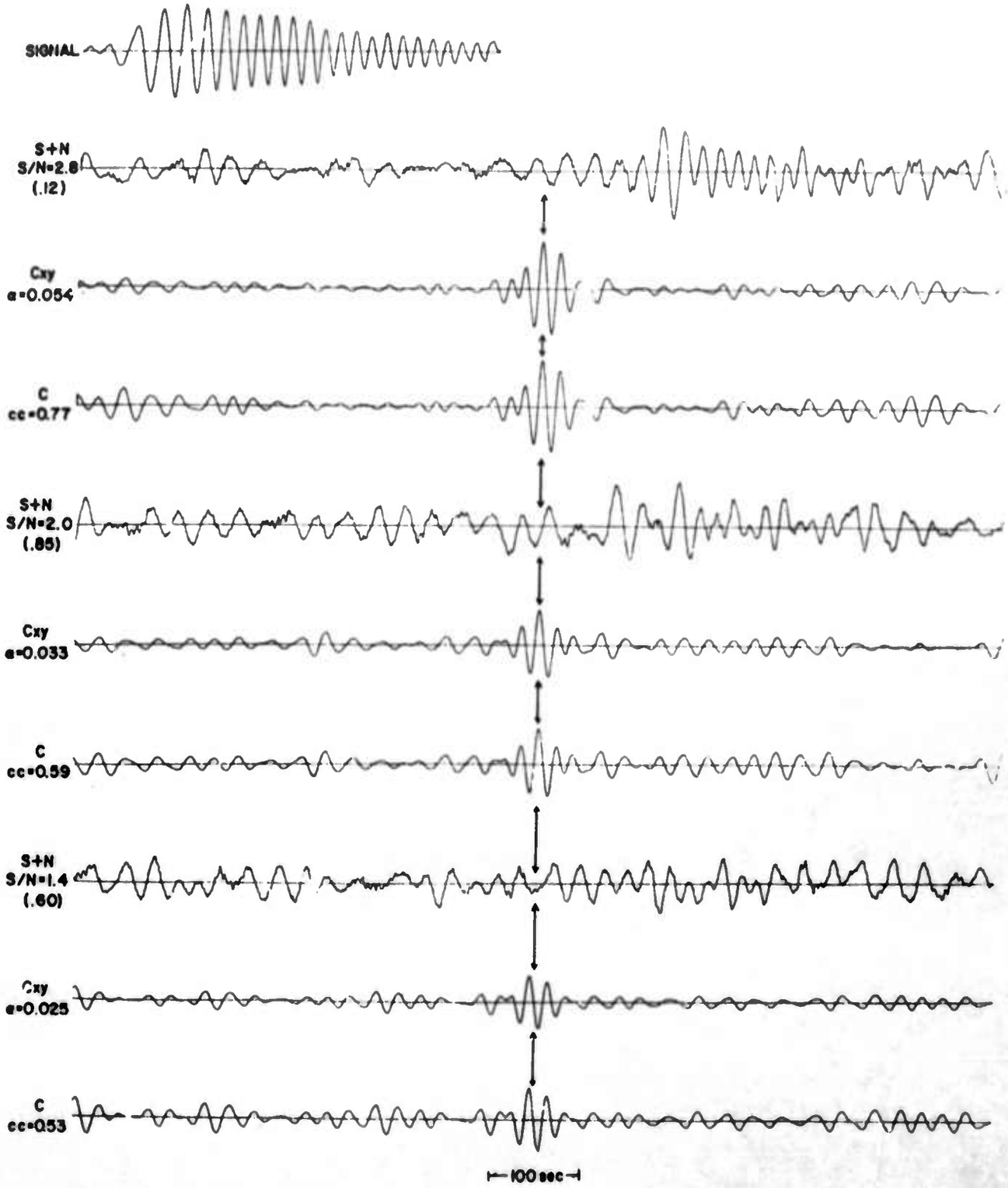

Figure 17. Real Signal Test Case

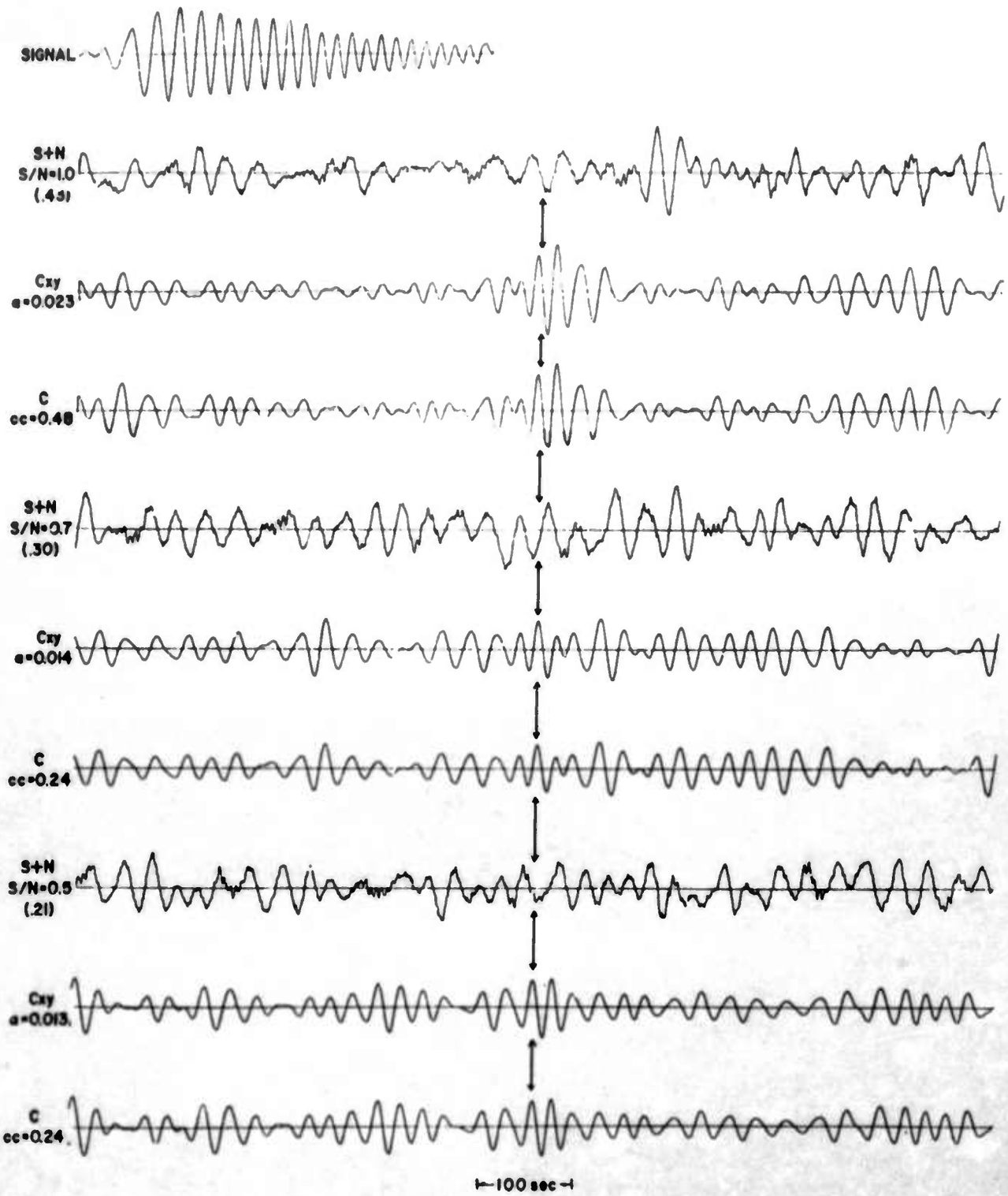

Figure 18. Real Signal Test Case

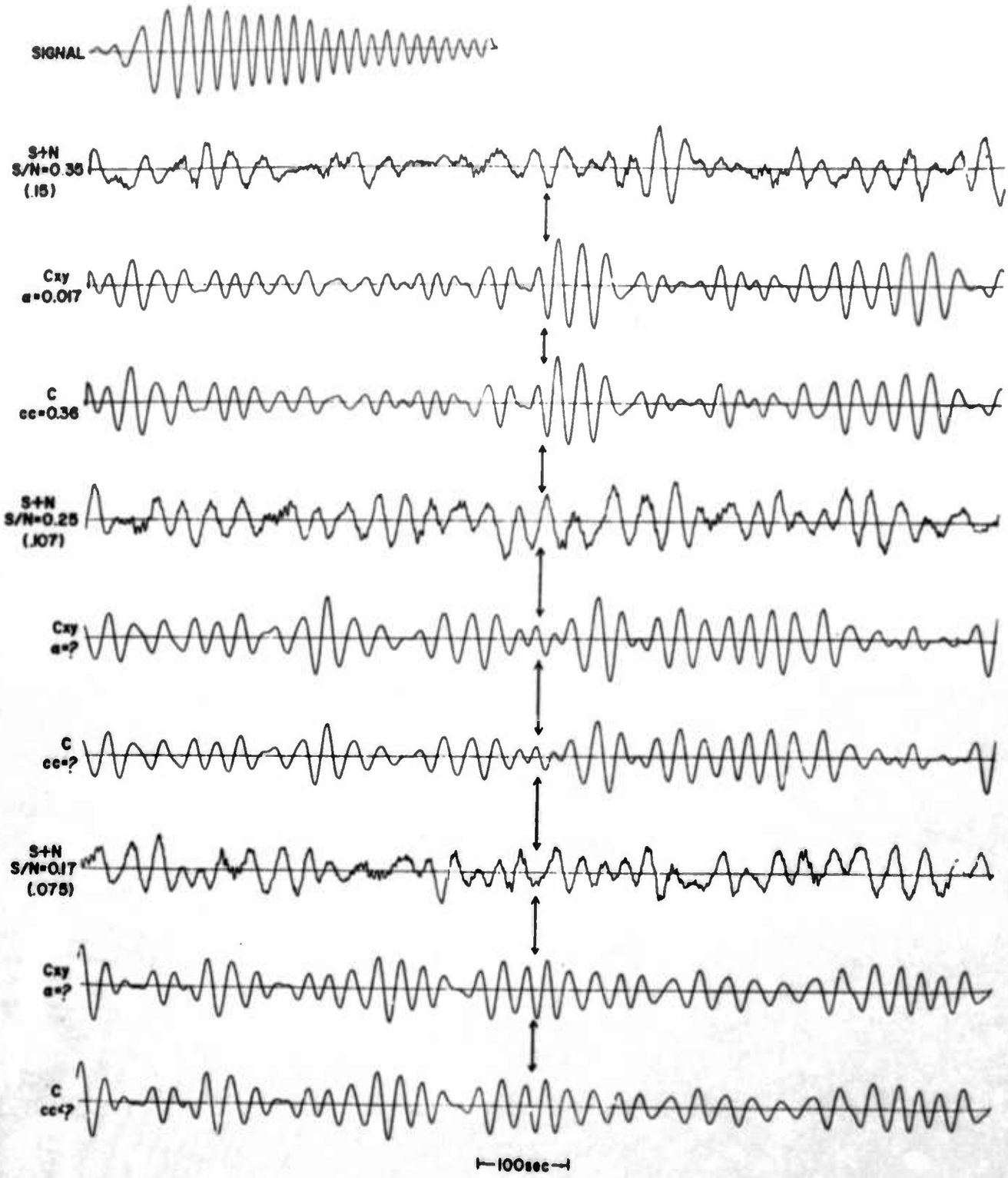

Figure 19. Real Signal Test Case

beginning time for the signal in each instance. In this example the signal is detected for S/N (S/N) as low as .35 (.15), where visual detection is impossible. Notice also that the $\hat{a}$'s are approximately in proportion to the S/N used as expected.

The reason the results appear to be as good or better for S/N = .35 compared to S/N = .5 is that the noise level was not uniform over the entire noise trace used to establish the RMS of the noise and the .35 signal was buried at a position where the actual noise level over the filter length was low relative to that where the .5 signal was buried.

On the basis of this investigation we conclude that:

1. In principle the matched filter approach can be used:

(a) to detect weak surface wave signals for signal to noise ratios as low as about 0.35;

(b) to make reliable relative magnitude estimates for S/N as low as .5;

(c) to determine radiation pattern relative to a reference event;

(d) to estimate the general shape of a small event's amplitude spectrum relative to that of the reference event.

2. The results presented for a number of actual events have demonstrated the practical applicability and usefulness of the matched filter approach in studying weak teleseismic surface waves.

3. The matched filter used in conjunction with the surface wave arrival time patterns appropriate for different source regions of interest allows one to discriminate against all but those events in the particular source region of interest.

F. Rectilinear Motion Detection

The studies of rectilinear motion detection are summarized in three sections. The first section defines the rectilinear motion detectors (REMODE) as non-linear filters based upon a correlation function between the vertical and radial components. The section described three variations of REMODE, exhibits the application of these filters to a suite of real seismograms from a Peruvian earthquake, and comments on the different behavior of the various types.

The second section describes some controlled tests of an actual seismic noise. This section shows for one particular REMODE operator that:

a. with input S/N ratios of 18 db or more the output signal size is not changed by REMODE and an average S/N ratio gain of 9 db results;

b. with input S/N ratios of 9 db to 18 db the output signal size may be changed by REMODE but a gain in S/N does occur;

c. with input S/N ratios less than 9 db the output signal size is changed by REMODE and a loss in S/N occurs.

The third section describes some controlled tests of an actual signal buried in a portion of polarized noise generated in the coda of a large earthquake. The study compares REMODE operators with various parameter settings in detecting a rectilinear signal in both shear and rectilinearly polarized noise. The results show how much more effective REMODE is in detecting rectilinearly polarized signals in shear noise than in rectilinearly polarized compressional noise.

1. Applications and Development of Polarization (REMODE) Filters

The polarization of particle motion in three-component seismic recordings is useful in the detection and identification of seismic phases. Operators have been described which use the behavior of the integrated product of two components to detect and identify phases. More general polarization filters, called REMODE, have been developed in which the filter functions are based on the correlation functions of two components.

If the original vertical and radial components z(t) and r(t) of a seismic recording are used as inputs to a REMODE process, the output traces z'(t) and r'(t) are the input traces filtered by the time-varying REMODE filter ϕ_t:

$$z'(t_o;\ WT) = \int_{t_o-T/2}^{t_o+T/2} \phi_{t_o,w}\,(t_o-t)\ z(t)\ dt$$

where $\phi_{t_o,w}$ is a filter function of length T, derived from the lagged cross-products between z(t) and r(t) in a time window of length W centered on t_o. The filter function varies as the window is moved along the seismogram.

The filter functions differ as follows. The filter functions for REMODE 2 are time-varying estimates of the real parts of cross-correlation functions.

The filter functions for REMODE 3 are the REMODE 2 filters normalized by time-varying estimates of average power in the input traces over the same time windows as the cross-correlation estimates.

The suffix A on filters 2 and 3 designates a modification to reject rectilinear motion due to shear phases moving in the same general direction as the compressional phases.

REMODE 5 is an experimental polarization filter of greater selectivity than REMODE 2 and 3. It is designed to attenuate noise having nearly rectilinear polarization, such as signal-generated noise, which is not effectively rejected by REMODE 2 or 3.

As a test, the filters were applied to short-period LRSM recordings of eight large teleseismic events, for which reliable focal depth estimates were available. The phases pP or sP could be identified with confidence from three of the events.

Phases which were clearly visible on the unfiltered seismograms were more clearly visible on the normalized filtered seismograms, and outstanding on the un-normalized filtered seismograms. All of the depth phases which were identifiable on the filtered seismograms were also identifiable on the unfiltered seismograms.

An example of the application of various REMODE filters is shown in Figure 20.

None of the filters effectively enhanced weak signals. A weak sP phase, on the unfiltered seismograms of the Peru event, was slightly more evident on the filtered records. A tentative sP phase for a Bonin Islands event, visible on several of the unfiltered records as a wavelet broader than the REMODE window, was degraded by un-normalized filtering and unimproved by normalized filtering.

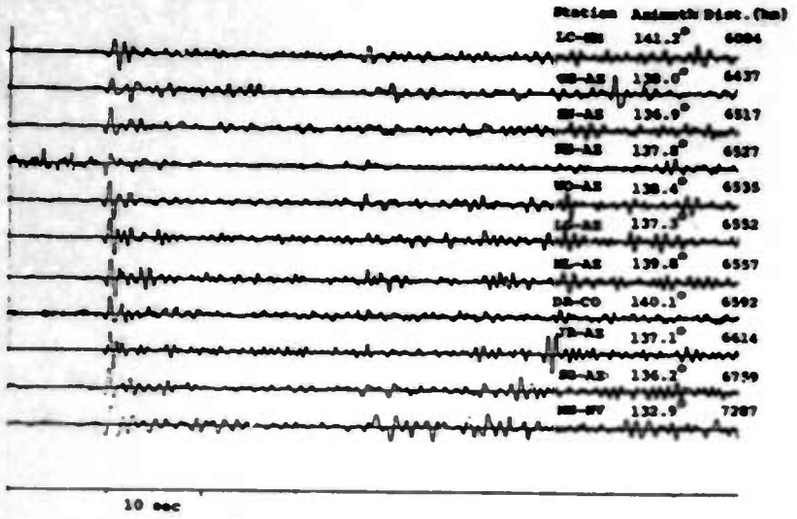

UNFILTERED Z-COMPONENT SEISMOGRAMS (ROTATED)

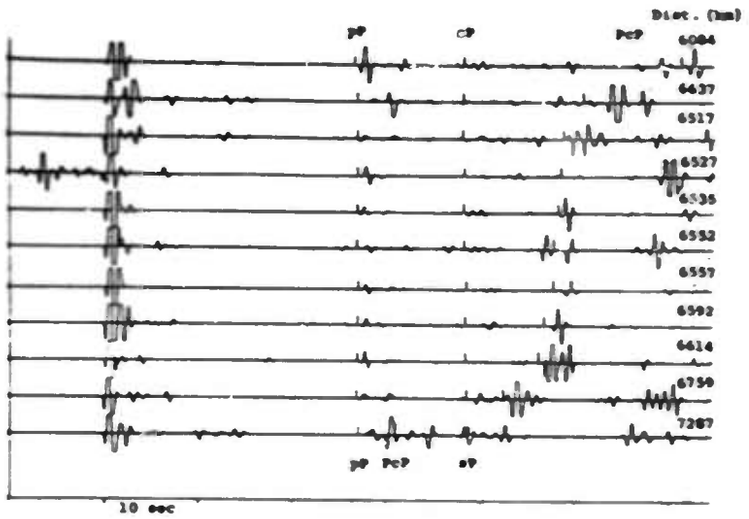

Z-COMPONENTS PROCESSED BY UN-NORMALIZED REMODE (2A)

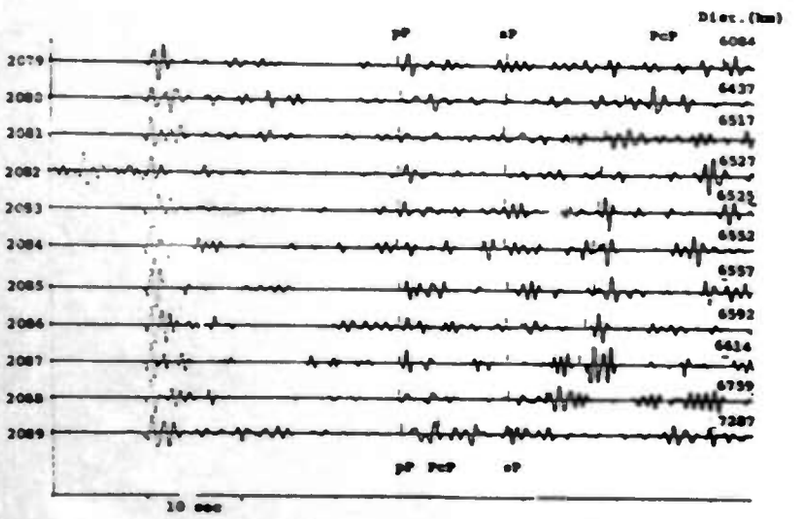

Z-COMPONENTS PROCESSED BY NORMALIZED REMODE (3A)

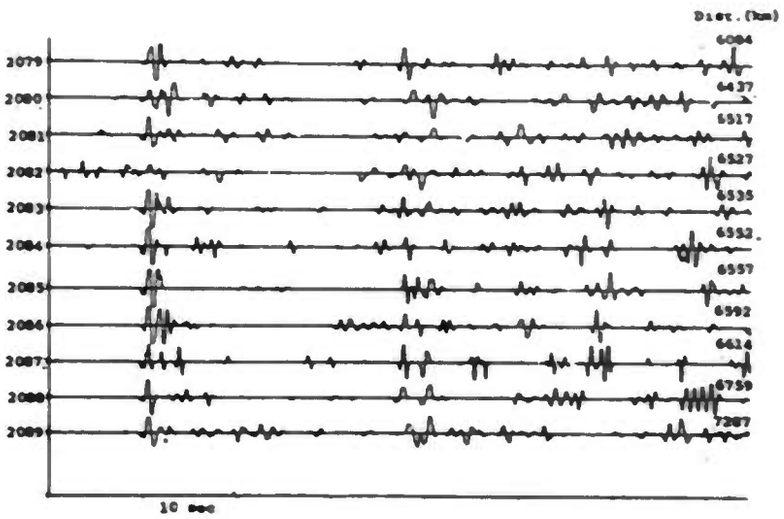

Z-COMPONENTS PROCESSED BY NORMALIZED REMODE (5)

PREFILTERED: Q=1.0, fo=1.0 cps REMODE WINDOW LENGTH = 1.0 sec

Figure 2C. PERU EVENT

If no trace of a depth phase could be recognized across the suite of unfiltered seismograms, then it was not recognizable on the REMODE-processed seismograms. No sP phase could be found on any seismograms for a Colombia event, nor could any of the depth phases be found for three other events. The PcP phase could not be identified for several events. Although such phases could be presumed to exist, there is no reason to assume that they contain enough energy to be detectable.

2. Feasibility of Linear Polarization Measurements for Detecting and Measuring Seismic Body Waves

The objective of this study was to compare at teleseismic distances the detectability of P on the vertical component with polarization measurements.

The vertical and radial component of a strong teleseismic event was added to noise so that the S/N ratio was known a priori. Vertical component measurements and polarized vertical component measurements were compared on twenty different noise samples at approximately twenty different noise levels. In addition, a theoretical evaluation was made assuming Gaussian linearly additive noise. The sample mean amplitude was based on twenty samples. On the assumption that the noise and signal were randomly phased, the estimate of the signal amplitude was the square root of the difference of the squared signal plus noise and squared noise. The signal-to-noise ratio was computed by dividing the above sampled mean of signal by that of noise.

Results of the evaluation for zero lags are shown on Figure 21 . For signals with input S/N greater than 18 db, no bias in the amplitude measurement occurred and an average gain in S/N ratio of 9 db was obtained without signal distortion. For input S/N greater than 18 db, a second pass of the operator resulted in further enhancement of several db. For input S/N from 9 to 18 db, gains were obtained from 0 db to 9 db, respectively; but at the expense of large bias in amplitude measurements as shown at the bottom of Figure 21 . For inputs less than a 9 db threshold, the polarization measurements showed a loss in S/N ratio.

Similar results were obtained using the even part of the correlation coefficient up to $\pm$ ½ second of lag. Using lags, input greater than 18 db was required for unbiased amplitude measurements, but a gain of 14 db resulted. With lags, the detection threshold was near 5 db.

The gain obtained in measuring the linearly polarized component on Z and R was analyzed theoretically, assuming the signal is linearly polarized and the ambient noise was Gaussian and linearly additive. In order to evaluate the expected gain of the linearly polarized measurement compared to the vertical component measurement, the signal-to-noise ratio of cross correlated energy fluctuations of the two components was compared to the signal-to-noise ratio of the energy fluctuations of the vertical component. It was found that this measure of gain depends only on the noise power, noise coherency, and ratio of horizontal to vertical component amplitude of the signal.

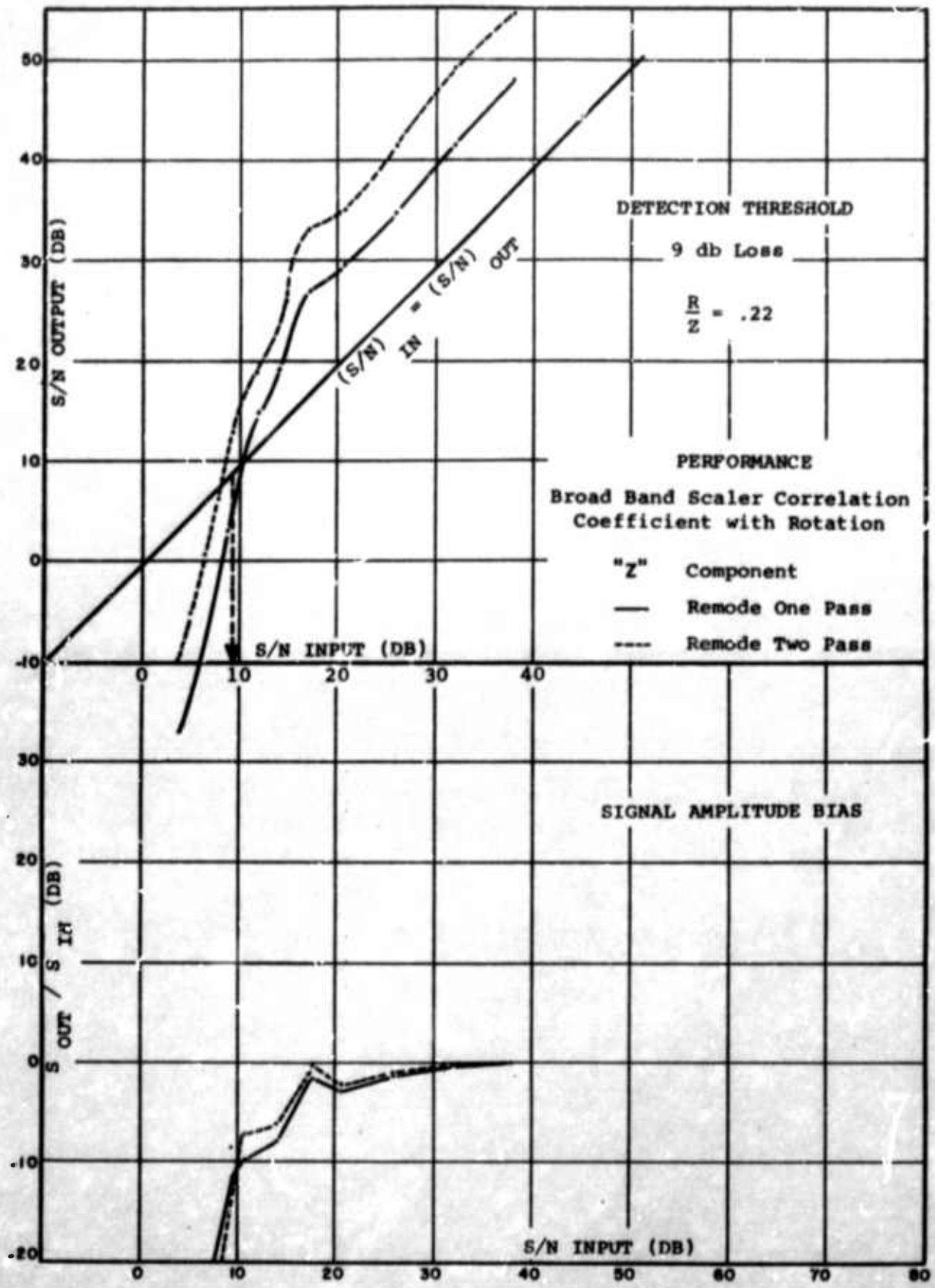

Figure 21. Polarization Measurements Using REMODE Filters

Based on the test for polarization measurements used, no significant detection gain can be expected using polarization criteria to detect weak teleseismic P-waves; they can be used to isolate and measure stronger events. For Gaussian noise, the measurements of linear polarization should be useful at epicentral distances less than 40° for which several db gain can be expected.

3. REMODE Signal-to-Noise Tests in Polarized Noise

Much of the noise following the P phase had frequency content and polarization so similar to signal that REMODE processing did not isolate weak signals effectively.

The REMODE 5 processor is designed to pass input motion which is rectilinear to a specified degree in a specified range of directions. Its sensitivity to rectilinear motion can be controlled by variation of parameters.

Short-period test tapes were generated to compare different REMODE 5 processes at low S/N ratios. The test tapes consisted of a P-phase embedded in its own signal-generated noise, to simulate a depth phase in its typical noise environment.

A teleseism from the Sea of Okhotsk was selected which had a strong, well-recorded P-phase at one of the LRSM stations. The first four-cycle segment of the P phase on the Z component was multiplied by a factor and added to both the Z and R components of the noise sample. The same data were used to represent signal in shear noise, by reversing the polarity of the radial-component noise before addition of signal.

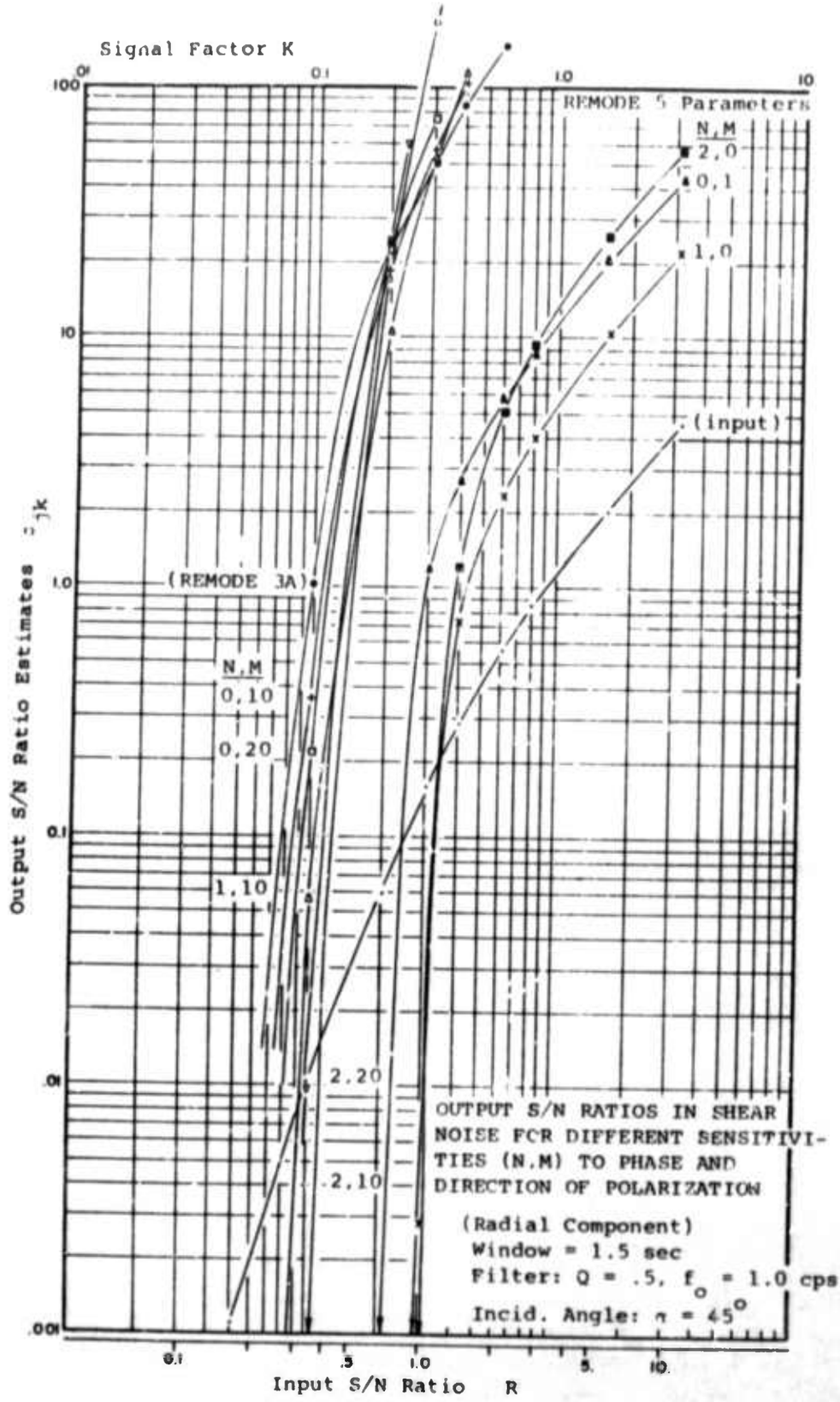
Signal Factor K
.01
0.1
1.0
10
100
REMODE 5 Parameters
N,M
2,0
0,1
1,0
(input)
(REMODE 3A)
N,M
0,10
0,20
1,10
2,20
2,10
Output S/N Ratio Estimates
.001
.01
0.1
1.0
.1
.5
1.0
5.
10.
Input S/N Ratio R
OUTPUT S/N RATIOS IN SHEAR NOISE FOR DIFFERENT SENSITIVITIES (N,M) TO PHASE AND DIRECTION OF POLARIZATION
(Radial Component)
Window = 1.5 sec
Filter: Q = .5, f_o = 1.0 cps
Incid. Angle: α = 45°

Figure 22.

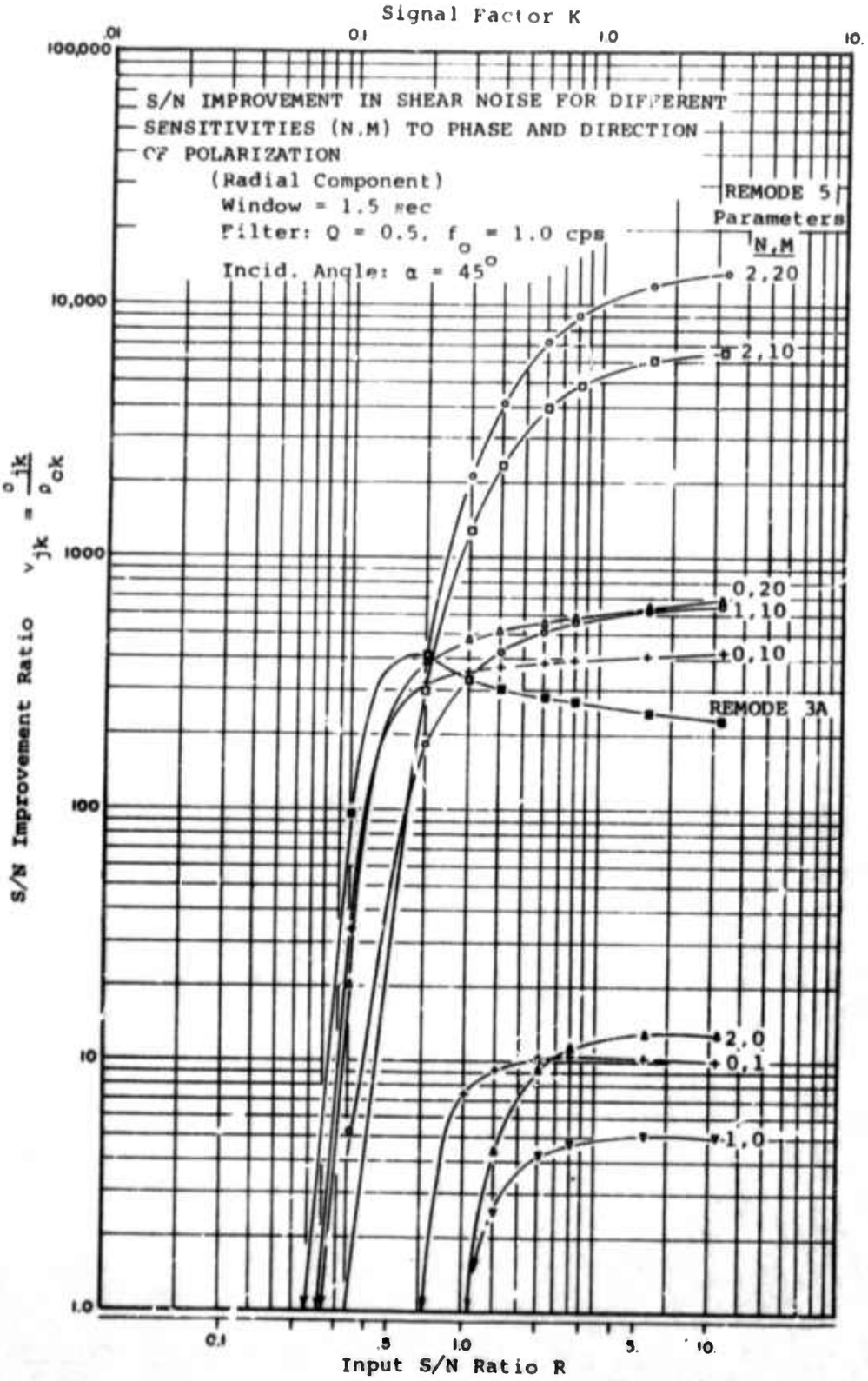
Signal Factor K
.01
0.1
1.0
10.
100,000
10,000
1000
100
10
1.0
S/N IMPROVEMENT IN SHEAR NOISE FOR DIFFERENT SENSITIVITIES (N,M) TO PHASE AND DIRECTION OF POLARIZATION
(Radial Component)
Window = 1.5 sec
Filter: Q = 0.5, f_o = 1.0 cps
Incid. Angle: $\alpha = 45^o$
REMODE 5 Parameters N,M
2,20
2,10
0,20
1,10
0,10
REMODE 3A
2,0
0,1
1,0
S/N Improvement Ratio $v_{jk} = \frac{\rho_{ik}}{\rho_{ck}}$
0.1
.5
1.0
5.
10.
Input S/N Ratio R

Figure 23.

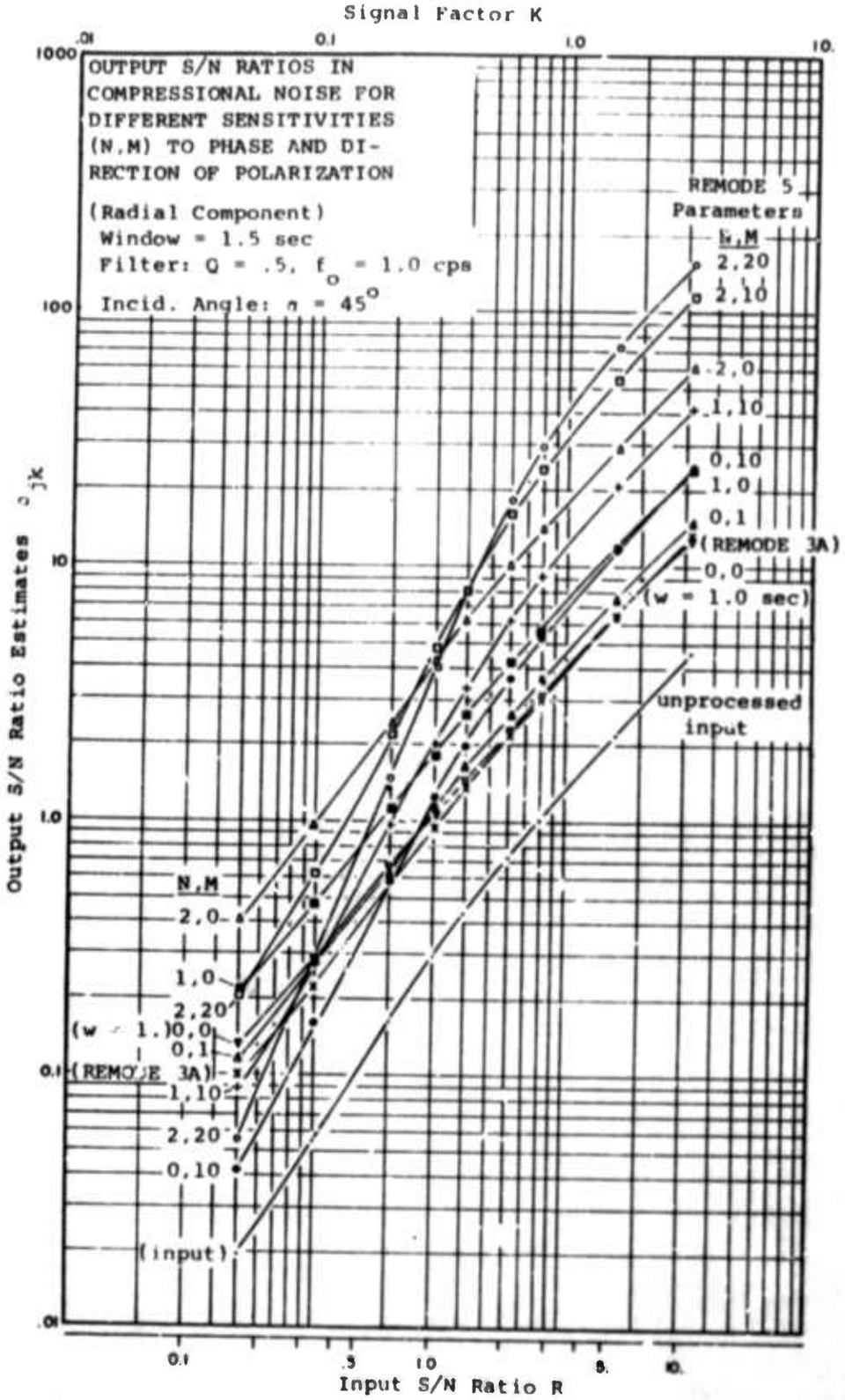
Signal Factor K
.01
0.1
1.0
10.
1000
100
10
1.0
0.1
.01
OUTPUT S/N RATIOS IN COMPRESSIONAL NOISE FOR DIFFERENT SENSITIVITIES (N,M) TO PHASE AND DIRECTION OF POLARIZATION
(Radial Component)
Window = 1.5 sec
Filter: Q = .5, f_o = 1.0 cps
Incid. Angle: α = 45°
REMODE 5 Parameters
N,M
2,20
2,10
2,0
1,10
0,10
1.0
0.1
(REMODE 3A)
0,0
(w = 1.0 sec)
unprocessed input
N,M
2,0
1,0
2,20
(w = 1.)0,0
0,1
(REMODE 3A)
1,10
2,20
0,10
(input)
Output S/N Ratio Estimates η_{jk}
0.1
.5
1.0
5.
10.
Input S/N Ratio R

Figure 24.

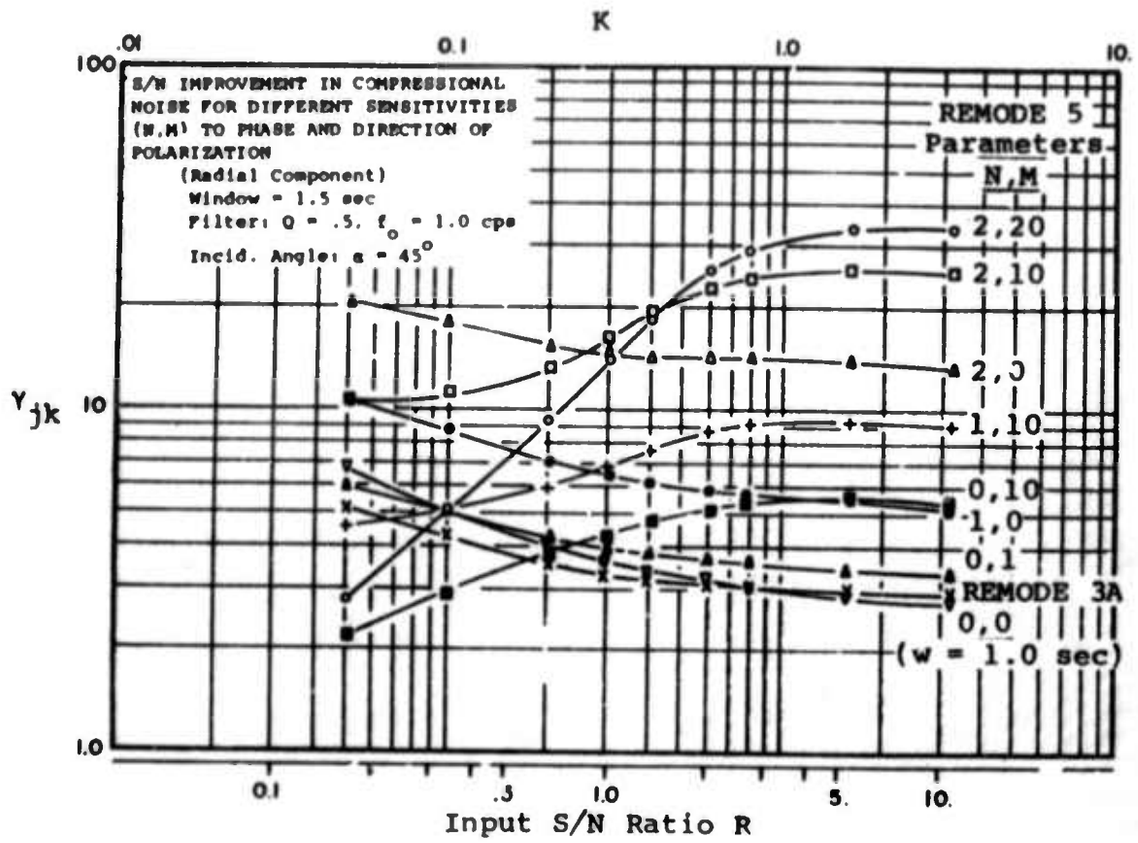
K
.01
0.1
1.0
10.
100
10
1.0
S/N IMPROVEMENT IN COMPRESSIONAL NOISE FOR DIFFERENT SENSITIVITIES (N,M) TO PHASE AND DIRECTION OF POLARIZATION
(Radial Component)
Window = 1.5 sec
Filter: Q = .5, f_o = 1.0 cps
Incid. Angle: α = 45°
REMODE 5
Parameters
N,M
2,20
2,10
2,0
1,10
0,10
1,0
0,1
REMODE 3A
0,0
(w = 1.0 sec)
Y_{jk}
0.1
.3
1.0
5.
10.
Input S/N Ratio R

Figure 25.

REMODE Parameters N,M	Window Width W	Prefilter Parameters Q,Fo	Input S/N Level at Detection Threshold	S/N Improvement Ratio at Maximum Input S/N Level of +21 dB (Radial Component) Compressional Noise	Shear Noise
0,1	3.	.5,1	-10 to -3 dB	4	-
0,1	1.5	.5,1	-10 to -3 dB	3.3	10
0,10	1.5	.5,1	-10 to -3 dB	5	420
0,20	1.5	.5,1	-10 to -3 dB	-	680
1,0	1.5	.5,1	-3 to 0 dB	5	5
2,0	1.5	.5,1	-3 to 0 dB	13	13
2,10	1.5	.5,1	-10 to -3 dB	25	6,500
2,20	1.5	.5,1	-10 to -3 dB	34	13,500
2,20	.75	.5,1	-10 to -3 dB	22	-
2,20	3.	.5,1	0 to +6 dB	40	-
2,20	1.5	2.,1	-10 to -3 dB	15	-
(REMODE 3A	1.5	.5,1	-10 to -3 dB	2.9	230

Table 5. REMODE Comparisons for Detection Thresholds and S/N Improvements

Figure 22 shows radial-component output S/N ratio estimates ρ_{jk} as functions of "true" input S/N ratios R, for several different processors. The "input" curve represents input S/N estimated in the same way as output S/N, to show the bias in the S/N estimator ρ. Ideally the "input" curve would be a straight line of slope 1.0. Actually its slope increases with decreasing S/N because of cancellation between signal and noise of opposite polarity. Figure 23 shows output S/N estimates normalized to the input S/N estimate, and represents the S/N improvement or gain γ_{jk} of each processor as a function of the "true" input S/N ratio R. The processors having large M severely attenuate shear noise, providing large S/N improvement for input S/N ratios greater than 1.0. At low input S/N ratios, transverse-polarized noise overrides signal polarization.

Figures 24 and 25 show the output S/N ratios and S/N improvement ratios in compressional noise for the radial component. Output S/N ratios for most of the processors are orders of magnitude smaller than they were for shear noise, because compressional noise is not strongly attenuated by polarization filtering. REMODE gain (Figure 25) increases noticeably with increasing input S/N for the more selective processors. The negative slopes at low S/N ratios are due to differences in bias between output S/N estimates and the input S/N estimates to which they are normalized.

The advantages of changes in REMODE selectivity were most evident at high input S/N ratios. Although the processors differed markedly in their ability to improve strong signal, they differed much less in their ability to detect signal at low S/N ratios. This is shown in Table 5, which summarizes the detection thresholds and maximum S/N improvements for several different processors.

Conclusions regarding the use of REMODE 5 in the detection and identification of depth phases include the following.

1. Increase in REMODE selectivity are more effective for isolating visible signals than for revealing obscure signals.

2. There exists an input S/N level below which REMODE operators will provide little or no signal enhancement. This limit is below the S/N level at which signal is recognizable on the unprocessed records.

3. Signal enhancement in the presence of compressional noise does not necessarily improve signal detectability at low S/N levels, because nearby compressional noise phases larger than the signal can be enhanced even more than the signal.

G. Energy Fluctuations in Seismic Noise

In recent years, statistical methods have been successfully used to predict the change in ambient seismic noise power sensed by burying a seismometer beneath the surface of the earth. Observations of seismic noise has indicated a large standing wave or isotropic component composed of the admixture of many propagation modes. Statistical theories such as equipartition of energy have been reasonably successful for deriving the excitation of the propagation modes.

Since such models are classically described by waves from a zero-mean Gaussian population, the purpose of this study was to tentatively assume that the seismic noise is Gaussian and to try to reject the hypothesis by measuring the relative frequency of occurrence of specific particle energies sequentially observed on samples of seismic noise. As control for the study, the same frequency of occurrence observations were made of a thermal noise sample recorded on tape from a Gaussian noise generator. The energy envelope of Gaussian noise is theoretically described by a Boltzman or exponential probability function. Thus the fit of a straight line to the log of the relative frequency of occurrence is a test of the Gaussian hypothesis. Two tests were used; one was the chi-square test of the deviation from the least squares straight line; the other, more powerful test compared the variance of the seismic noise and that of the Gaussian noise generator.

Three hours of seismic noise was selected which appeared to be typical of the normal ambient background. The noise was measured at a depth of 7,452 feet in a deepwell near Apache, Oklahoma. The near surface layering is described as high velocity

limestones of approximately 6 km/sec overlying an igneous basement complex of velocities in the neighborhood of 5 km/sec.

As shown on Figure 26 for seismic noise, the relative frequency of occurrence is given by the vertical axis, and the class interval in order of increasing energy is shown on the horizontal axis. On each plot, the center frequency and effective bandwidth of the filter is labeled. On Figure 27 , the same information is shown for the Gaussian noise generator. Comparing Figure 26 with Figure 27 , the scatter from a linear trend is the same overall for both sets of data, seismic and Gaussian generator.

Based on the chi-square test, it is more than 99% probable that samples at all of the frequencies are from a zero mean Gaussian population. The hypothesis that the class deviation of the seismic noise sample and the thermal noise sample are from the same random population is rejected only for the sample at 1.4 cps, suggesting that a non-Gaussian component may be included with the noise in this band. If we accept the Gaussian hypothesis, theoretical interest in the power spectral density of the noise may bear ultimately on dissipation mechanisms and may possibly lead to analysis of geological structure, with the real changes in the power spectrum in a region depending primarily on changes in structure. Of more practical interest is that modern literature on detection and filtering is most meaningful in the context of seismic signals added to Gaussian noise.

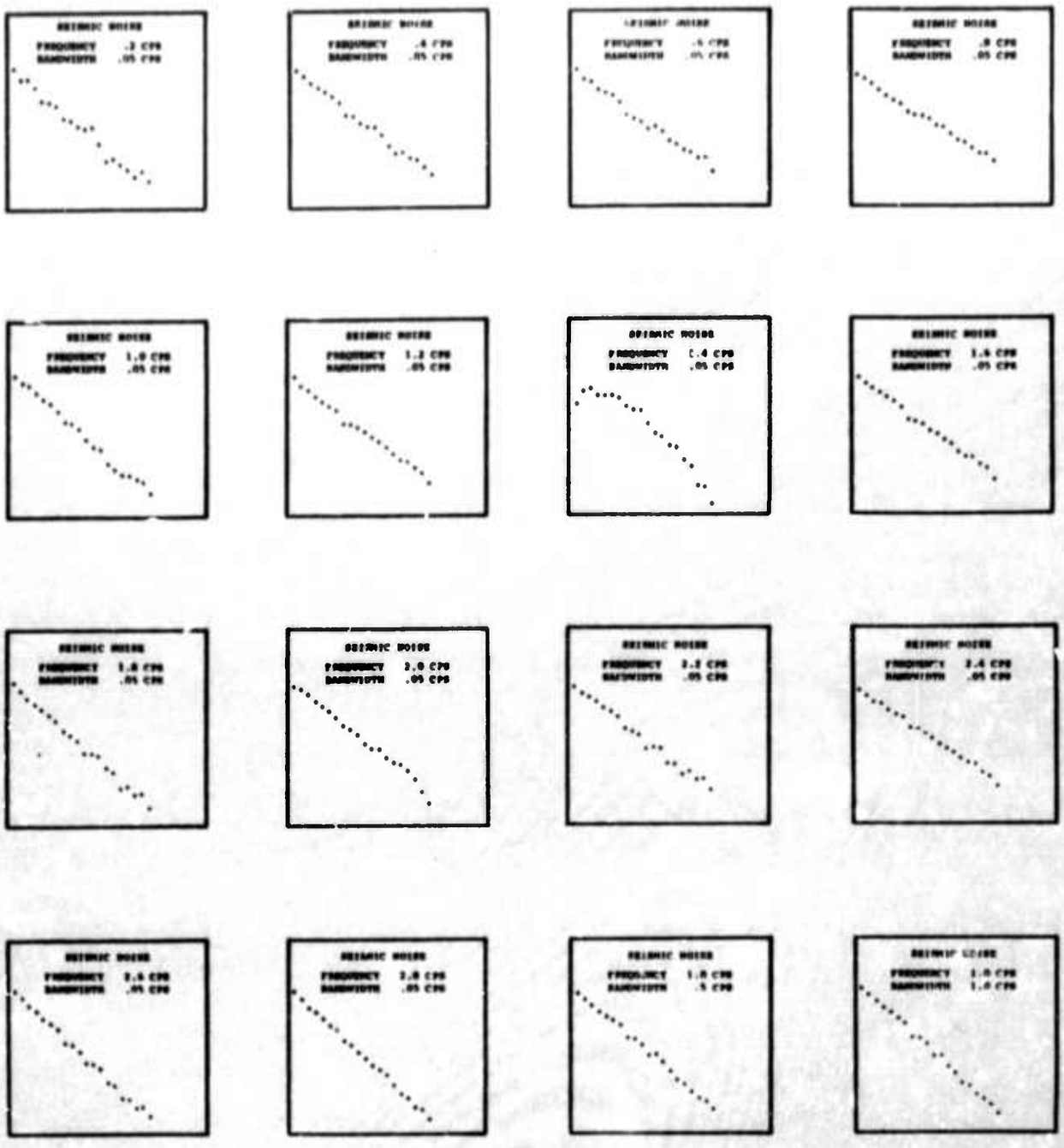

Figure 26. Relative Frequency of Occurrence (Ordinate) Versus Energy Level (Abscissa)

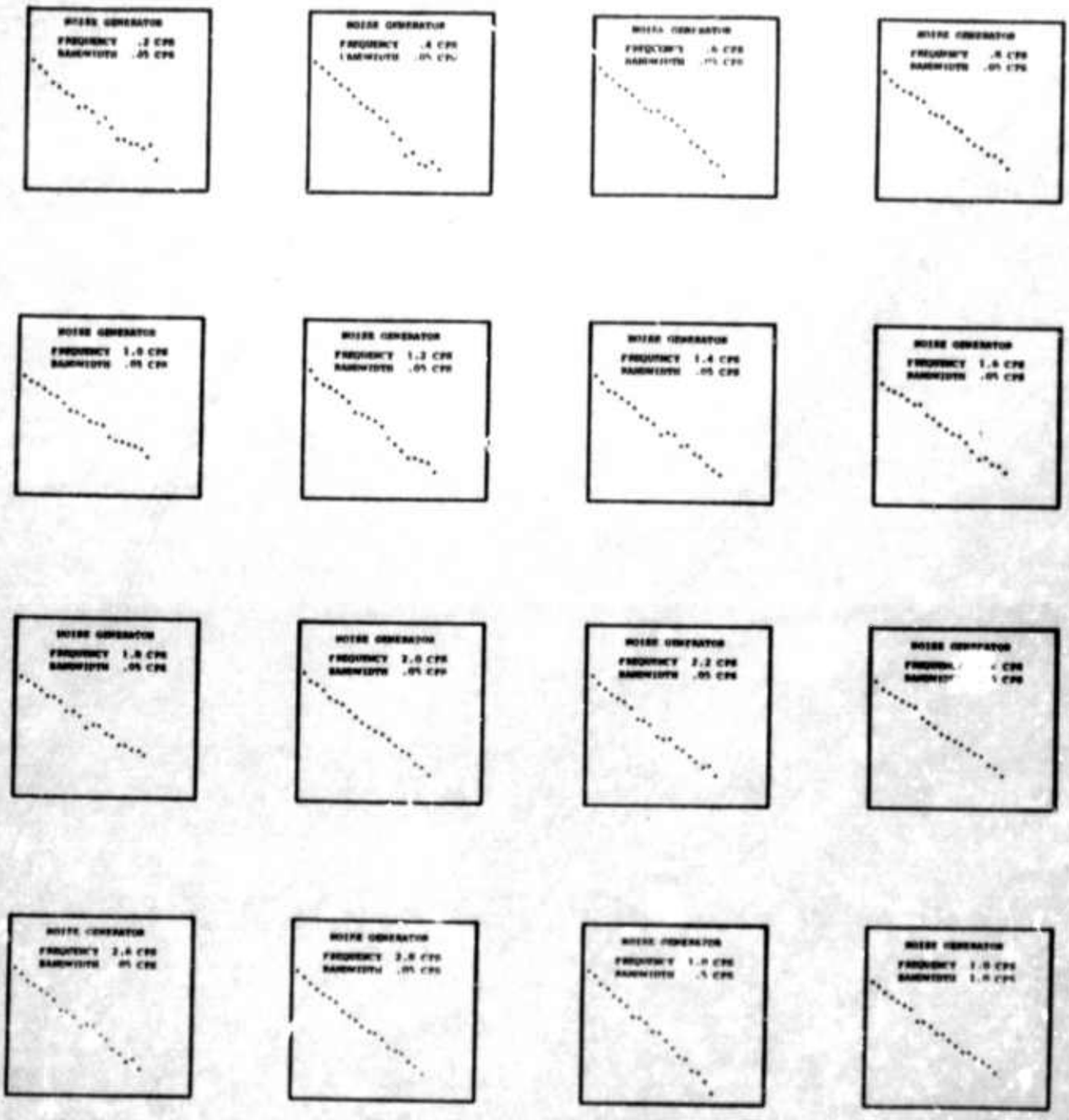

Figure 27. Relative Frequency of Occurrence (Ordinate) Versus Energy Level (Abscissa)

H. The Coherency Analysis of Seismic Noise

In the coherency analysis of seismic noise at arrays, we would like to know the fraction of noise which is correlated and uncorrelated at each frequency, the linear relations between seismometer outputs, the stationarity of the noise, and other properties in an effort to predict how well optimum filters could be made to work if computer limitations were no problem. The theory is used to estimate frequency response functions, ordinary coherence functions, partial coherence functions, and multiple coherence functions.

The parameters being estimated may be qualitatively interpreted as follows. The value of a frequency response function at frequency point f can be expressed in terms of gain and phase. The gain describes the change in amplitude and the phase describes the phase shift, or equivalently the time delay, experienced by a sinusoid of frequency f passing through the linear time invariant system characterized by the frequency response function. The ordinary coherence function provides a measure of the degree of linear relationship between two variables when they are considered as the input and output of the time invariant linear system. An alternative equivalent interpretation is that of the percentage of power or variance which is common to the two random variables.

The partial coherence function is a quantitative measure of linear relationship between two variables when they are considered as being related by a linear time invariant system and linear least squares estimates of other measured variables have been subtracted out. Under appropriate conditions, the

partial coherence between two variables will provide a more pertinent measure of their relationship than will ordinary coherence functions. The multiple coherence function provides a measure of the degree of linear relationship between a single record considered as an output variable and several other variables considered input variables. An alternative interpretation of multiple coherence is the percentage of power or variance which is accounted for via linear relationships with all the input variables simultaneously.

The multiple coherence function can assist in determining how many seismometer outputs in an array should be processed to properly determine the seismic noise field. The partial coherence functions and ordinary coherence functions can assist in the determination of where pertinent strong linear relationships exist from seismometer to seismometer to help direct efforts eventually intended toward noise suppression with a minimum of computational effort.

Digital computer programs were developed and sets of numerical experiments were made. These numerical experiments illustrated that the multiple coherence function acts basically as predicted. It attains a low value when there are less seismometer outputs being measured than there are underlying noise traces, and it increases and approaches unity as the number of seismometers increases past the number of underlying independent noise traces.

The partial coherence function is, in general, more difficult to interpret in that residual coherences can exist between linear combinations of extraneous noise. However, it

would appear that if some assumptions are made concerning the character of the incoherent extraneous noise (e.g., constant power spectra throughout the seismometer array) then one should be able to predict the residual partial coherence. This prediction can be subtracted out such that the remainder is close to zero.

The gain and phase information relating the seismometer output has yet to be exploited in detail, but it should be useful in determining direction and speed of the noise components. Other information available from the program is the conditional power spectral density functions. This is the power remaining after linear combinations of other variables have been subtracted out. This gives additional data to provide more insight into the structure of the noise.

As an example of the kind of approach that might be applied to an array using coherency theory, the Cumberland Plateau seismic array given in Figure 28 was examined. The subarray analyzed contained nine seismometers with the basic data being a noise sample of the nine traces, 400 seconds long, taken at 5 points per second with 50 lags. A first consideration was the determination of characteristics of this noise field which related the amount of noise power in seismometer 10 that could be predicted or accounted for by taking various combinations of other elements in the array. Thus, the center was considered an "output" and various combinations of other seismometers were sequentially added as "inputs" to determine the change in the multiple coherence, i.e. the additional proportion of power accounted for by each set.

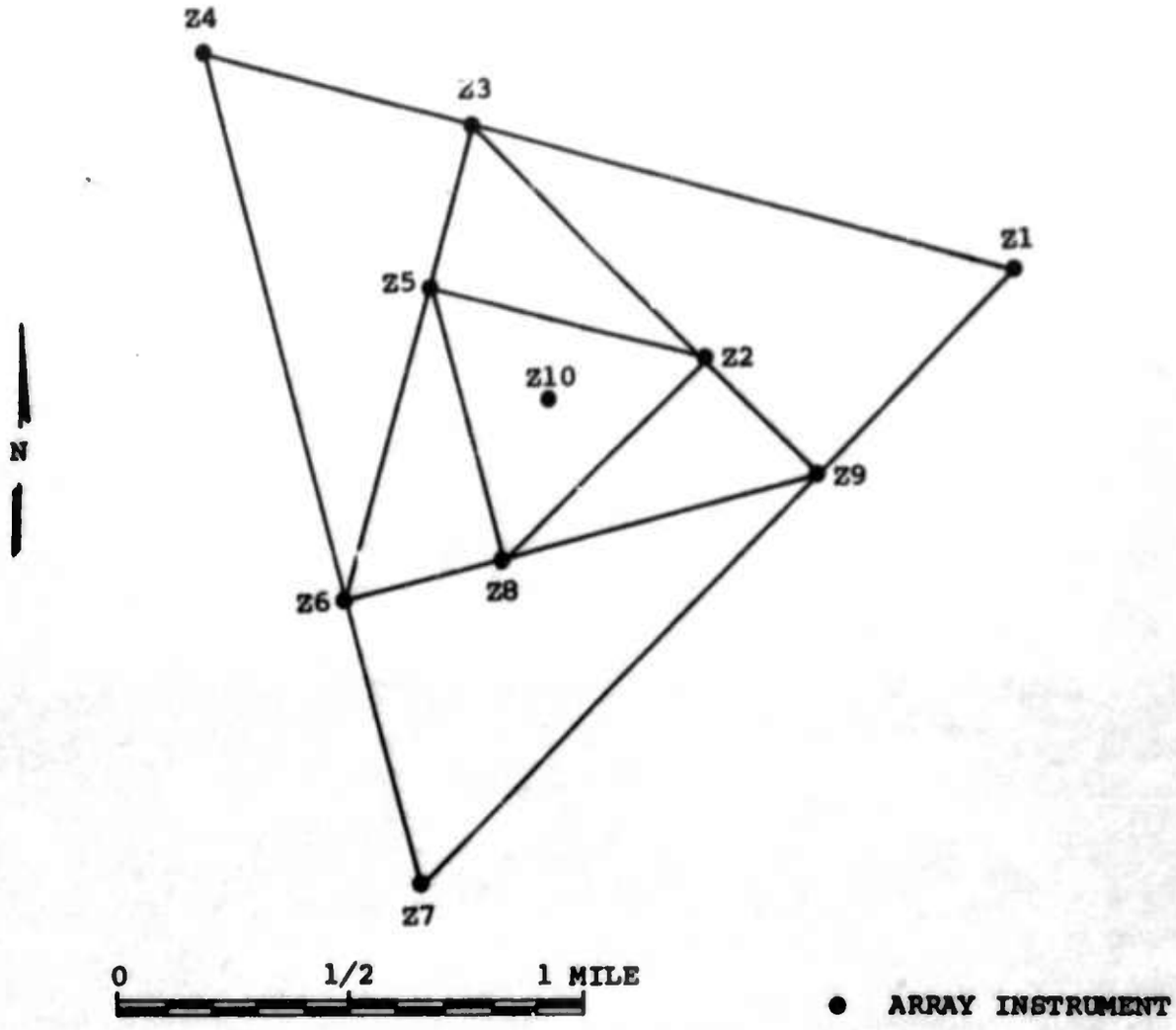

Figure 28. Seismic Array at CPSO

Figure 29 gives the multiple coherence or the proportion of the noise power in 10 which was accounted for by 3, 4, 5,..., 9 component seismometer arrays, respectively, at five different frequencies. The outer seismometers were added in first in this case. We note that much of the power (94.9%) in the .2 cps band is already accounted for by the first three seismometers. Figure 29 also shows the rate of increase in the proportion of power in 10 accounted for, as the number of seismometers increases. At low frequencies, most of the power is accounted for by the time seven seismometers are present while at 1.8 cps the full set accounts for only 60 percent of the noise power. By examining the ordinary coherence as given in Table 6, one notices that seismometer 10 is highly coherent with most of the other seismometers tending to verify that 10 is a reasonable candidate for the "output" variable in one particular linear system represented by the array. However, the high ordinary coherence between 10 and 2, 8 or 6 at low frequencies suggests that adding those closer seismometers first would have accounted for more of the coherent noise power. In fact it can be seen from the ordinary coherence in Table 6 that adding seismometer 8 into the array first would have produced a two-element array which accounted for between 30 and 98% of the noise power, an arrangement clearly superior to the first three-element array in Figure 28. Thus, by choosing certain seismometers in the array one could improve the slope of the "proportion of noise power accounted for" curve in Figure 29.

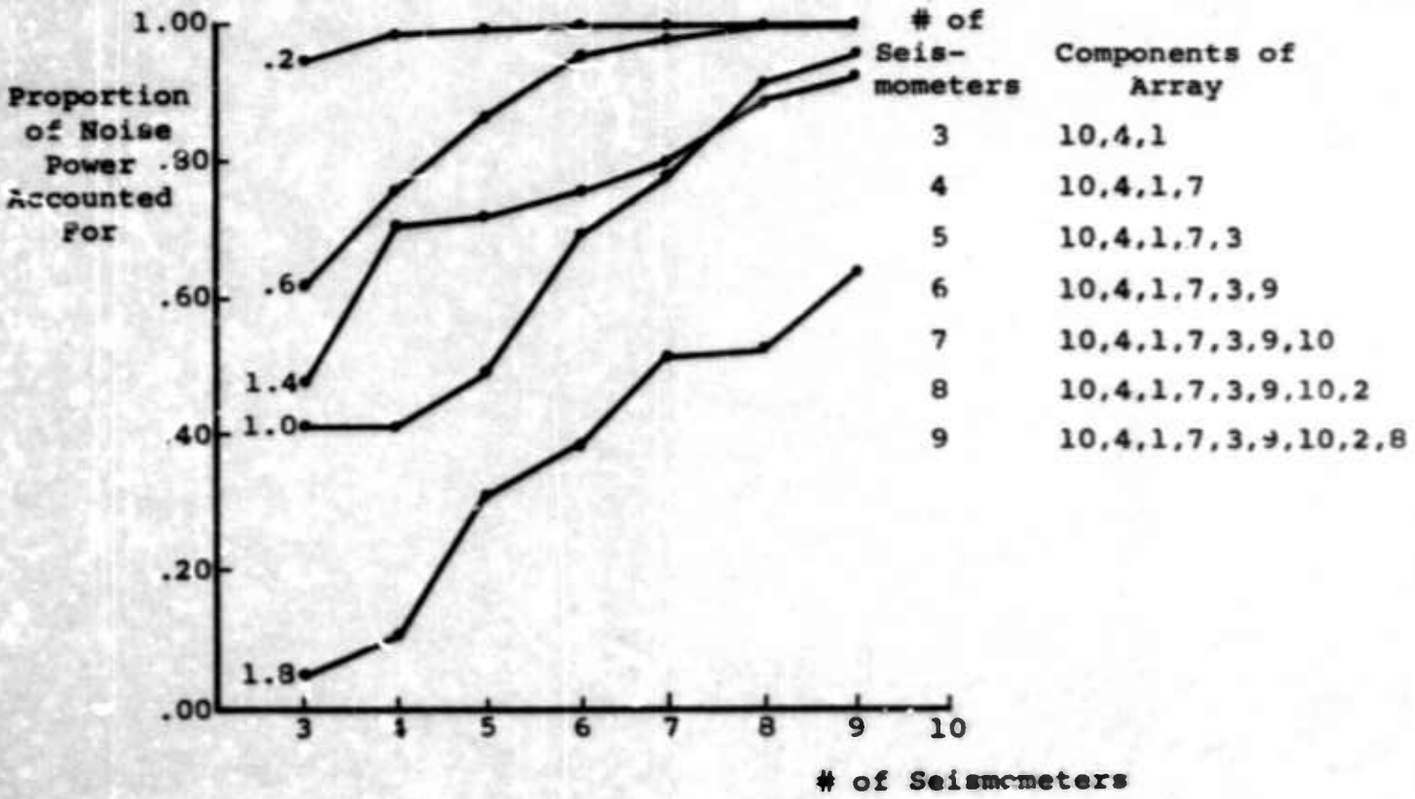

Figure 29. Sample A -- Proportion of Noise Power Accounted For With Outer Seismometers Added First

SAMPLE A

	①	④	⑦	③	⑨	⑥	②	⑧
.2	.87	.85	.86	.93	.95	.96	.98	.98
.6	.38	.52	.43	.70	.75	.79	.89	.90
1.0	.17	.31	.05	.41	.43	.23	.69	.64
1.4	.13	.45	.56	.30	.35	.49	.71	.56
1.8	.01	.06	.05	.23	.10	.30	.01	.31

SAMPLE B

	③	⑨	⑥	②	⑧
.2	.92	.96	.94	.98	.97
.6	.74	.76	.77	.89	.90
1.0	.37	.33	.28	.59	.65
1.4	.48	.36	.48	.71	.55
1.8	.15	.14	.30	.00	.14

Table 6. Ordinary Coherence of 10 with other Seismometers

In Figure 30, the same sample (A) is considered with the difference being the addition of the close-in seismometers first. This time the proportion of power accounted for increases much more sharply as the number of seismometers increases and by the time six are present the noise accounted for compares favorably with the previous situation when all nine are present. In fact more than 90% of the power in the low three bands is accounted for by a three-element array, consisting of the three close-in seismometers.

The data in both Samples A and B indicate that the outer elements are coherent with the center seismometer 10 (Table 6). This suggests that much of the noise power in the first two bands could be eliminated by replacing each seismometer by its residual trace (i.e., with the effect of 10 eliminated). With this in mind the simple linear filter relations between 10 and the other seismometers (given in Table 7) were examined and found to be quite consistent over the two recording samples. This shows that for the inner seismometers (See Table 6) between 92 and 100% of the noise power can be accounted for at each seismometer for .2 cps noise and 70 through 90% of the noise power at .6 cps merely by subtracting out the effect of 10 and furthermore, that it is done in both situations with the same set of filter coefficients. This still leaves plenty of degrees of freedom left for estimating the signal and gets rid of the noise with the same set of filters in both situations.

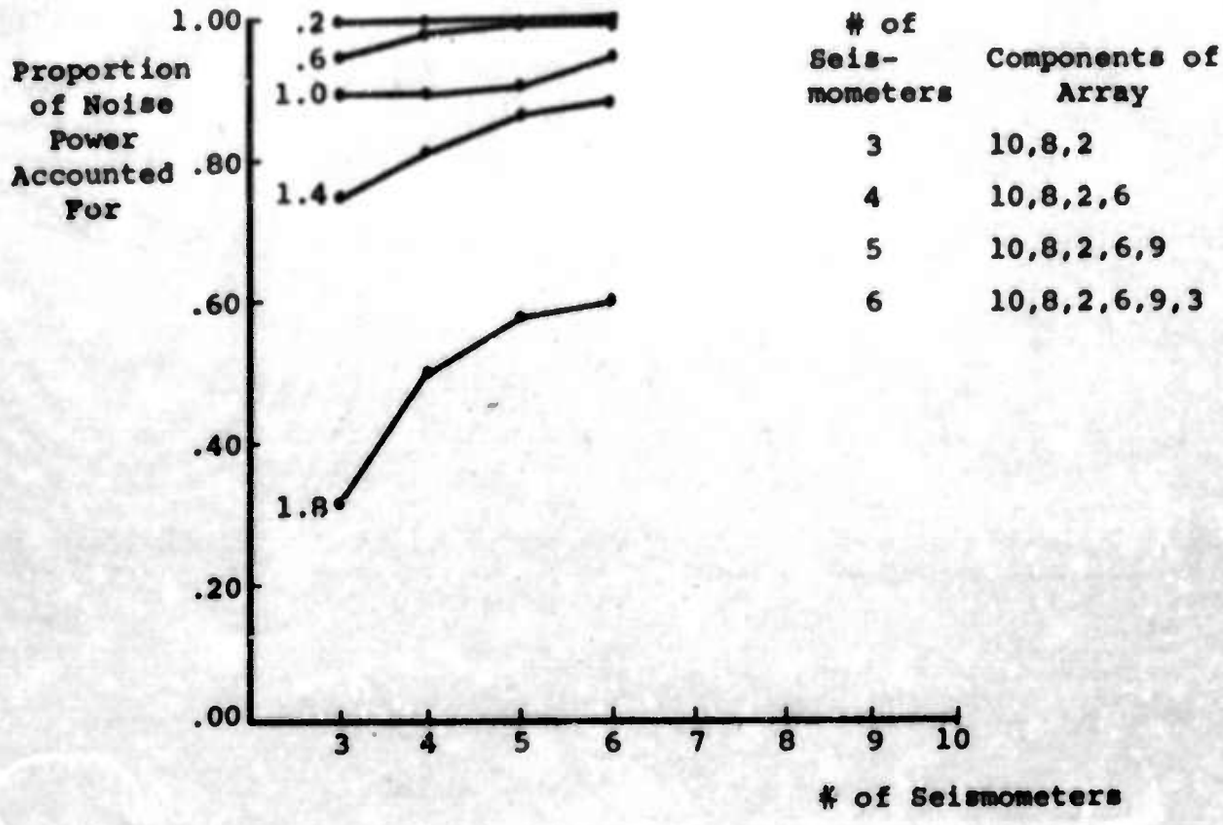

Figure 30. Sample A -- Proportion of Noise Power Accounted For With Inner Seismometers Added First

	$H_{8,10}$	$H_{2,10}$	$H_{6,10}$	$H_{9,10}$	$H_{3,10}$
Sample A (.2 cps)					
Real	1.35	1.16	.94	1.06	1.87
Imaginary	.56	.20	.39	.14	.33
Sample B (.2 cps)					
Real	1.33	1.19	.91	1.08	1.79
Imaginary	.54	.19	.38	.13	.39
Sample A (.6 cps)					
Real	1.24	.96	.89	.66	.46
Imaginary	.09	-.14	.12	-.60	1.08
Sample B (.6 cps)					
Real	1.16	.98	.81	.63	.62
Imaginary	.11	-.11	.13	-.61	1.13

Table 7. Linear Filter Relation Between Sub-Array Elements and Center Element (10)

I. Analysis of Seismic Noise at the Yellowknife Array, Canada

From data supplied by the United Kingdom Atomic Energy Authority (UKAEA) a quiet day noise analysis was performed for the Yellowknife array (YKC), Canada. The data was supplied in the form of a twenty-four channel magnetic tape recording of the amplified outputs of short-period, vertical-component, Willmore Mark II, seismometers. Both an original recording and a transcription were supplied. The UKAEA transcription process was analyzed for fidelity by examining several noise samples, taken at the same time intervals, from the original and transcription tapes. Although the noise samples of the transcription looked very much like the original recordings, power spectral analysis indicated generally high fidelity only below about 1.5 cps. Above 1.5 cps system generated noise led to poorer reproduction.

Analysis of the noise field is advantageously performed in terms of the power in the field as a function of frequency and vector wave-number i.e., 3-D power spectral analysis where, for any frequency, the power is given as a function of the vector wave-number, k. However, the relative spacing of the seismometers at YKC caused severe aliasing leading to uninterpretable spectra. Thus an attempt was made to arrive at a meaningful picture of the vertical component of the noise field by calculating auto- and cross-correlation functions, single channel power spectra, cross-power spectra, and coherencies. The array geometry and total system response are shown in Figures 31 and 32, respectively.

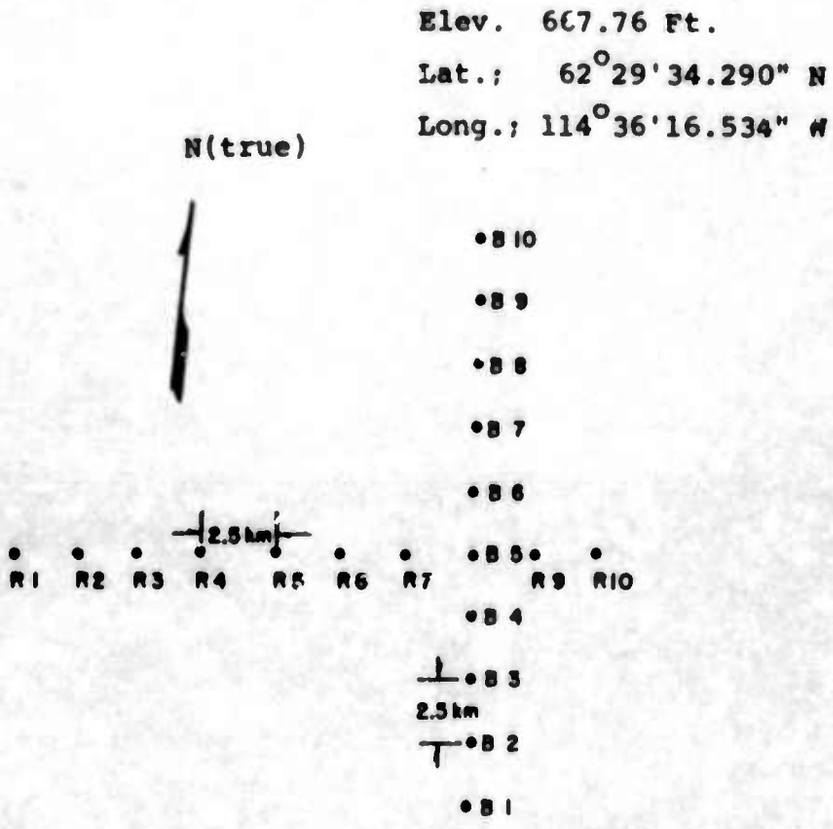

Figure 31. Yellowknife Array

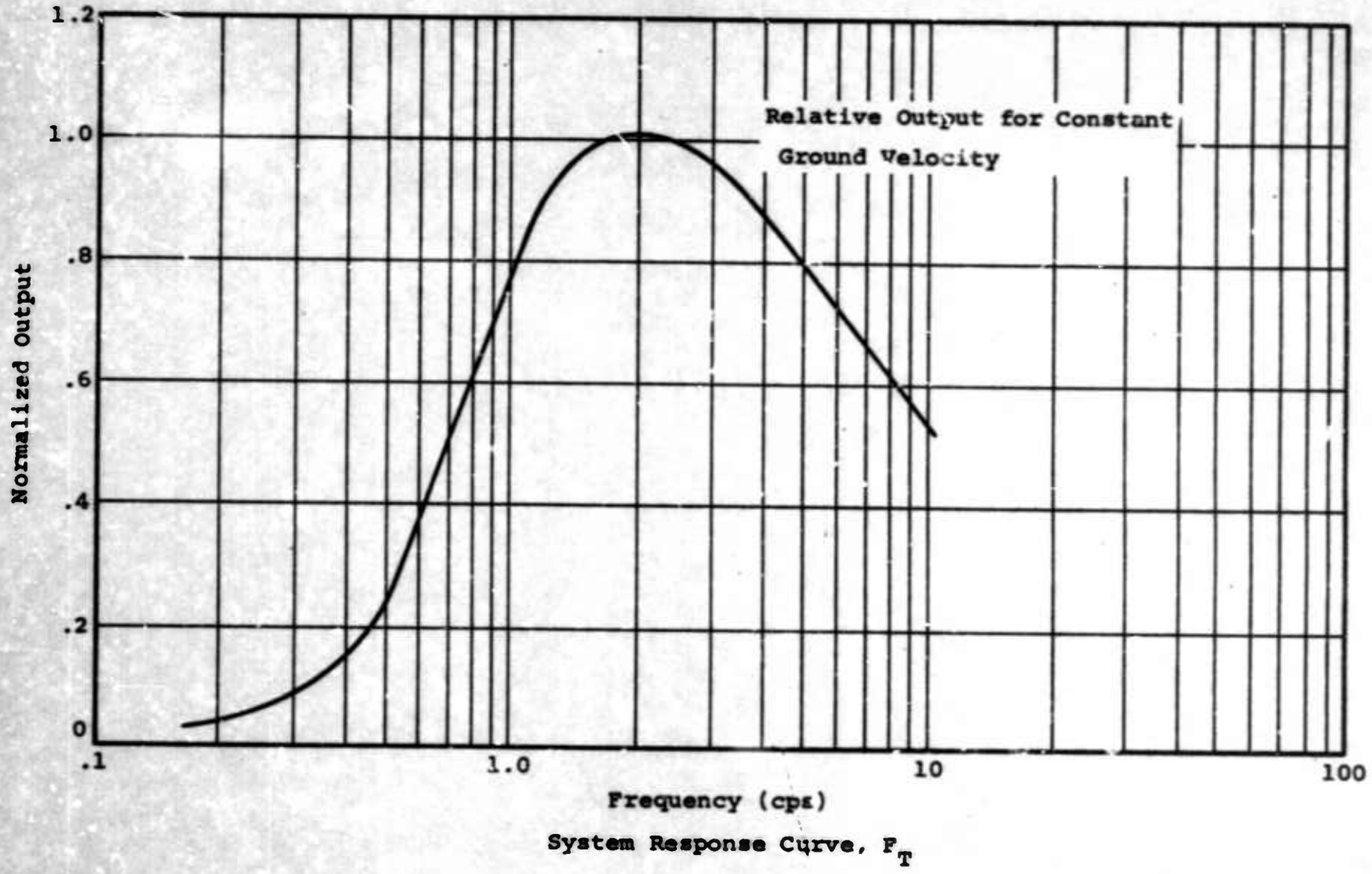

System Response Curve, F_T

Figure 32. System Response at Yellowknife Array

The field appears to be divided into coherent and incoherent (random) noise where the coherency depends on frequency, seismometer spacing and direction. The noise below about .4 cps generally exhibits the highest coherency with a peak of 90% for a 2.5 km spacing along the B arm of the array and decreases with increasing frequency and seismometer separation. The peak coherency for a 2.5 km separation along the R seismometers is 72%, and drops more rapidly with increasing spacing than along the B arm. Instrumental noise appears to contribute to incoherent power at all frequencies and to coherent power at several frequencies. In particular, instrumental noise was found to contribute such large amounts of incoherent as well as coherent power as to make analysis above about 1.5 cps impossible.

The peak microseismic energy was found to occur at a period of 4.5 seconds, at about 20 db above the 1 cps noise power as seen on spectra which were uncorrected for the system response. The 4.5 second peak appears to consist of a wave or group of waves traveling at about 3.6 km/sec. in an easterly direction with a small northerly component. This dominant microseismic energy hits the B seismometers almost broadside thus accounting for the apparent directional dependence of the low frequency coherence. Corrected for system response, the peak occurs at about 8.0 seconds at 70-80 db above the 1 cps power.

It is obvious from the above discussion that the dynamic range of the instrumentation must be known in detail and that analysis of the noise field above about 1.5 cps requires either increasing the overall dynamic range or eliminating the dominant low frequency energy before sensing and recording. The geometry

of the array determines the spatial spectral window and thus the power in the noise field that is "seen" in k-space. That is, analogous to the Nyquist folding frequency, the spatial sampling determines the spatial folding vector wave-number and also the shape and position (in k-space) of the sidelobes. For YKC the seismometers were too far apart causing severe alissing thus making a k-space noise analysis impossible. The regular spacing of the array is desirable since this causes shape peaks in the side lobes, but a closer spacing (at most .5 km apart) is necessary in order to increase the spatial folding wave-number to the point where a meaningful k-space analysis is possible.

Figures 33 and 34 are illustrative of the type of anslysis made for this study. Figure 33 shows the original and associated transcription of one sample taken at the R1 seismometer. Figure 34 shows low resolution auto-spectra computed for the R1 seismometer for the sample given in Figure 33.

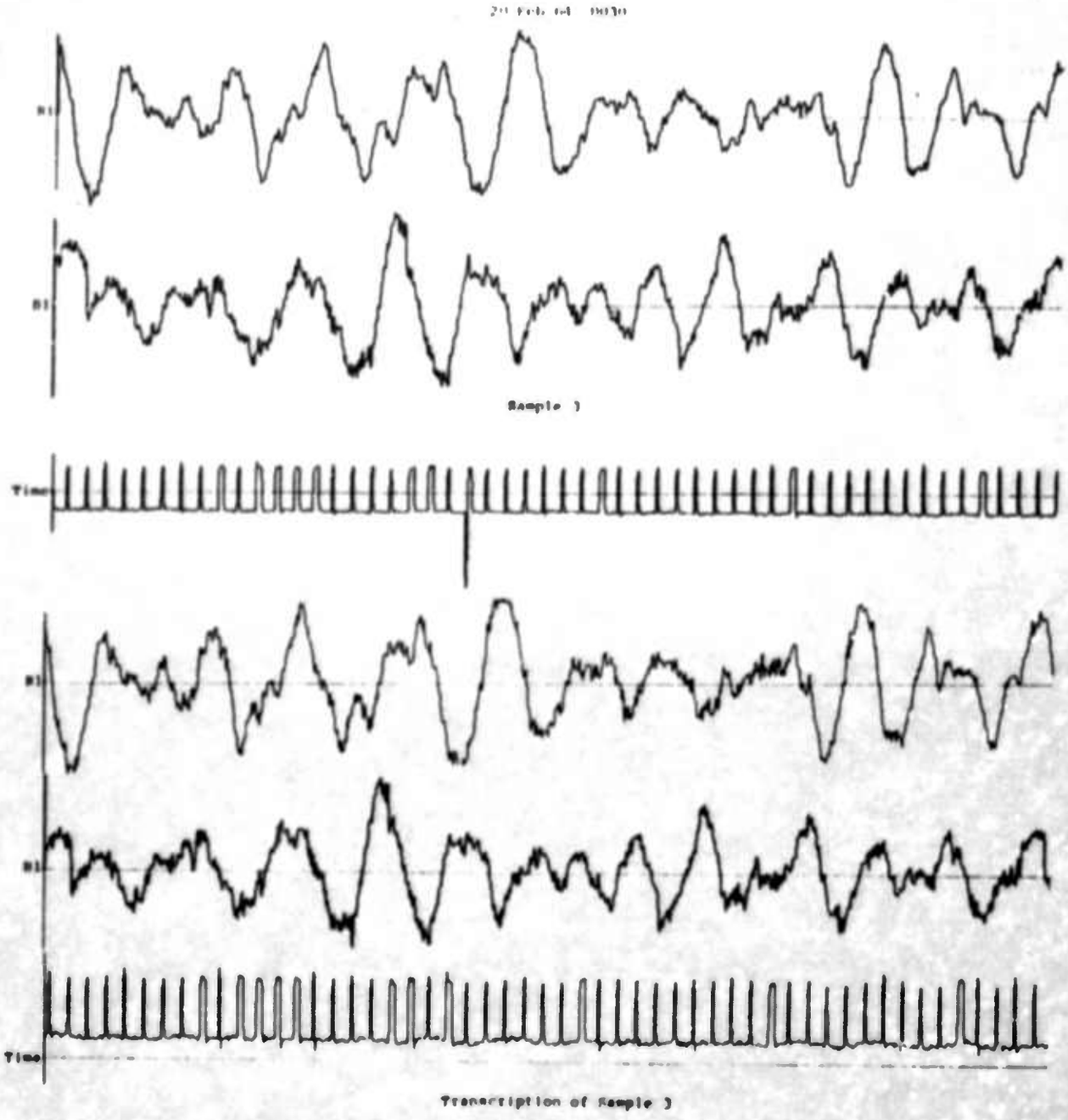

Figure 33. Yellowknife Array Noise Sample: Original and Transcription

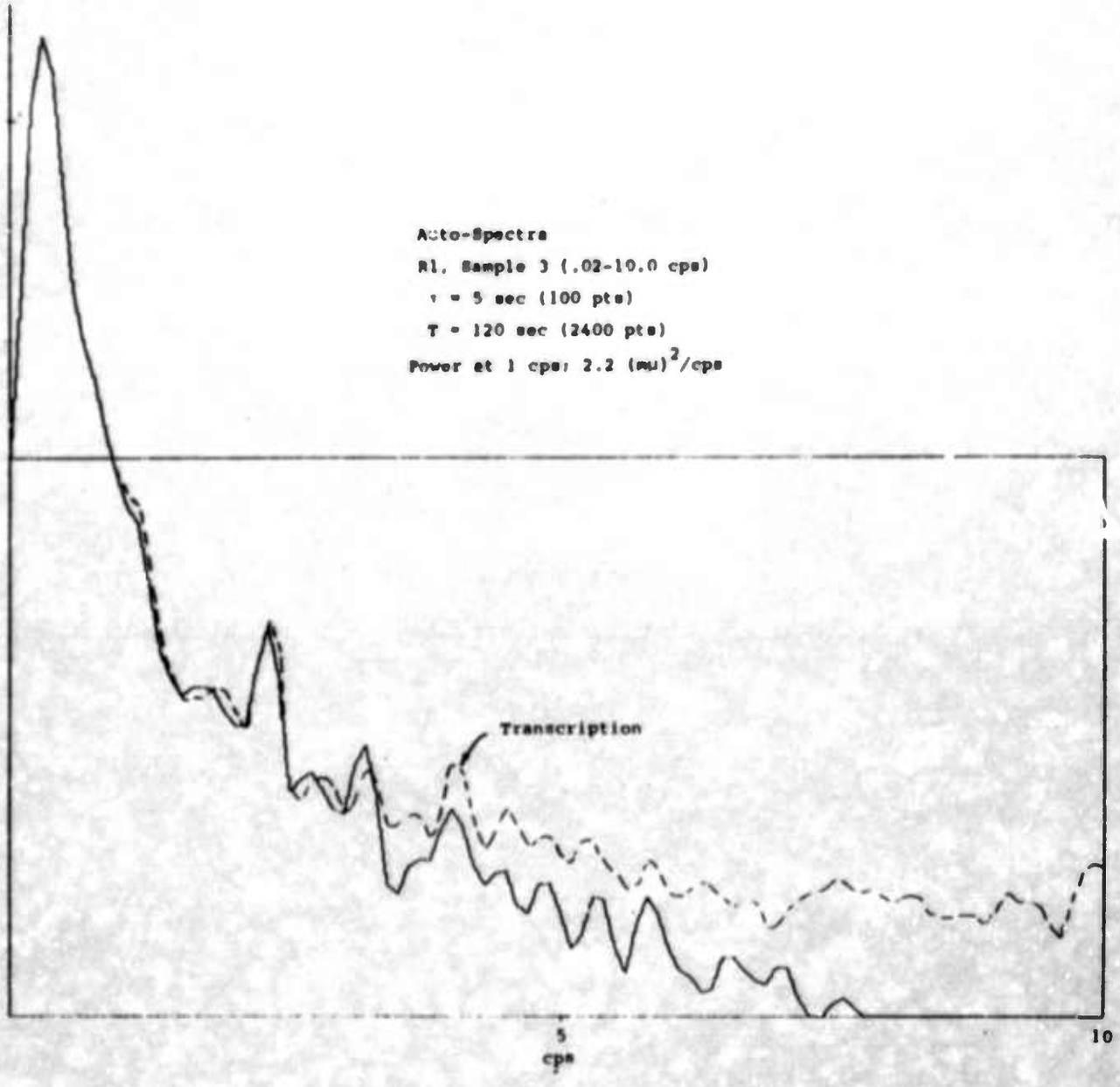

Figure 34. Auto-Spectra, R1, Low Resolution (.2 cps) for Yellowknife Array Noise

J. Finite Fourier Transform Theory and Its Application to the Computation of Convolutions, Correlations, and Spectra

Practical and computational aspects of the theory of Fourier Transforms have been examined in connection with various SDL research analyses. These efforts have resulted in a set of programs for performing operations on time series based on the Cooley-Tukey hyper-rapid Fourier transform method. Using this method, computations on seismic array data such as the calculation of convolutions, correlations, spectra, and digital filters have been speeded up by factors of three or four and sometimes even ten. Following is a brief description of the procedures followed and the results obtained from these procedures.

1. Finite and Discrete Fourier Transforms

In the case of continuous data of infinite length, the Fourier transform pair is the direct transform and the inverse transform. Sometimes the direct transform is written with a factor of 1 in front on the integral and the inverse with a factor of $1/2\pi$. Quantities of interest, such as spectra, etc., involve magnitudes or squares of one transform and the factor must be inserted or taken out, depending on which definition is used, to preserve the proper dimensions.

Two drawbacks of these definitions for digital computations are apparent: First, the integrals must be approximated by sums in the digital computer, which implies that both transforms involve sampled variables. Second, the infinite limits on the sums are impossible in practice. Clearly, these sums must be truncated, as they do not in general converge over a finite interval. As a result, Fourier transforms as such are never really

computed by a digital computer. Instead, the complex samples of a direct transform are approximated by the cosine and sine coefficients of Fourier series representation of the input data.

If N samples of the data are taken at equally spaced intervals $\Delta t = T/N$, the integrals become sums, and the frequency sum goes from DC to the folding frequency. It was found that a great deal of symmetry between the two transforms could be preserved if the sum is summed up to N-1. Redundant points in the spectrum are included (since the transforms are periodic) but the computational procedures are simplified.

It was shown that the set of direct Fourier transform points, between DC and the folding frequency, contained the same amount of information as the real data series, which suggested that the existence of one transform should imply the existence of the other.

2. Two-and-Three-Dimensional Fourier Transforms

Two- and three-dimensional direct Fourier transforms are seen to be

$$A(k_1,k_2) = \frac{1}{\sqrt{N_1 N_2}} \sum_{j_1=0}^{N_1-1} \sum_{j_2=0}^{N_2-1} x(j_1,j_2)\, w_1^{-j_1 k_1}\, w_2^{-j_2 k_2} \qquad (1)$$

and

$$A(k_1,k_2,k_3) = \frac{1}{\sqrt{N_1 N_2 N_3}} \sum_{j_1=0}^{N_1-1} \sum_{j_2=0}^{N_2-1} \sum_{j_3=0}^{N_3-1} x(j_1,j_2,j_3)\, w_1^{-j_1 k_1} \cdot w_2^{-j_2 k_2}\, w_3^{-j_3 k_3} \qquad (2)$$

By separating and breaking up these equations, it was calculated that $N_1 + N_2$ one-dimensional transforms are required to compute the single two-dimensional transform, and that $N_1 N_2$ one-dimensional transforms and N_3 two-dimensional transforms are needed to compute the single three-dimensional transform.

3. Speed-Up of Transform Computing Time

It was shown that the process of transforming is equivalent to matrix multiplication by a matrix W, which preserves "length" between two domains. The Cooley-Tukey method factors the W matrix, if its order is a power of two, into L + 1 sparse matrices, where L is the power of two. Multiplying L + 1 times by these sparse matrices can in some cases reduce the computing time by many tens of times.

4. High-Speed Correlations and Convolutions

By computing Fourier transforms with a finite Fourier series-like method an important condition is put on the time series. As in regular Fourier series the input is assumed to be periodic with period T and the integrals or sums are computed over a single period. There is also the effect of cutting off the spectrum at the folding frequency. Sines and cosines of finite wavelength will repeat again outside the region of interest. This fact in itself is not bothersome but becomes a serious complication in the computation of convolutions and correlations. Convolutions and correlations as usually computed assume the time series to be zero outside the region of interest. Therefore, the integrals or sums in computing them are summed out only over the non-zero terms. When multiplying together two finite Fourier transforms (or the complex conjugate of one times the other) the periodicity of the time

series means that elements which have been shifted past the end of a period reappear at the beginning. This process is called circular convolution or correlation and its effects are unavoidable when straightforwardly computing lagged products with finite Fourier transforms.

Circular convolution is written:

$$R_{ij}^{C}(t) = \sum_{\tau=0}^{T-1} x_i(\tau)\, x_j(t+\tau) \qquad (3)$$

where $x_m(t + T) = x_m(t)$ for all m.

It was shown that this kind of correlation is equal to the transform of the absolute product of the two finite transforms.

On the other hand the transient correlation for positive lags is defined by the following:

$$R_{ij}^{T}(t) = \sum_{\tau=0}^{T-1-t} x_i(\tau)\, x_j(t+\tau) \qquad (4)$$

where the upper limit on the sum simulates the desired zeros in the time series outside the region of interest. The finite Fourier transform of this R^T is thus not the product of the two individual transforms. However, by filling zeros into the second half of each data series and computing their transforms out to twice their actual length, a good estimate of the spectrum may be obtained. In addition, the negative lags in the correlation appear, thus giving a more mathematically satisfying result.

Transient correlations for 100% lags were shown to be computed by forming the absolute product of two transforms, each computed out to twice the length of the original data series with zeros filled into the second halves.

Non-circular or transient convolutions were also computed in much the same way, except that the transforms had to be computed out to a length equal to the sum of the lengths of the time series and the filter, with the appropriate number of zeros filled into each. The convolution theorem was proved in the same fashion and were computed by forming the product of the two transforms, each computed out to a length equal to their sum with zeros filled into the extra lengths.

K. Perturbation Theory for the Inversion of Travel Time Data

Estimation of the internal elastic structure of the earth from body wave travel times ordinarily requires both arrival time data and the slope of a curve fitted to the observed travel time. There are well-known difficulties in fitting such curves, particularly in cases where the observed travel times suggest a multivalue travel time function. We have considered methods which make use of later arrival information in order to account for possible multiplicities in the travel time curves. An additional advantage to be gained from multiple phase inversion is the reduction in the number of station observations necessary to determine earth structure. The usefulness of the body phase amplitudes, in addition to the travel time information, was also demonstrated, since the amplitude information in the region of multiplicities can be used to confirm the actual presence of a multiplicity, and in addition, the nature of the velocity variation giving rise to the multiplicity.

It is clear that an effective means of including later arrival data, as well as data from any number of different phases, is through use of an iteration scheme. Such an approach, which does not require travel time slope information, can incorporate constraints and information from sources other than the travel time data. In particular, simultaneous inclusion of amplitude and travel time information in an inversion process using both perturbation and iteration can be accomplished, although the amplitude information would serve only as a condition of acceptance for structure which otherwise satisfied the travel time

data in the least squares sense. What is required for the implementation of an iteration procedure is a general, systematic and accurate means of generating the correction to be applied to the structure at each iteration stage. A properly conceived variational treatment has been used to supply this analytical information.

The inference of earth structure from body wave data has been developed, using procedures similar to those used in determining elastic and anelastic earth structure from surface wave amplitude and dispersion. The method developed iteratively perturbs an initial velocity distribution (which may be shown to be in agreement with surface wave dispersion data over the region in question) until the theoretical travel time function is in agreement, in the least squares sense, with the observed data. The method does not require any estimate of the curve slope or multiplicities, nor does it require a particularly dense and complete data coverage over the entire distance range. Several phases can be used simultaneously.

It was shown that the method is not only feasible but that it may be almost completely automated and combined with analysis of other data, including surface wave dispersion and amplitude spectra, for the determination of a more precise and accurate planetary structure.

APPENDIX A

BIBLIOGRAPHY OF REPORTS ISSUED UNDER CONTRACT AF33(657)-15919

NUMBER	TITLE	AUTHOR
133	Longshot	Clark, D. M.
134	Auk	Clark, D. M.
135	Par	Clark, D. M.
136	Cup	Clark, D. M.
137	Chase IV	Clark, D. M.
138	Charcoal	Clark, D. M.
139	An Evaluation of Maximum Likelihood Filtering Applied to LASA Data	Flinn, E.A. Hartenberger, R. A. McCowan, D. W.
140	Yuba	Flinn, E.A. Hartenberger, R. A. McCowan, D.W.
141	Applications & Development of Polarization (REMODE) Filters	Griffin, J. M.
142	Perturbation Theory for the Inversion of Body Waves Travel-Time Data	Archambeau, C. B. Flinn, E.A.
143	Buff	Archambeau, C. B. Flinn, E. A.
144	Palanquin	Archambeau, C. B. Flinn, E. A.
145	Red Hot	Archambeau, C. B. Flinn, E. A.
146	Progress Report on the Partial Coherency Study	Enochson, L. D. Shumway, R. H.
147	Relative Travel-Time Anomalies at LASA & the Location of Epicenters using "SHIFT"	Chiburis, E. F.
148	Two Examples of Maximum Likelihood Filtering of LASA Seismograms	Flinn, E. A. Hartenberger, R. A. McCowan, D. W.
149	Maximum Likelihood Filtering of LASA Noise Seismograms	Flinn, E. A. Hartenberger, R. A. McCowan, D. W.

APPENDIX A

BIBLIOGRAPHY OF REPORTS ISSUED UNDER CONTRACT AF 33(657)-15919
(continued)

NUMBER	TITLE	AUTHOR
150	The Crosswise Sum Method For Maximum Likelihood Filtering of LASA Seismograms	Flinn, E. A. Hartenberger, R. A. McCowan, D. W.
151	LASA Signal and Noise Amplitudes for Three Teleseismic Events	Chiburis, E. F. Hartenberger, R.A.
152	Rex	Chiburis, E. F. Hartenberger, R.A.
153	Duryea	Chiburis, E. F. Hartenberger, R.A.
154	Pin Stripe	Chiburis, E. F. Hartenberger, R. A.
155	The Coherency Analysis of Seismic Noise	Dean, W. C. Enochson, L. D. Shumway, R. H.
156	Chartreuse	Dean, W. C. Enochson, L.D. Shumway, R. H.
157	Analysis of Seismic Noise at the Yellow-Knife Array, Canada	Plutchok, Robert
158	Rockville Dam	Plutchok, Robert
159	LASA Travel-Time Anomalies for Various Epicentral Regions	Chiburis, E. F.
160	Dumont	Chiburis, E. F.
161	SDL Digital-to-Analog (DAC) System	Botello, R. J.
162	REMODE Signal/Noise Tests in Polarized Noise	Griffin, J. N.
163	Feasibility of Linear Polarization Measurements for Detecting & Measuring Seismic Body Waves	Sax, R. L.
164	Signal-to-Noise Ratio Improvement by Time-Shifting & Summing LASA Seismograms	Chiburis, E. F. Hartenberger, R.A.

APPENDIX A

BIBLIOGRAPHY OF REPORTS ISSUED
UNDER CONTRACT AF 33(657)-15919
(continued)

NUMBER	TITLE	AUTHOR
165	Pile Driver	Chiburis, E. F. Hartenberger, R.A.
166	Rayleigh Wave Rejection by Optimum Filtering of Vertical Arrays	Dean, W. C.
167	Energy Fluctuations in Seismic Noise	Sax, R. L. Rabenstine, D.B. Marine, R. N.
168	Finite Fourier Transform Theory & its Application to the Computation of Convolutions, Correlations & Spectra	McCowan, D. W.
169	Tan	McCowan, D.W.
170	Vertical Array Teleseismic Signal Measurements	Sax, R. L. Hawkins, R. L.
171	Half Break	Sax, R. L. Hawkins, R. L.
172	Travel-Time Data at the SDL	Chiburis, E. F. Ahner, R. O.
173	Signal-to-Noise Ratio Improvement by Beamforming LASA Seismograms	Chiburis, E. F. Hartenberger, R.A.
174	The Detection Threshold at the Montana LASA	Chiburis, E. F. Hartenberger, R.A.
175	Detection of Surface Waves From Small Events at Teleseismic Distances	Rabenstine, D. B. Alexander, S. S.

Unclassified
Security Classification

DOCUMENT CONTROL DATA · R&D

(Security classification of title, body of abstract and indexing annotation must be entered when the overall report is classified)

1. ORIGINATING ACTIVITY (Corporate author)

EARTH SCIENCES, TELEDYNE INDUSTRIES
ALEXANDRIA, VIRGINIA 22314

2a. REPORT SECURITY CLASSIFICATION
Unclassified

2b. GROUP
---

3. REPORT TITLE

FINAL REPORT CONTRACT AF 33(657)-15919 SDL OPERATIONS
18 FEBRUARY 1966 - 1 MARCH 1967

4. DESCRIPTIVE NOTES (Type of report and inclusive dates)

Scientific

5. AUTHOR(S) (Last name, first name, initial)

Dean, William C.

6. REPORT DATE	7a. TOTAL NO. OF PAGES	7b. NO. OF REFS
July 31, 1967	108	

8a. CONTRACT OR GRANT NO.	9a. ORIGINATOR'S REPORT NUMBER(S)
AF33(657)-15919	
b. PROJECT NO. VELA T/6702	
c. ARPA Order 624	9b. OTHER REPORT NO(S) (Any other numbers that may be assigned this report)
d. ARPA Program Code No. 5810	

10. AVAILABILITY/LIMITATION NOTICES

This document is subject to special export controls and each transmittal to foreign governments or foreign national may be made only with prior approval of Chief, AFTAC.

11. SUPPLEMENTARY NOTES	12. SPONSORING MILITARY ACTIVITY
	ADVANCED RESEARCH PROJECTS AGENCY NUCLEAR TEST DETECTION OFFICE WASHINGTON, D. C.

13. ABSTRACT

DD FORM 1 JAN 64 1473

Unclassified
Security Classification

14 KEY WORDS	LINK A		LINK B		LINK C	
	ROLE	WT	ROLE	WT	ROLE	WT
Seismic Data Laboratory						
VELA-UNIFORM						
LASA						
Vertical Arrays						
Surface Waves						
Rectilinear Motion						
Seismic Noise						
Seismic Coherency						
Finite Fourier Transform						

INSTRUCTIONS

1. ORIGINATING ACTIVITY: Enter the name and address of the contractor, subcontractor, grantee, Department of Defense activity or other organization *(corporate author)* issuing the report.

2a. REPORT SECURITY CLASSIFICATION: Enter the overall security classification of the report. Indicate whether "Restricted Data" is included. Marking is to be in accordance with appropriate security regulations.

2b. GROUP: Automatic downgrading is specified in DoD Directive 5200.10 and Armed Forces Industrial Manual. Enter the group number. Also, when applicable, show that optional markings have been used for Group 3 and Group 4 as authorized.

3. REPORT TITLE: Enter the complete report title in all capital letters. Titles in all cases should be unclassified. If a meaningful title cannot be selected without classification, show title classification in all capitals in parenthesis immediately following the title.

4. DESCRIPTIVE NOTES: If appropriate, enter the type of report, e.g., interim, progress, summary, annual, or final. Give the inclusive dates when a specific reporting period is covered.

5. AUTHOR(S): Enter the name(s) of author(s) as shown on or in the report. Enter last name, first name, middle initial. If military, show rank and branch of service. The name of the principal author is an absolute minimum requirement.

6. REPORT DATE: Enter the date of the report as day, month, year; or month, year. If more than one date appears on the report, use date of publication.

7a. TOTAL NUMBER OF PAGES: The total page count should follow normal pagination procedures, i.e., enter the number of pages containing information.

7b. NUMBER OF REFERENCES: Enter the total number of references cited in the report.

8a. CONTRACT OR GRANT NUMBER: If appropriate, enter the applicable number of the contract or grant under which the report was written.

8b, 8c, & 8d. PROJECT NUMBER: Enter the appropriate military department identification, such as project number, subproject number, system numbers, task number, etc.

9a. ORIGINATOR'S REPORT NUMBER(S): Enter the official report number by which the document will be identified and controlled by the originating activity. This number must be unique to this report.

9b. OTHER REPORT NUMBER(S): If the report has been assigned any other report numbers *(either by the originator or by the sponsor)*, also enter this number(s).

10. AVAILABILITY/LIMITATION NOTICES: Enter any limitations on further dissemination of the report, other than those imposed by security classification, using standard statements such as:

(1) "Qualified requesters may obtain copies of this report from DDC."

(2) "Foreign announcement and dissemination of this report by DDC is not authorized."

(3) "U. S. Government agencies may obtain copies of this report directly from DDC. Other qualified DDC users shall request through _____."

(4) "U. S. military agencies may obtain copies of this report directly from DDC. Other qualified users shall request through _____."

(5) "All distribution of this report is controlled. Qualified DDC users shall request through _____."

If the report has been furnished to the Office of Technical Services, Department of Commerce, for sale to the public, indicate this fact and enter the price, if known.

11. SUPPLEMENTARY NOTES: Use for additional explanatory notes.

12. SPONSORING MILITARY ACTIVITY: Enter the name of the departmental project office or laboratory sponsoring *(paying for)* the research and development. Include address.

13. ABSTRACT: Enter an abstract giving a brief and factual summary of the document indicative of the report, even though it may also appear elsewhere in the body of the technical report. If additional space is required, a continuation sheet shall be attached.

It is highly desirable that the abstract of classified reports be unclassified. Each paragraph of the abstract shall end with an indication of the military security classification of the information in the paragraph, represented as *(TS)*, *(S)*, *(C)*, or *(U)*.

There is no limitation on the length of the abstract. However, the suggested length is from 150 to 225 words.

14. KEY WORDS: Key words are technically meaningful terms or short phrases that characterize a report and may be used as index entries for cataloging the report. Key words must be selected so that no security classification is required. Identifiers, such as equipment model designation, trade name, military project code name, geographic location, may be used as key words but will be followed by an indication of technical context. The assignment of links, rules and weights is optional.

GPO 886-551